FACULTY OF HEALTH SCIENCES

DIVISION OF MEDICAL PHYSICS

Assessment of Imaging Dose from the Kilovoltage Cone Beam Computed Tomography System on Board the Varian Halcyon Linear Accelerator

Author:

Jonathan Mbewe

(MBWJON001)

Supervisor:

Dr Annemari Groenewald

Submitted to the Department of Radiation Medicine at the University of Cape Town in fulfilment of the academic requirements for the degree of MSc(Med) in Medical Physics by dissertation.

December 2023

Declaration

I, Jonathan Mbewe, hereby declare that the work on which this dissertation is based is my original work (except where acknowledgements indicate otherwise) and that neither the whole work or any part of it has been, is being, or is to be submitted for another degree in this or any other university.

I empower the university to reproduce for the purpose of research either the whole or any portion of the contents in any manner whatsoever.

Signed: Signed by candidate

Date: 17 APRIL 2024

Abstract

Daily cone-beam computed tomography (CBCT) is mandatory for cancer patients receiving radiotherapy treatment using advanced techniques on the Varian Halcyon linear accelerator for setup verification, correction and adaptation of the treatment plan. The frequent nature of imaging sessions mostly using kilovoltage (kV) x-ray energies has raised concerns about the contribution of low-energy radiation dose to the overall integral dose and possible induction of secondary primary tumours. In this study, the dose to organs and tissues located in the pelvic and thoracic regions of the body from kV CBCT imaging was estimated using the GATE Monte Carlo toolkit.

The spectral, dose output, and filtration characteristics of the x-ray source on the Halcyon kV CBCT system were derived through measurements using a calibrated ionisation chamber and analytical calculations. The outcomes of this process were used to build a geometry for the Monte Carlo model of the beamline, and then validate it by comparing the computed Percentage Depth Dose and Crossline profiles to those measured in a water phantom using calibrated parallel plate and thimble ionisation chambers. In-phantom dose measurements using Radiochromic film in RANDO pelvic and thoracic phantoms were used to generate a Normalisation Factor to relate the measured and simulated absorbed doses. To estimate the patient doses, Monte Carlo simulations were performed on the Adult Female reference computational phantom from the International Commission for Radiation Protection (ICRP) publication 110.

The highest doses to the pelvic region resulted from the "Pelvis Large" imaging protocol, with organ doses ranging from 5.11 mGy to 174.96 mGy per CBCT scan. In the thoracic region, the "Thorax" protocol resulted in the highest doses, ranging from 2.75 mGy to 54.63 mGy per CBCT scan.

Depending on the fractionation regimen in use, there is a possibility that the imaging doses may exceed 5% of the prescribed therapeutic dose, in which case the imaging dose may need to be added to the treatment plan per recommendation of the AAPM Task Group 180 report.

Dedication

To Noko, Helen, and Potego. Thank you for believing in me.

Acknowledgements

I wish to thank my supervisor for proposing an interesting research topic, as well as for her patience during the investigation and writeup.

Contents

List of Figures **ix**

List of Tables **xiv**

1 Introduction **1**

1.1 Introduction 2

1.1.1 Problem statement 2

1.2 Literature review 4

1.2.1 Imaging in external beam radiotherapy 4

1.2.2 Computed Tomography 5

1.2.3 Gantry mounted kV imaging systems 6

1.2.4 Dosimetry of kilovoltage Cone Beam Computed Tomography (kV CBCT) 7

1.2.5 Measurement-based dosimetry 8

1.2.6 Model based dosimetry 14

1.2.7 Monte Carlo based dosimetry 15

1.2.8 Summary 15

2 Materials and methods **16**

2.1 Halcyon kV CBCT system 17

2.1.1 Characterisation of the Halcyon kilovoltage (kV) source 18

2.1.2 Determination of equivalent energy spectra . . . 19
2.2 Radiochromic film dosimetry . . . 27
2.2.1 Measurement of reference air kerma . . . 27
2.2.2 Preparation of radiochromic film . . . 27
2.2.3 Irradiation of radiochromic film . . . 28
2.2.4 Characterisation of radiochromic film response . . . 29
2.2.5 In-phantom dose profile measurements . . . 33
2.3 Monte Carlo model of the X-ray source . . . 35
2.3.1 Geometry . . . 36
2.3.2 Physics processes . . . 44
2.3.3 Simulating dynamic acquisitions . . . 44
2.3.4 Analysis of output . . . 47
2.3.5 Conclusion . . . 48

3 Results and discussion **49**

3.1 Equivalent spectra . . . 50
3.2 Bowtie filter . . . 51
3.3 Percentage Depth Dose and off-axis profiles . . . 53
3.4 Reference air kerma . . . 54
3.5 Radiochromic film response . . . 56
3.6 In-phantom dose profile measurements . . . 71
3.7 Validation of the Monte Carlo model . . . 74
3.8 RANDO phantom: GATE dose output . . . 78
3.9 Normalisation factor . . . 78
3.10 Organ doses . . . 80

4 Conclusion and Future Work **83**

4.1 Conclusion and Future Work 84

4.2 Strengths and limitations 84

5 Bibliography **86**

6 Appendices **94**

6.1 GATE macros 94

6.2 Energy spectrum files 131

6.3 MATLAB Scripts 150

List of Figures

List of Abbreviations xv

1.1 Computed Tomography Dose Index (CTDI) dose profile (Dose Spread Function, DSF) showing contributions from the primary beam and scattered photons in the tails [6] 9

1.2 Central and peripheral $CTDI_{100}$ measurement positions to derive $CTDI_w$. $D_{opt(i)}$ denotes the value of the ion chamber measurement at the $i-$th position. [25] 9

1.3 Absorbed dose (normalised) as a function of z for scan lengths of 10 mm, 50 mm, 100 mm, 150 mm, 200 mm, 300 mm, 400 mm, 500 mm, and 600 mm [9]. 11

1.4 $D_L(0)$ as a function of L from measurements at the phantom centre and a peripheral location in the central slice [15]. 12

1.5 International Commission for Radiation Units (ICRU)/American Association of Physicists in Medicine (AAPM) phantoms for determination of Computed Tomography (CT) $\overline{D}_{eq}$ [19]. 12

1.6 TLD chips and rods [13]. 13

2.1 Illustration of kV and Megavoltage (MV) beamline arrangments on the Halcyon 2.0. (Image by author.) 18

2.2 IBA Dosimetry XR detector and MagicMax^{TM} dosimetry system used for Half Value Layer (HVL) measurements. The laptop is the control and display console, while the green-coloured device is the MagicMax^{TM} electrometer. The XR detector is the white-coloured rectangular device to the immediate right of the laptop. 20

2.3 Experimental setup for HVL measurements at the Halcyon. The red square represents the detector position, the grey vertical rectangles represent the styrofoam blocks, while the blue horizontal immediately above the styrofoam blocks represents the aluminium filter position. (Image by author.) 21

2.4 SPEKTR 3.0 Graphical User Interface, showing (A) spectra plots, (B) definition of added filtration, (C) reset button to clear the current entries, (D) loading and saving spectra files to and from storage media, (E) spectrum characteristics, and (F) x-ray tube settings. . . . 22

2.5 Ionisation chamber position for bowtie profile measurements on the Halcyon. 23

2.6 Experimental setup for bowtie profile measurement at the Halcyon. (Image by author.) . . 24

2.7 Coordinates of the bowtie filter's curved surface. The y-axis coincides with the central beam axis. y_2 is the position of the filter's distal surface, t_0 is the bowtie thickness through the central beam axis. ϕ is the angle between any ray through the filter and the central beam axis. The ray is transmitted through a path length $L_{BT}(\phi)$ of the filter. (Image by author.) 25

2.8 A Radcal 10X6-6 ionisation chamber positioned at the Halcyon virtual isocentre. The chamber height above the couchtop is meant to minimise the effect of backscatter on the Air Kerma measurement. 28

2.9 Experimental setup for irradiating Radiochromic film (RCF) pieces. The pieces are placed on a platform made from masking tape atop air-equivalent supports made from cardboard. (Image by author.) 29

2.10 Phantom placement of a long film strip to measure the dose distribution horizontally. . . . 33

2.11 The architecture of GATE Monte Carlo toolkit. [34] 35

2.12 GATE corrdinate system [60]. 38

2.13 OpenGL visualisation of the collimator box (in white wireframe), half bowtie filter (magenta), and the lower and upper collimator blades (gray and red), respectively. 39

2.14 A DAWN visualisation of the source capsule, collimator blades, half bowtie filter, and water phantom in the simulation geometry. 42
2.15 A 3D volumetric rendering of the ICRP AF computational phantom generated in ParaView from a Metaimage file. 44
2.16 Extraction of line profiles from 3D dose maps co-registered to the input RANDO image set. 47

3.1 SPEKTR-derived energy spectra of the 100 kV beam used on Halcyon for kV CBCT imaging. The mean energy in each case is indicated in the top right corner. 50
3.2 SPEKTR-derived energy spectra of the 125 kV beam used on Halcyon for kV CBCT imaging. 51
3.3 SPEKTR-derived energy spectra of the 140 kV beam used on Halcyon for kV CBCT imaging. 51
3.4 Profile of the curved portion of the bowtie filter in the Halcyon kV beamline. It was obatined from ionisation chamber measurements and analytical calculations. 52
3.5 A 3 Dimensional rendering of the bowtie filter in the Halcyon kV beamline created in FreeCAD. 52
3.6 Percentage depth dose curves measured in water at 100 cm Source Surface Distance for 100 kV, 125 kV, and 140 kV. The curves were normalised to 100% at the maximum dose. 53
3.7 Crossline dose profiles for 100, 125, and 140 kV beams. The curves are normalised to 100% at the maximum dose. 54
3.8 An exponential analytical function fit to RCF net reflectance - reference air kerma at 100 kV. 58
3.9 A logarithmic analytical function fit to RCF net reflectance - reference air kerma at 100 kV. 58
3.10 A power analytical function fit to RCF net reflectance - reference air kerma at 100 kV. . . 59
3.11 Uncertainty analysis of the exponential analytical model fit at 100kV. 59
3.12 Uncertainty analysis of the logarithmic analytical model fit at 100kV. 60

3.13 Uncertainty analysis of the power analytical model fit at 100kV. 60

3.14 (%) difference between measured and exponential fit derived air kerma at 100 kV. 61

3.15 (%) difference between measured and logarithmic fit derived air kerma at 100 kV. 61

3.16 (%) difference between measured and power fit derived air kerma at 100 kV. 62

3.17 An exponential analytical function fit to RCF net reflectance - reference air kerma at 125kV. 62

3.18 A logarithmic analytical function fit to RCF net reflectance - reference air kerma at 125 kV. 63

3.19 A power analytical function fit to RCF net reflectance - reference air kerma at 125 kV. . . 63

3.20 Uncertainty analysis of the exponential analytical model fit at 125 kV. 64

3.21 Uncertainty analysis of the logarithmic analytical model fit at 125 kV. 64

3.22 Uncertainty analysis of the power analytical model fit at 125 kV. 65

3.23 (%) difference between measured and exponential fit derived air kerma at 125 kV. 65

3.24 (%) difference between measured and logarithmic fit derived air kerma at 125 kV. 66

3.25 (%) difference between measured and power fit derived air kerma at 125 kV. 66

3.26 140 kV exponential fit 67

3.27 140 kV logarithmic fit 67

3.28 140 kV power fit 68

3.29 Uncertainty analysis of the exponential analytical model fit at 140 kV. 68

3.30 Uncertainty analysis of the logarithmic analytical model fit at 140 kV. 69

3.31 Uncertainty analysis of the power analytical model fit at 140 kV. 69

3.32 (%) difference between measured and exponential fit derived air kerma at 140 kV. 70

3.33 (%) difference between measured and logarithmic fit derived air kerma at 140 kV. 70

3.34 Dose distribution from Halcyon Thorax kV CBCT protocol. 71

3.35 Dose distribution from Halcyon Thorax Fast kV CBCT protocol. 72

3.36 Dose distribution from Halcyon Pelvis kV CBCT protocol. 72

3.37 Dose distribution from Halcyon Pelvis Large kV CBCT protocol. 73

3.38 Dose distribution from Halcyon Pelvis Large Fast kV CBCT protocol. 73

3.39 Comparison of measured and GATE Monte Carlo computed percentage depth dose profiles of the 100kV beam. 74
3.40 Comparison of measured and GATE Monte Carlo computed percentage depth dose profiles of the 125 kV beam. 75
3.41 Comparison of measured and GATE Monte Carlo computed percentage depth dose profiles of the 140 kV beam. 75
3.42 Comparison of measured and GATE Monte Carlo computed crossline dose profiles of the 100kV beam. 76
3.43 Comparison of measured and GATE Monte Carlo computed crossline dose profiles of the 125 kV beam. 76
3.44 Comparison of measured and GATE Monte Carlo computed crossline dose profiles of the 140 kV beam. 77
3.45 The normalised dose distribution computed by GATE Monte Carlo through the central slice of RANDO pelvis, using the Pelvis protocol with 125 kV. Voxel values were renormalised to allow visualisation using a colour map. 78
3.46 The normalised dose distribution computed by GATE Monte Carlo through the central slice of RANDO pelvis, using the Breast protocol with 125 kV. Voxel values were renormalised to allow visualisation using a colour map. 79
3.47 The normalised dose distribution computed by GATE Monte Carlo through the central slice of RANDO pelvis, using the Pelvis Large Fast protocol with 140 kV. Voxel values were renormalised to allow visualisation using a colour map. 79

List of Tables

2.1 Preconfigured kV CBCT protocols on Halcyon 19

2.2 ICRP organs and tissues of interest to the current study with their corresponding labels. . 45

3.1 Halcyon kV beamline HVL1, HVL2, and output 50

3.2 Exposure parameters and reference air kerma measured on the Haclyon kV beamline at 100 kV. 55

3.3 Exposure parameters and reference air kerma measured on the Haclyon kV beamline at 125 kV. 55

3.4 Exposure parameters and reference air kerma measured on the Haclyon kV beamline at 140 kV. 56

3.5 Values of the fitting parameters and associated uncertainties for the Exponential, Logarithmic, and Power analytical functions. 57

3.6 Maximum dose-to-water measured in-phantom from Halcyon kV CBCT body imaging protocols. 71

3.7 Protocol-specific doses to organs in the pelvic region. 80

3.8 Protocol-specific doses to organs in the thoracic region. 81

List of Abbreviations

2D Two Dimensional

3D Three Dimensional

AAPM American Association of Physicists in Medicine

CAD Computer Aided Design

CBCT Cone Beam Computed Tomography

CCD Charge Coupled Device

CTDI Computed Tomography Dose Index

CT Computed Tomography

Co-60 Cobalt 60

DICOM Digital Imaging and Communications in Medicine

DLP Dose Length Product

DRR Digitally Reconstructed Radiographs

DSF Dose Spread Function

EPID Electronic Portal Imaging Device

FOV Field of View

FPI Flat Panel Imager

GUI Graphical User Interface

HVL Half Value Layer

IAEA International Atomic Energy Agency

ICRP Internation Commission for Radiation Protection

ICRU International Commission for Radiation Units

IEC International Electrotechnical Commission

IGRT Image Guided Radiotherapy

IMRT Intensity Modulated Radiotherapy

kV kilovoltage

kV CBCT kilovoltage Cone Beam Computed Tomography

LINAC Linear Accelerator

mA milliAmpere

mAs milliampere-second

MC Monte Carlo

MRI Magnetic Resonance Imaging

ms millisecond

MV CBCT Megavoltage Cone Beam Computed Tomography

MV Megavoltage

OAR Organs-at-risk

OSLD Optically Stimulated Luminescent Dosimeters

PDD Percentage Depth Dose

PET Positron Emission Tomography

PV Pixel Value

RCF Radiochromic film

RPM Rotations Per Minute

SBRT Stereotactic Body Radiotherapy

SID Source Imager Distance

SPECT Single Photon Emission Computed Tomography

SRS Stereotatctic Radiosurgery

SSDE Size Specific Dose Estimates

SSD Source Surface Distance

TASMICS Tungsten Anode Spectral Model using Interpolating Cubic Splines

TG Task Group

TIFF Tagged Image File Format

TLD Thermoluminescent dosimeter

VMAT Volumetric Modulated Arc Therapy

Chapter 1

Introduction

1.1 Introduction

Daily Cone Beam Computed Tomography (CBCT) is either strongly recommended or mandatory for cancer patients receiving radiotherapy treatment using advanced techniques like Intensity Modulated Radiotherapy (IMRT), Volumetric Modulated Arc Therapy (VMAT), and Stereotactic Body Radiotherapy (SBRT) for setup verification and adaptation of the treatment plan. This is the rationale for Image Guided Radiotherapy (IGRT), and the benefits to patients in terms of reduced normal tissue complications, improved disease control, the possibility for dose escalation and the subsequent reduction in the overall treatment time are well documented. The frequent nature of imaging sessions mostly using kilovoltage x-ray energies has raised concerns about the contribution of low-energy radiation dose to the overall integral dose and possible induction of secondary primary tumours. To this end several studies have investigated and quantified this dose for several versions of the On Board Imager from Varian Medical Systems, and X-ray Volume Imaging from Elekta. Both CBCT systems are implemented on C-arm linear accelerators.

In recent years, Varian Medical Systems introduced the Halcyon O-ring linear accelerator. The initial version had Megavoltage Cone Beam Computed Tomography (MV CBCT) capability, while the second incorporated both kV CBCT and MV CBCT. On both versions acquisition of CBCT images prior to treatment delivery is a requirement at each fraction. This project aims to quantify concomitant imaging dose from Halcyon's kV CBCT using Monte Carlo (MC) simulations.

1.1.1 Problem statement

The report of Task Group (TG) 180 of the AAPM recommends a threshold for imaging dose of 5% of the therapeutic target dose beyond which the imaging dose should be added to the treatment plan. Quantifying the imaging dose contribution of daily kV CBCT imaging sessions to the overall patient dose will aid in the decision whether or not to account for it, as well as to deduce better estimates of the chances of inducing late effects. Several research publications exist characterising imaging dose from popular C-arm

linac based kV CBCT systems and the Halcyon MV CBCT. However, no substantial literature dedicated to the Halcyon kV CBCT exists.

This project aims to fill that gap by addressing the research questions below:

1. What are the organ doses from imaging with the preconfigured thorax and pelvis protocols?

2. How likely is it that this dose may exceed 5% of therapeutic target doses?

1.2 Literature review

1.2.1 Imaging in external beam radiotherapy

The need for imaging as a tool to improve geometric accuracy in external-beam radiotherapy was recognised as early as the 1940s as shown in the publication "Some Experimental and Clinical Lights on the Rotation Therapy, its Bases and Possibilities" by Nielsen and Jensen[52]. The article proposed a system to actively monitor the treatment by rotational therapy, of oesophageal cancer using the exit beam captured on a phosphor screen to create a portal image. This live image would be used to recentre the treatment field "if the oesophagus should fall outside of the beam during rotation of the patient". Between 1950 and 1960 several attempts were made to capture treatment portal images using radiographic film [63]. These were unsuccessful because of either long film processing times or the poor contrast of images acquired at MV energies. This changed when a 1966 publication "Beam Localization in Cobalt and Megavoltage Therapy during Treatment" by Swain and Steckel successfully used the Adlux® film manufactured by DuPont Company to record portal images from a Cobalt 60 (Co-60) teletherapy unit and a 2 MV Van de Graaf accelerator [63]. The film could be processed in a 90s chemical processor which at that time had been in wide clinical use. The radiographs demonstrated superior contrast and could be processed faster without having to move the patient. Since the film was exposed without intensifying screens and lead filters - as had been the state of practise, patient discomfort was minimised because the film could be placed in holders made from thin cardboard paper. This film was later distributed as Kodak RP/V2 "Verification Film" [26].

Film based MV portable imaging not only presented an opportunity to improve geometric accuracy, but also created another challenge: using the treatment unit for both patient markup and treatment delivery was uneconomical and created bottlenecks. A 1968 article by Jong et al. [36], "Roentgen stand for field positioning in high-energy radiotherapy" proposed designs for what would become the radiotherapy simulator. As the name suggests, the simulator had the same geometric characteristics as an isocentric teletherapy unit, the only significant difference being the diagnostic kV energy x-ray tube as the radiation

source. The same article also proposed a clinical workflow incorporating the simulator: after diagnosis, a patient would have a session at the simulator where mostly orthogonal radiographs of the general disease site would be acquired. Using bony landmarks, the oncologist then determined the extent of treatment-field borders and shielding of organs-at-risk. With this information marked on the radiographs, the patient would return for a final simulation session during which treatment fields and reference marks would be tattooed on the skin. Reference setup images for comparison with subsequent treatment portal images - and geometric parameters for patient setup at the treatment unit were obtained at this stage.

Radiotherapy simulators became an important equipment in what would be called Two Dimensional (2D) radiotherapy and were a de-facto requirement for Radiation Oncology centres. The introduction of digital simulators and Electronic Portal Imaging Device (EPID) on treatment machines meant that online setup verification and correction protocols could be implemented routinely [12].

1.2.2 Computed Tomography

Several reports published in the mid 1970s discussed the potential benefits of CT in radiotherapy planning: the superior soft tissue contrast for a more precise definition of disease extent, delineation of normal organs as well as correction for tissue heterogeneity. A report published in 1978 by Sontag and Cunningham was arguably the first to offer practical demonstration, albeit on a non-deformable RANDO phantom [62]. Later the same year, Battista et al. presented their experience using a CT scanner in clinical radiotherapy for patient simulation, treatment planning and dose calculation [5]. Since then CT scanners have become the imaging modality of choice for treatment planning in Three Dimensional (3D) conformal radiotherapy. Other modalities such as Magnetic Resonance Imaging (MRI), Single Photon Emission Computed Tomography (SPECT), and Positron Emission Tomography (PET) have been useful but their purpose has been to supplement CT imaging. The introduction of wide-aperture scanners, movable lasers, and sythentic Digitally Reconstructed Radiographs (DRR) ushered in virtual simulation, a facility that relegated the physical simulator to the role of clinical mark-up imaging of mostly palliative radiotherapy

cases [61].

Although CT imaging is the gold standard for radiotherapy treatment planning, it has found limited use for routine patient setup verification. In-room CT scanners installed as movable CT-on-rails were pioneered by Japanese researchers in the mid 1990s for frameless Stereotatctic Radiosurgery (SRS) [69] and has seen adoption mainly in particle therapy and to a smaller extent intracranial SRS [40, 55].

1.2.3 Gantry mounted kV imaging systems

Megavoltage portal images suffered from low soft tissue contrast. Setup verification therefore relied on bony tissue as surrogates for the position of Organs-at-risk (OAR). This limitation was recognised by Biggs et al [7] when they proposed a solution to mount a diagnostic x-ray tube isocentrically at 45^o to the Linear Accelerator (LINAC) gantry. This solution had one position of a cassette holder for MV portal acquisition, and second for kV verification image acquisition. In this way the patient positioning and shielding of OAR could be verified in a single session. Before treatment delivery, a double exposure protocol would be followed to acquire a kV image of the open field - with the gantry rotated to 45^o, and a MV portal image. The two images would then be blended together to produce a double exposure image for portal verification and soft-tissue visualisation. This setup was developed further by placing the kV x-ray tube and a Charge Coupled Device (CCD) camera perpendicular to the MV beam of an Elekta SL-20 LINAC - a system subsequently used for what was the first demonstration of a gantry mounted kV CBCT acquisition [32, 56]. Less than a year later, Jaffray and Siewerdsen reported kV CBCT with a Flat Panel Imager (FPI) in place of the CCD detector [33], a practice which continues to this day. Other source-detector arrangements exist besides the perpendicular kV imaging setup, but these are installed on specialised treatment systems and strictly for 2D projection radiography [35, 48].

1.2.4 Dosimetry of kV CBCT

Radiation dosimetry refers to a set of methods used to convert the energy deposited by ionising radiation in unit mass of tissue (absorbed dose, D) to its effect in tissue [23]. Absorbed dose (D) is expressed mathematically in Equation (1.1) and has a unit of Gray (1 Gy = 1 J/kg).

$$D = \frac{dE}{dm} \tag{1.1}$$

dE is the energy deposited in matter of unit mass dm. Equation (1.1) provides a conceptual definition of a physical quantity which may be directly measured only under a set of limited conditions in practice, and certainly not for the routine determination of patient imaging doses from CBCT procedures. A more useful quantity that reflects the risk of damage to tissue arising from absorbed dose is the effective dose (E), given by Equation (1.2).

$$E = \sum_T W_T \sum_R W_R \cdot D_{T,R} \tag{1.2}$$

W_T is a weighting factor that represents an organ or tissue's radiosensitivity and its likelihood of experiencing damage from ionising radiation R. The radiation weighting factor, W_R expresses the likelihood of causing radiation damage to tissue. $D_{T,R}$ is the absorbed dose to tissue T from exposure to radiation R. Tables of weighting factors are available in publications such as Report 103 of the Internation Commission for Radiation Protection (ICRP) [57]. Imaging with kV CBCT exclusively uses x-ray photons having a radiation weighting factor of unity.

Dosimetry methods employed in kV CBCT can be categorised as measurement based, model based, and MC based [20].

1.2.5 Measurement-based dosimetry

Computed Tomography Dose Index

Routine direct measurement of absorbed doses to patients' internal organs is not feasible currently, except in the case of dose to the skin, body cavities and orifices. In lieu of absorbed dose, measurements of surrogate quantities are made in-air or in standard acrylic phantoms. Using conversion factors, the effective doses are calculated in anthropomorphic mathematical phantoms representing the standard man, woman or child [44]. Effective doses derived in this manner are used as radiation-risk estimates, with uncertainties of up to 30% [24]. To reduce these uncertainties, Size Specific Dose Estimates (SSDE) that consider metrics of patient size were introduced into clinical practice [8, 41].

In fan beam CT dosimetry, the CTDI has been the surrogate quantity of choice for patient dose. CTDI is traditionally measured in a cylindrical phantom using a 100 mm long pencil ionisation chamber, in which case it is denoted CTDI_{100} and defined in equation ((1.3)).

$$CTDI_{100} = \frac{1}{nT}\int_{-50mm}^{+50mm} D(z)dz \tag{1.3}$$

n is the number of detector rows, and T is the individual row thickness. CTDI_{100} is measured for a thin slice ($\leq$ 10 mm) and a single rotation of the tube with the couch stationary. As shown in figure (1.1), it measures the dose to air over a volume which includes the slice width and the scatter-generated tails of the fan beam profile on both sides of the slice [64].

To estimate the average absorbed dose in the scan plane, several CTDI_{100} measurements are made with the ionisation chamber positioned at the phantom centre and positions along the periphery at the four cardinal angles, as illustrated in figure (1.2).

The weighted sum of the central and mean peripheral CTDI_{100}, Equation (1.4) yields the weighted CTDI (CTDI_w).

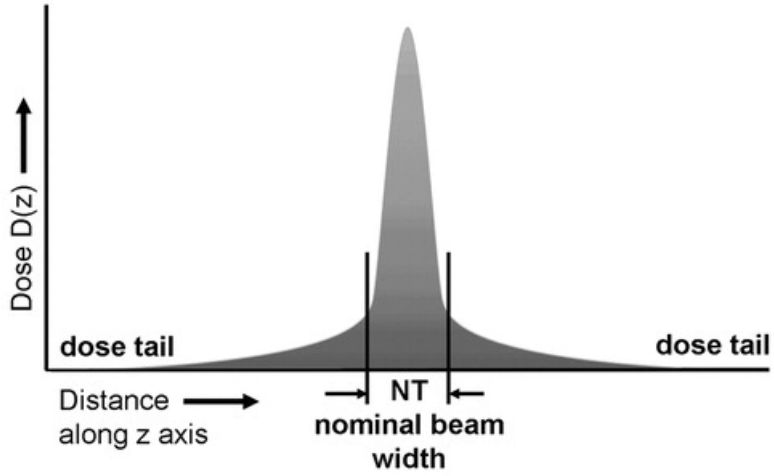

Figure 1.1: CTDI dose profile (Dose Spread Function, DSF) showing contributions from the primary beam and scattered photons in the tails [6]

.

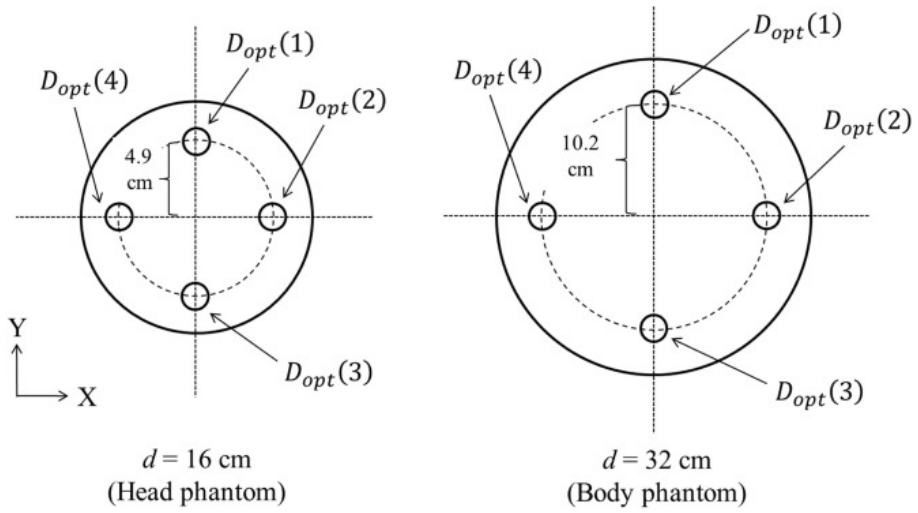

Figure 1.2: Central and peripheral CTDI_{100} measurement positions to derive CTDI_w. $D_{opt(i)}$ denotes the value of the ion chamber measurement at the $i-$th position. [25]

.

$$CTDI_w = \frac{1}{3}CTDI_{centre} + \frac{2}{3}CTDI_{periphery} \tag{1.4}$$

CTDI_w is defined for a pitch of unity, i.e., no couch translation per tube rotation. For values of pitch different from 1, CTDI_{vol} given by Equation (1.5) applies.

$$CTDI_{vol} = \frac{CTDI_w}{pitch} \tag{1.5}$$

Finally, the product of $CTDI_{vol}$ and the scan length yields the Dose Length Product (DLP) that expresses the mean absorbed dose to the entire volume within the scan region (Equation (1.6)).

$$DLP = CTDI_{vol} \cdot scanlength \tag{1.6}$$

Together with tissue weighting factors, DLP is used to determine approximations of population-wide risks of stochastic effects from CT examinations [29, 57].

The definition of $CTDI_{100}$ is valid for fan-beams. However, the concept begins to break down with increasing cone angles where the 100 mm detector length and amount of material in 150 mm cylindrical phantom are insufficient to measure the primary beam and scatter dose profile. As a possible solution, the International Atomic Energy Agency (IAEA) in its report "Status of Computed Tomography dosimetry for wide cone-beam scanners" [30], proposed a two-pronged solution based on International Electrotechnical Commission (IEC) report 60601-2-44. [14]. For CT slice thickness of up to 40 mm the existing $CTDI_{100}$ method is maintained, while for beam widths greater than 40 mm, the formalism expressed in Equation (1.7) must be used.

$$CTDI_{100,(n\times T)>40} = CTDI_{100,ref} \times \left(\frac{CTDI_{free-in-air,N\times T}}{CTDI_{free-in-air,ref}} \right) \tag{1.7}$$

Equation (1.7) states that the $CTDI_{100}$ for the user slice thickness ($n\times T$) greater than 40 mm is equal to the product of the $CTDI_{100}$ measured in-phantom for a reference slice thickness and the ratio of user and reference slice CTD_{100} measured free in-air.

The IAEA method has been demonstrated to underestimate the absorbed dose owing to the inability of the 100 mm detector to capture the entire cone beam dose profile [54].

Average planar equilibrium dose

As a means to mitigate this issue, Dixon et al. [18] introduced the quantities Integral Dose (E_{tot}) (synonymous to DLP) and Planar Average Equilibrium Dose ($\overline{D}_{eq}$) (synonymous to $CTDI_{vol}$) in a formalism based on the measurement of a point dose in a cylindrical phantom using a small-volume integrating ionisation chamber (1.8). The phantom must be sufficiently long to provide full scatter conditions for the irradiated scan length.

$$E_{tot} = \rho\pi R^2 L\overline{D}_{eq} \tag{1.8}$$

ρ is the phantom mass density and R is phantom radius. Suppose $D_L(z=0)$ is the absorbed dose at the centre of the field of view for a scan length L, in the z direction. Figure 1.1 illustrates the DSF from a single, stationary rotation of a narrowly collimated primary beam. $D_L(z=0)$ increases with L, as illustrated in Figure 1.3.

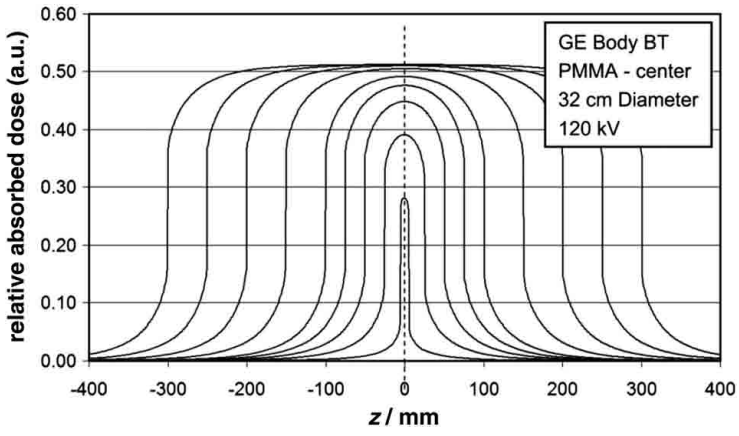

Figure 1.3: Absorbed dose (normalised) as a function of z for scan lengths of 10 mm, 50 mm, 100 mm, 150 mm, 200 mm, 300 mm, 400 mm, 500 mm, and 600 mm [9].

If L were to increase infinitely, $D_L(z=0)$ would asymptotically approach a limit - the planar average equilibrium dose, ($\overline{D}_{eq}$), as illustrated in Figure 1.4 for measurements at the phantom centre and a peripheral location in the central plane.

Practical measurements are performed in an appropriate phantom, such as the ICRU/AAPM phantom

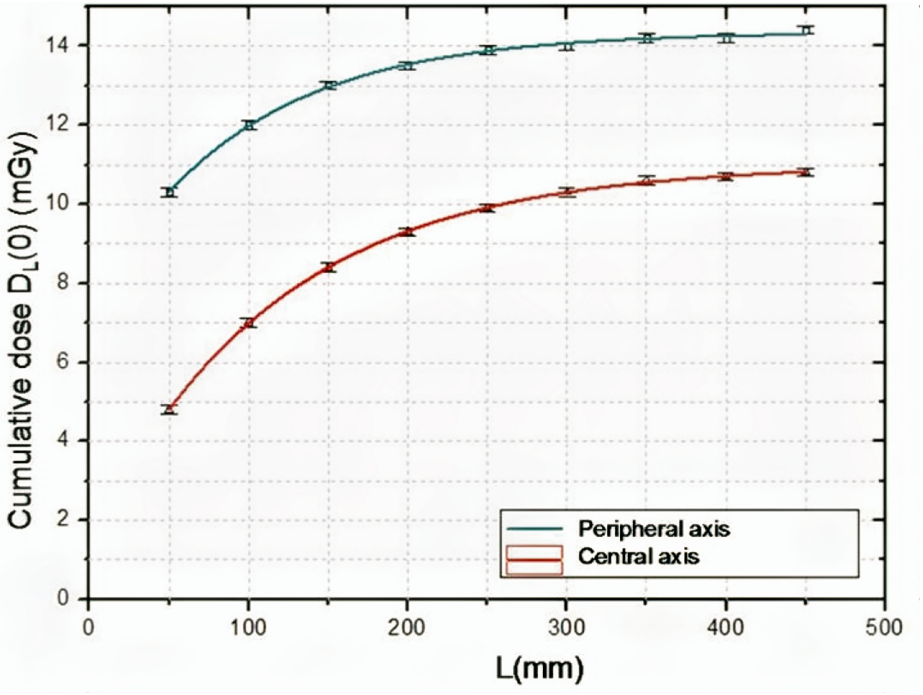

Figure 1.4: $D_L(0)$ as a function of L from measurements at the phantom centre and a peripheral location in the central slice [15].

recommended by AAPM TG 200 [19], illustrated in Figure 1.5. The detector should be a calibrated, integrating thimble or Farmer type ionisation chamber. The phantom is made from polyethylene ($\rho = 0.97 g/cm^3$), has a length of 600 mm, diameter 300 mm, with inserts at the central location and a second, peripheral location in the central plane.

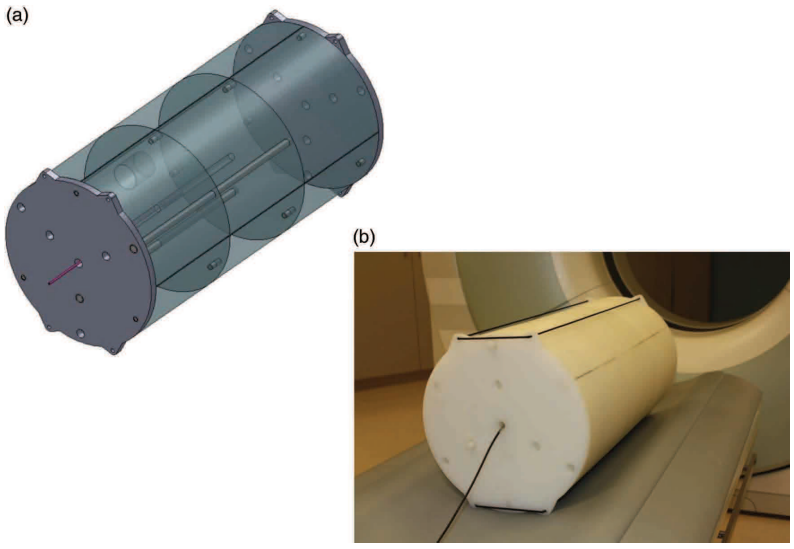

Figure 1.5: ICRU/AAPM phantoms for determination of CT $\overline{D}_{eq}$ [19].

Several publications comparing CTDI and TG 111 CT dosimetry methodologies concluded that the TG 111 method yielded more accurate results [28, 10, 3]. A major advantage of the TG 111 formalism over the CTDI is that it may be used to evaluate the dosimetry of all forms rotational CT, for both stationary-table and helical scanning regardless of the cone angle. Similar to CTDI concept however, this method effectively measures CT scanner radiation output and may only be related to risk quantities in patient populations via conversion factors. Although useful for tracking and comparing the output constancy of CT scanners, neither method is effective for determining the absorbed dose in patients.

Thermoluminescent dosimetry

Thermoluminescent dosimeter (TLD) relies on the ability of imperfect crystals to store the energy from ionising radiation. This energy is emitted as visible light when the crystals are subsequently heated under controlled conditions, and related to the absorbed dose by a calibration factor. Several different materials may be used as TLD, however Lithium Fluoride doped with some impurity such as Magnesium or Titanium is the material that has been most characterised for radiation dosimetry [43]. TLD may take the form of powder or small cylindrical chips,as illustrated in Figure 1.6.

Figure 1.6: TLD chips and rods [13].

Practical TLD dosimetry involves a process of cleaning the dosimeters to remove dirt from the surfaces, annealing to remove any latent signal, calibration to relate the radiation dose to the light signal emitted,

actual measurement exposure and finally the readout. Many of these steps are now almost completely automated in current TLD readers [71].

Optically Stimulated Luminescence

A more recent development has been the Optically Stimulated Luminescent Dosimeters (OSLD), or 'glass dosimeters'. The operational principles are similar to TLDs, except that OSLDs use visible light for signal generation instead of heat [46]. An important advantage that OSLDs have over TLDs is that they may be taken through the readout cycle several times with minimal loss of information [39].

Radiochromic film

RCF has been used to determine the in-phantom absorbed dose due to kV CBCT imaging. Despite posessing superior spatial resolution, capability for 2D measurement of dose distribution, and near-water equivalence, the use of RCF for dosimetry in the kV imaging range has been hampered by the energy dependence of reponse. For this reason RCF is used primarily in MV radiotherapy dosimetry. Giaddui et. al [21] used GafChromic XR-QA film to evaluate in-phantom, the imaging dose from kV CBCT systems of two competing manufacturers. Rampado et. al [59] characterised the energy response of the same model and found it to be highly dependent on beam quality. Tomic et. al [67] characterised Gafchromic XR-QA2, the immediate successor to XR-QA and also found its response to be energy dependent. XR-QA2 was supplanted in 2021 by GafChromic LD-V1, whose response characteristics were investigated in the Mammography kV range by Satoshi and Nakajima [49], and in the diagnostic range by Mbewe [45]. Initial results suggested the energy dependence was not significant, and therefore the film could be used for in-phantom dose measurements with a single response-dose calibration curve.

1.2.6 Model based dosimetry

This method of dosimetry is not as widespread as measurement and MC based tools, but relies on adding to regular treatment planning systems the capability to calculate radiation dose in the kV range. Such an

adaptation was successfully implemented by Alaei et. al in the Pinnacle treatment planning system [2]. It is not generally available, however.

1.2.7 Monte Carlo based dosimetry

MC modelling uses random number generation to simulate radiation sources, track particle interactions in material and quantify radiation dose deposition [4]. Most MC packages are general-purpose and may be used for all radiation physics problems. Marchant and Joshi [42] developed a model of Varian's XI CBCT using the GEANT4 toolkit [1] to estimate patient doses arising from CBCT imaging to the pelvic region. Since the model used patients' actual Digital Imaging and Communications in Medicine (DICOM) image sets for patient geometry, the dosimetry was patient-specific as opposed to being generalised estimates. Several authors used this model as the basis for simulating CBCT systems from different vendors by simply modifying the beam source specification and geometry [73, 22]. Another less popular package that has been used for kV CBCT dosimetry are EGSnrc and BEAMnrc [50]. The main downside of MC modelling is the need for accurate geometry and material specification of the kV CBCT system, and not all manufacturers are willing to make such information public.

1.2.8 Summary

Dosimetry in CT and kV CBCT for IGRT is measurement based, model based or monte carlo based. Direct measurement of patient organ doses is not currently feasible. Instead, measurement of skin dose, surrogate quantities or organ doses in anthropomorphic phantoms is performed. Model based dosimetry relies on adding to regular treatment planning systems the capability to calculate radiation dose in the kV energy range. Well validated monte carlo models are the gold standard in radiation dosimetry.

Chapter 2

Materials and methods

2.1 Halcyon kV CBCT system

The Halcyon^{TM} from Varian Medical Systems (Palo Alto, CA, USA) is a radiotherapy delivery system consisting of a 6 MV inline linear accelerator, imaging devices and other peripherals all mounted on a ring gantry. The system was developed to improve access to advanced IGRT and reduce the complexity associated with commissioning such programs [11]. For this purpose, the Halcyon is delivered with preconfigured machine models, beam-source models and radiation dose calculation algorithms. The initial version of the Halcyon had MV CBCT using the therapy source for imaging. Subsequent versions included a kV CBCT system with a Feldkamp, Davis, and Kress (FDK) and a novel Iterative CBCT (iCBCT) algorithms for image reconstruction.

Halcyon's kV CBCT system consists of a kV x-ray tube source to which a single permanent half-bowtie filter is fixed. The source generates peak voltages ranging from 40 kV to 150 kV, with the focal spot located at 100 cm from the isocentre. The image receptor is a 43 cm x 43 cm amorphous Silicon device with 1028 x 1028 pixels, offering a scan Field of View (FOV) of 49.1 cm. The imager centre is laterally displaced from the isocentre by 17.5 cm, with a constant Source Imager Distance (SID) of 154 cm. The ring gantry geometry allows the CBCT system to reach a maximum speed of four Rotations Per Minute (RPM), for faster acquisitions than the conventional C-arm LINAC whose typical maximum RPM is one. Figure (2.1) illustrates the geometrical arrangement of the kV, MV source and imager pairs.

There are eleven kV CBCT clinical imaging protocols which are preconfigured and are not user adjustable. Table (2.1) provides a summary of the protocols.

Iterative reconstruction is available for all but three imaging protocols. Similar exposure techniques are used regardless of the choice of reconstruction algorithm, however, and the dose implications are invariant. The protocols 'Image Gently' and 'Image Gently Large' are used exclusively for paediatric imaging, and they will not be considered further in this investigation. As opposed to adult imaging, it is not advisable to use an average paediatric patient for estimating imaging dose owing to the large variability of patient sizes amongst this group. Instead, paediatric patients are stratified into age or weight

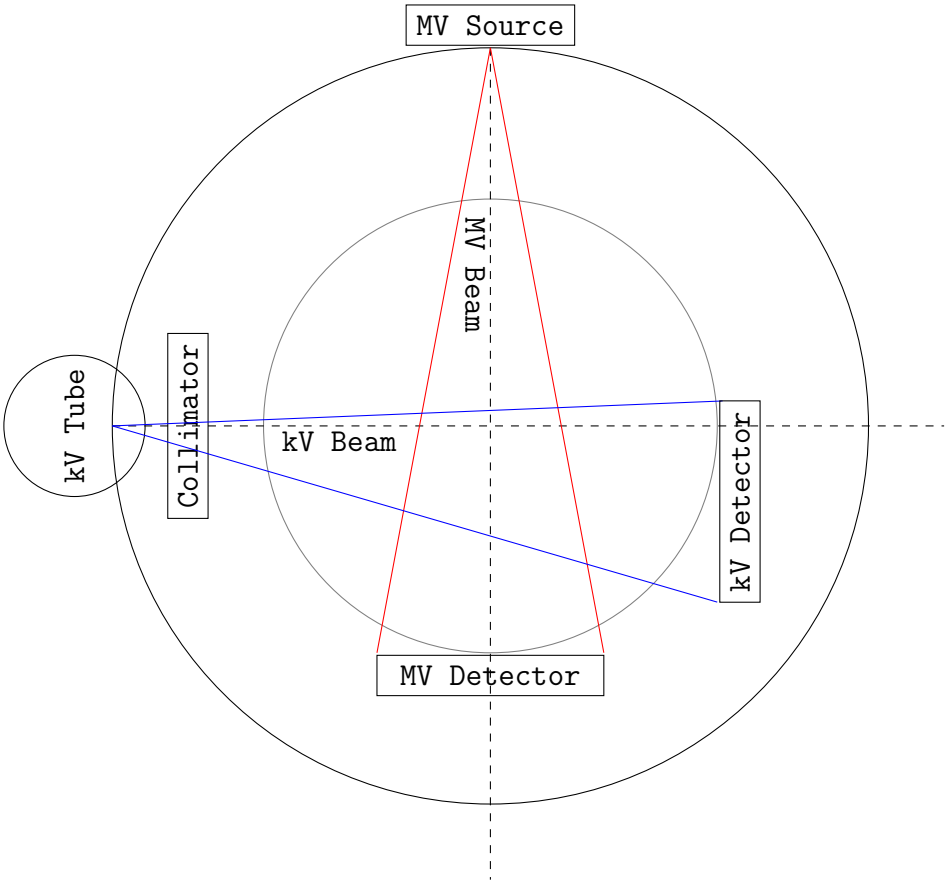

Figure 2.1: Illustration of kV and MV beamline arrangments on the Halcyon 2.0. (Image by author.)

bands per recommendation of ICRP 121 and ICRP 135 [38, 70]. A reference patient having a weight near each band's midway point is then used to fabricate anthropomorphic phantoms, whether physical or computational.

2.1.1 Characterisation of the Halcyon kV source

Detailed specifications of the x-ray kV source on the Halcyon kV CBCT, i.e., energy-fluence spectra, the geometry of bowtie filters and other attenuators, are not currently in the public domain. Therefore, equivalent spectral and filtration models were derived through measurement methods based on the work of Turner et al. [68], implemented originally for multi-detector CT, and applied to CBCT by McMillan et al. [47]. Using this method, no prior knowledge of an x-ray tube's spectral or filtration characteristics are required, except for the assumption that the spectra originate from a Tungsten target.

Table 2.1: Preconfigured kV CBCT protocols on Halcyon

Mode	Energy (kV)	Default (mAs)	Projections	mA/ms	Scan time (s)	FOV
Image Gently	80	93	463	20/10	16.6	281
Image Gently Large	100	98	491	20/10	16.6	384
Head	100	139	463	30/10	16.6	281
Head Low Dose	100	46	463	10./10	16.6	281
Breast	125	49	491	10/10	16.6	281
Thorax Fast	125	295	491	60/10	16.6	491
Pelvis Fast	125	592	592	100/10	21.2	491
Thorax	125	301	859	35/10	30.8	491
Pelvis	125	1074	895	80/15	36.7	491
Pelvis Large Fast	140	698	698	100/10	25	491
Pelvis Large	140	1456	809	90/20	40.6	491

2.1.2 Determination of equivalent energy spectra

The equivalent energy spectra are the calculated spectra that best match the characteristics of the real x-ray tube obtained from measurements. In particular, the equivalent specra have first and second HVLs (HVL_1 and HVL_2) and x-ray tube output (in mGy/mAs) that match measurements.

Measurement of HVL_1, HVL_2, and tube output

The measurement of HVLs was performed at the Halcyon with the MV source stationed at gantry angle 90^o and kV tube at 12 o'Clock position. For this purpose, the dosimetry system used was an IBA Dosimetry (IBA Dosimetry Gmbh, Schwarzenbruck, Germany) solid-state XR detector connected to a MagicMax^{TM} electrometer and control computer. Several absorbers made from 99.9% pure aluminium were used. The measurement of tube current was performed with a physical connection to the x-ray tube generator. The system is shown in figure (2.2)

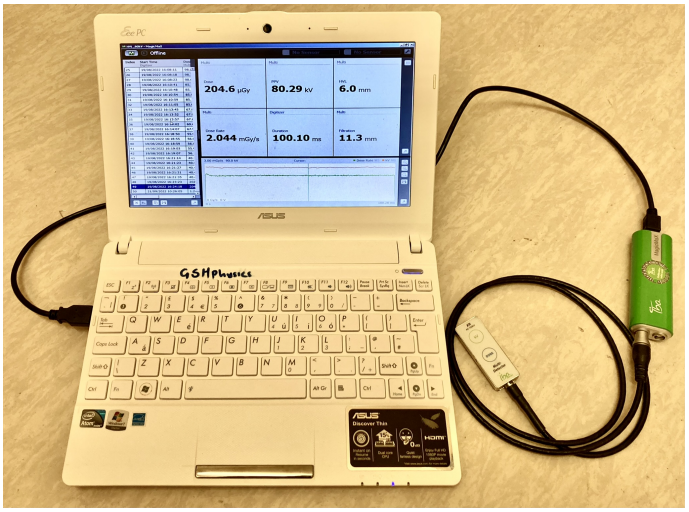

Figure 2.2: IBA Dosimetry XR detector and MagicMax^{TM} dosimetry system used for HVL measurements. The laptop is the control and display console, while the green-coloured device is the MagicMax^{TM} electrometer. The XR detector is the white-coloured rectangular device to the immediate right of the laptop.

The detector was positioned at the virtual isocentre, secured to the couch-top with masking tape, and sent to the true isocentre. In the XI View application using the default Bin1x1 imaging protocol, several static images were then acquired to finetune the lateral and vertical alignment of the dose measurement module of the XR detector at the true isocentre. Two styrofoam blocks of height 30 cm were then placed on either side of the detector to support the aluminium absorbers. For each kV setting of 100, 125, and 140 kV, the mA and ms settings of the imaging protocol were changed to 100 mA and 100 ms. Five exposures were taken without filters in place and the average was calculated. Exposures were subsequently repeated while progressively adding more aluminium filters until an average air kerma just below one-quarter of the initial no-filter measurement was obtained. These measurements were repeated for the three kV settings. In this manner, the HVL_1 and HVL_2 values of each kV were obtained. The experimental setup is illustrated in Figure (2.3). This setup was used without the Styrofoam blocks, for mA and mAs measurements with the MagicMax connected to the generator. mA and exposure time were set to 120 mA and 20 ms, respectively for all kVs.

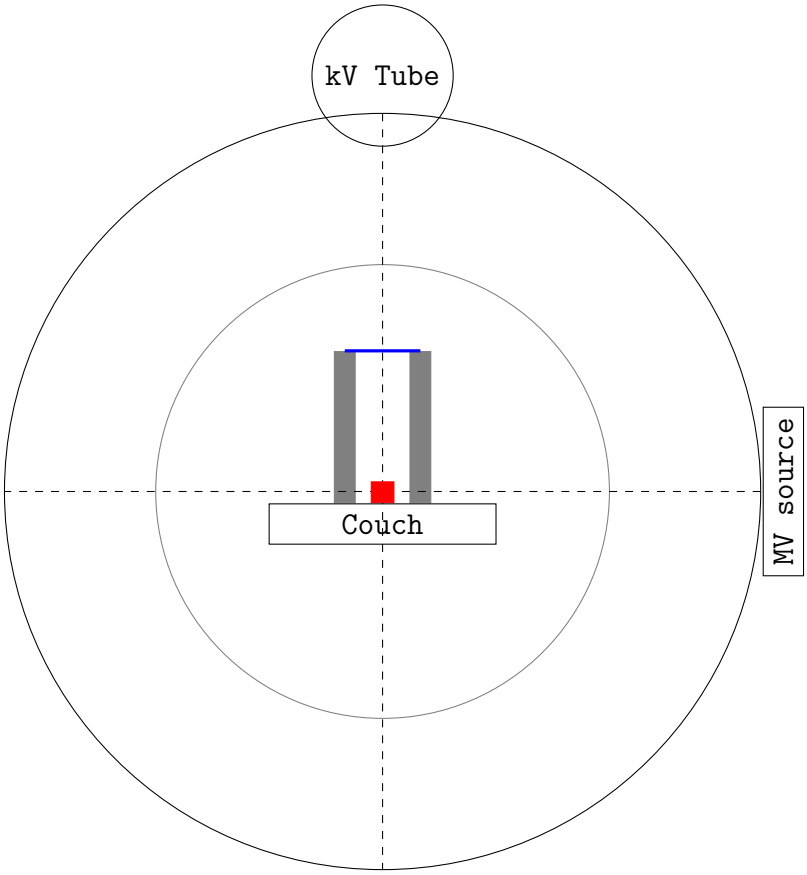

Figure 2.3: Experimental setup for HVL measurements at the Halcyon. The red square represents the detector position, the grey vertical rectangles represent the styrofoam blocks, while the blue horizontal immediately above the styrofoam blocks represents the aluminium filter position. (Image by author.)

Calculation of equivalent energy spectra

Calculation of the equivalent spectra started with the generation of initial unfiltered ("soft") energy spectra using the computer program SPEKTR (v3.0) - a computational tool for x-ray spectrum modeling and analysis [58]. The sotfware, written in MATLAB^{TM}, uses the so-called Tungsten Anode Spectral Model using Interpolating Cubic Splines (TASMICS), developed by Hernandez and Boone [27] to simulate and compute spectral and exposure characteristics of generic tungsten x-ray tubes. SPEKTR generates unfiltered energy spectra with a resolution of 1.0 keV from inputs of beam energy (kVp) and % ripple. A built-in function, $spektrTuner$, allows initial calculated spectra to be optimised ("tuned") such that measured and theoretical x-ray tube outputs (in mGy/mAs) are matched. Figure (2.4) shows the program's graphical user interface (GUI).

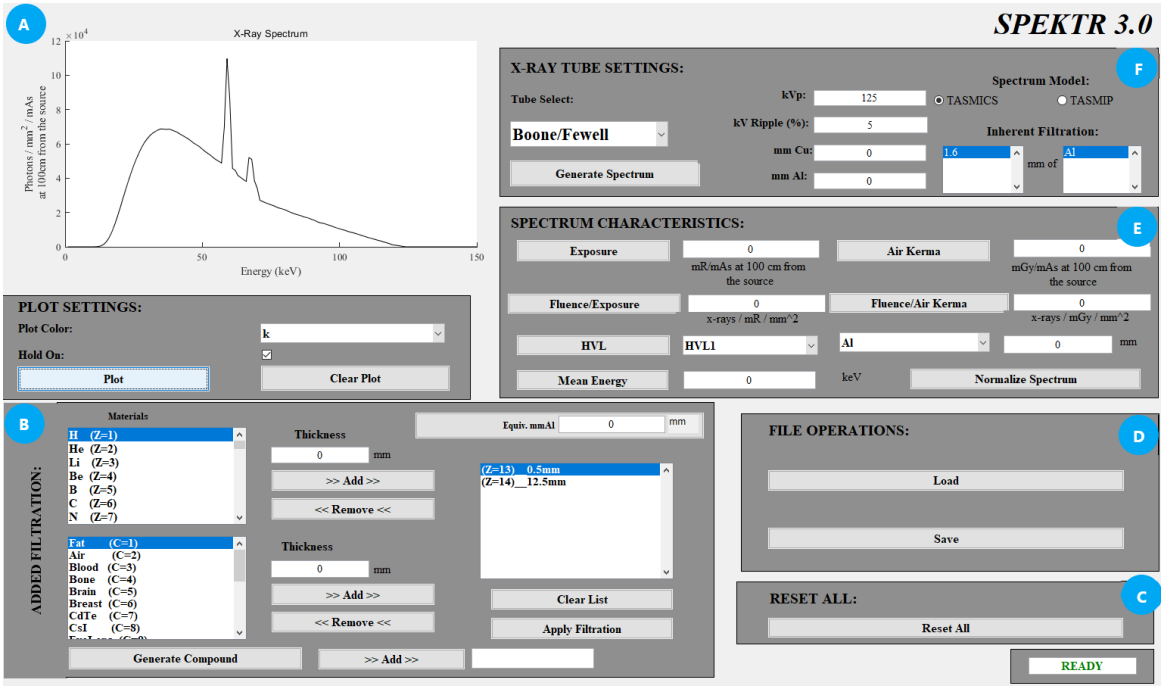

Figure 2.4: SPEKTR 3.0 Graphical User Interface, showing (A) spectra plots, (B) definition of added filtration, (C) reset button to clear the current entries, (D) loading and saving spectra files to and from storage media, (E) spectrum characteristics, and (F) x-ray tube settings.

Using SPEKTR, energy spectra were generated for the three kV settings and tuned to minimise the differences between measured and calculated tube output. With the initial spectra, an initial equivalent bowtie filter made of aluminium was assumed. In addition, two more absorbers were added: a hardening material representing the cumulative inherent filtration and an aluminium filter whose thickness was equal to the measured HVL_2 of each kV setting. The inherent filtration's thickness and material composition were altered iteratively until the calculated and measured HVL_2 were matched. The resulting spectrum was regarded as the spectrum transmitted through the central portion of the bowtie filter, assumed to be 0.5 mm thick. The final spectra were saved as two-column text files, where the first columns were the energy bins in 1 keV resolution up to 150 keV (x-values), and the second columns were the corresponding Photons/mm^2/mAs at isocentre (y-values). The y-values were normalised to the maximum value before the spectra were used in GATE for simulation.

Measurement of the bowtie profile

The equivalent bowtie's variable thicknesses were obtained from transmission measurements through the real, albeit unknown, half bowtie filter on the Halcyon's kV x-ray tube. The gantry was parked at angle 180^o to park the x-ray tube at the 3 o'Clock position. A PTW 30013 Farmer type ionisation chamber (PTW Freiburg, Freiburg im Breisgau, Germany) was secured to the superior edge of the couch in air (figure (2.5)) such that the chamber's stem rested on rectangular piece of Bostik Prestik^{TM} stuck onto the couch-top. A piece of masking tape kept the detector immobilised.

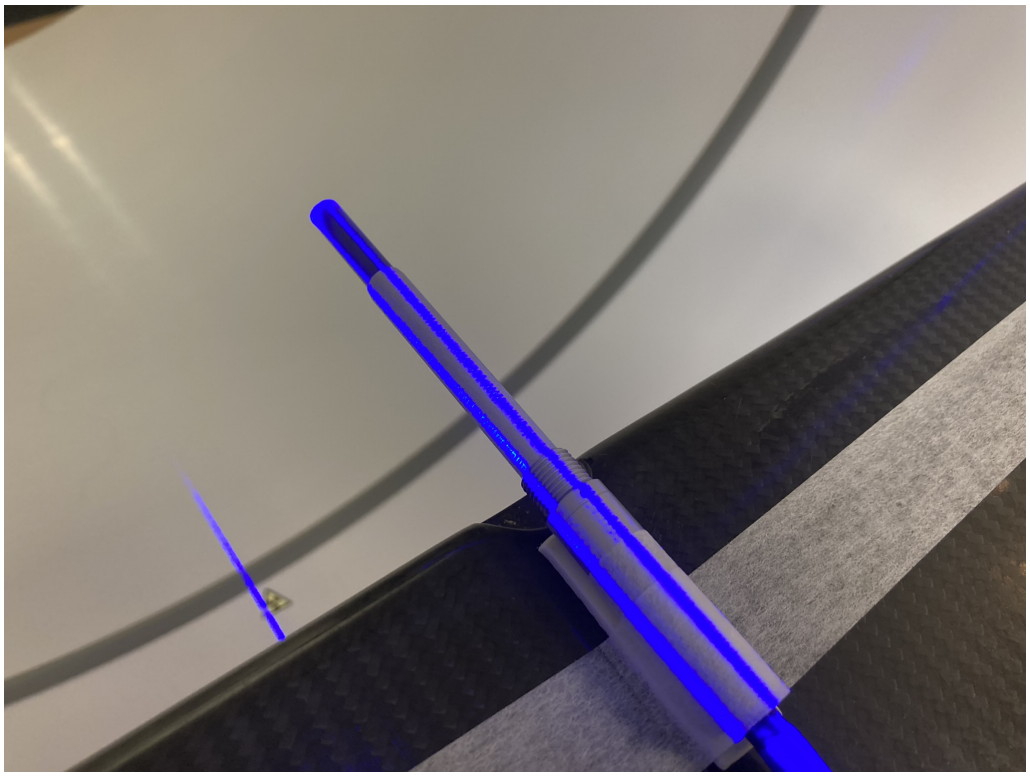

Figure 2.5: Ionisation chamber position for bowtie profile measurements on the Halcyon.

Starting from the anterior edge of imager, exposures were made and charge collected as the the chamber was moved in 0.5 to 1.0 cm steps across the bowtie until the imager's posterior edge was reached. The measurement setup is illustrated in figure 2.6).

The angle θ_i associated with each measurement position is determined from the focal-spot to isocentre distance L and the vertical ionisation chamber displacement, p_i using equation ((2.1)).

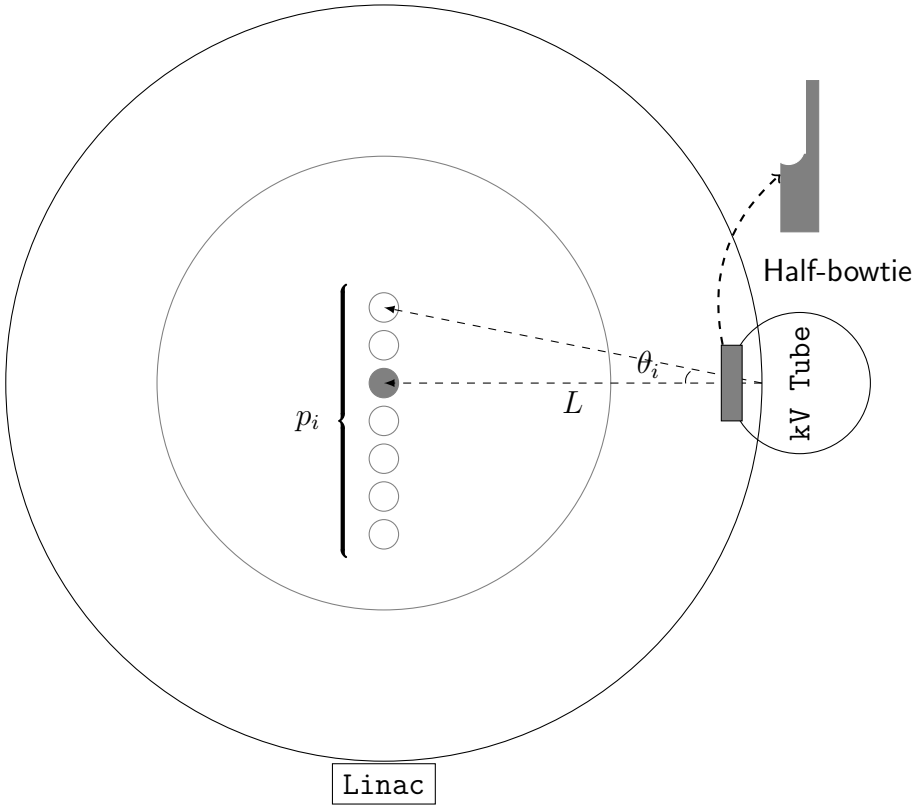

Figure 2.6: Experimental setup for bowtie profile measurement at the Halcyon. (Image by author.)

$$\theta_i = tan^{-1}(p_i/L) \tag{2.1}$$

The charge measured at the $p_i - th$ location with angle θ_i was expressed as a fraction of the charge measured at p_0, with $\theta_0 = 0$ (isocentre). To generate an equivalent bowtie filter, the steps below were followed:

1. Using SPEKTR, an aluminium filter of thickness 0.5 mm was added, representing the bowtie filter's centre portion, t_0. Using the equivalent spectrum derived in section 2.1.2, the KERMA in air was calculated.

2. An additional aluminium filter, t_1, representing the path length (L_{BT}) through the bowtie filter at angle θ_1 was added and the air KERMA again calculated. t_1 was varied until the ratio of the calculated air KERMA at θ_1 and θ_0 was matched with the corresponding ratio of charges.

3. Steps 1 and 2 above were repeated for all θ_i's

A plot of p_i vs t_i yields the bowtie filter profile. To find the coordinates of the filter's surface, the approach developed by Zhang et al.[74] was adopted. Consider Figure (2.7) depicting the bowtie filter's spatial location in the xy (axial), with the origin at the focal spot. By this approach, the (x, y) coordinates of the bowtie filter's curved surface are then given by equations (2.2) and (2.3).

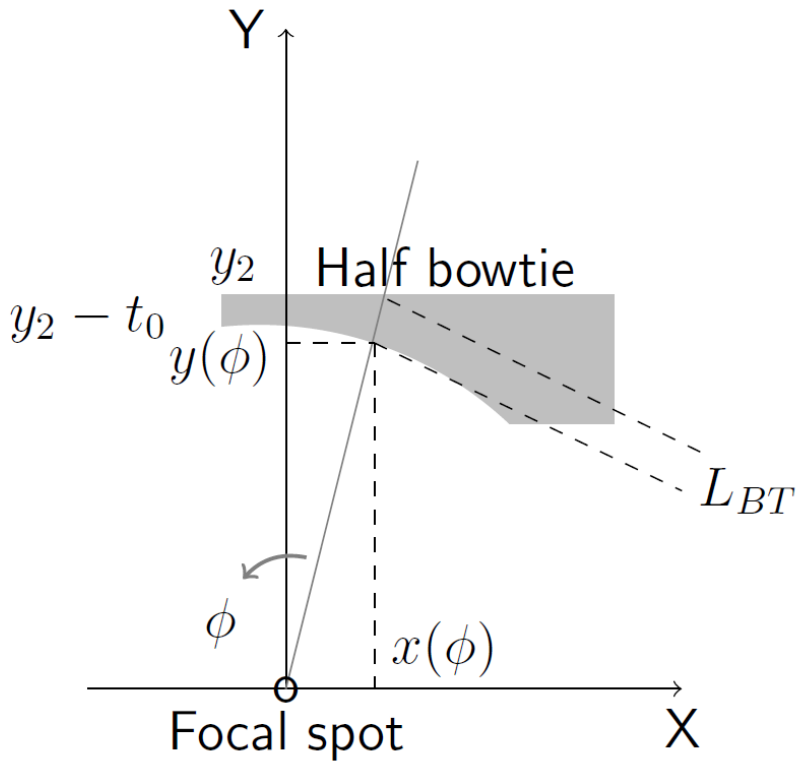

Figure 2.7: Coordinates of the bowtie filter's curved surface. The y-axis coincides with the central beam axis. y_2 is the position of the filter's distal surface, t_0 is the bowtie thickness through the central beam axis. ϕ is the angle between any ray through the filter and the central beam axis. The ray is transmitted through a path length $L_{BT}(\phi)$ of the filter. (Image by author.)

$$x(\phi) = y_2 \cdot tan\phi - L_{BT}(\phi) \cdot sin\phi \tag{2.2}$$

$$y(\phi) = y_2 - L_{BT}(\phi) \cdot cos\phi \tag{2.3}$$

Generating the 3D model of the bowtie filter

The (x,y) coordinates of the bowtie filter's curved section corresponding to each value of θ were obtained from Equations (2.2) and (2.3), with $y_2 = 147$ mm (obtained from the dimensions of an x-ray tube used in the kV CBCT system on the Varian TrueBeam LINAC, and $t_0 = 0.5$ mm from assumptions made in the equivalent bowtie filter model. The coordinates were used to plot points in the Computer Aided Design (CAD) software FreeCAD [37]. In doing so, a cartesian coordinate system was used in which the origin was placed at the tube focal spot. A cubic spline was then fit through the discrete points to create the curved section. Straight lines connected to the spline were used to model the filter's flat surfaces. The 2D sketch was extruded to generate the 3D model with dimensions 100.00 mm X 40.82 mm X 90.00 mm and saved as a Standard Tessellation Language (STL) file for later use in defining the bowtie filter geometry in the Monte Carlo model.

Measurement of Percentage Depth Dose (PDD) and off-axis profiles

The x-ray tube output at kVp settings of 100, 125, and 140 kV was characterised by measurement of depth dose and off-axis dose profiles in water. For this purpose, a PTW Beamscan water phantom was set up and positioned at 100 cm Source Surface Distance (SSD), with the collimator blades opened to 10 cm $\times$ 28 cm, the default aperture opening for kV CBCT acquisitions. A PTW Advanced Markus (PTW Freiburg, Freiburg im Breisgau, Germany) ionisation chamber was used for depth dose measurements, while a PTW Semiflex (PTW Freiburg, Freiburg im Breisgau, Germany) chamber was employed for measurement of off-axis dose profiles. PDD profiles were measured from a depth of 20 cm to the surface, while off-axis profiles were measured at a depth of 2 cm. The results were compared with those from the Geant4/GATE Monte Carlo model for verification.

2.2 Radiochromic film dosimetry

For this study, the RCF dosimetry systems comprised of Gafchromic LD-V1 films (Lot 08252201), and an EPSON 12000XL (Seiko Epson Corp., Nagano, Japan) RGB flatbed scanner. Calibration of the film was performed according to the method proposed by Declic et. al, [66], that established a relationship between air-kerma and reflective absorbance. For low dose applications, the sensitivity of radiochromic film was found to be higher when reflective scanning is used instead of transmission scanning [53].

2.2.1 Measurement of reference air kerma

Air kerma was measured at isocentre in the three beam qualities resulting from the combination of the kV settings, (100, 125, and 140 kV) and the permanent half bowtie filter for seven allowable combinations of tube current (mA) and exposure time (ms). The measurements were performed with the x-ray tube positioned at gantry 12 O'clock, aperture size of 20 $\times$ 20 cm^2 in stationary acquisition, with a calibrated RadCal 10X6-6 ionisation chamber (Radcal Corporation, CA, USA). The chamber was calibrated at an Accredited Secondary Standards Dosimetry Laboratory under reference conditions, using an S60 x-ray beam (nominal energy 60.1 kV). The uncertainty k=2 was 3.3%. Beam qualities were expressed as the HVL (in mm Al), the values of which were measured in section 2.1.2. The measurement setup is illustrated in Figure (2.8), showing the ionisation chamber mounted positioned at isocentre, at least 30 cm above the patient couch to minimise back-scattered radiation. At each kVp setting, seven air kerma measurements were taken by varying the mAs.

2.2.2 Preparation of radiochromic film

To generate calibration curves, the RCF was cut into pieces approximately 2.0×2.0 cm^2 in size. Seven sets of RCF were cut for each beam quality for seven air kerma values per beam quality. Three pieces were prepared for each beam quality, and an extra piece was designated the control film. The RCF pieces were handled according to the recommendations of AAPM TG 235, ensuring that there was minimal contact

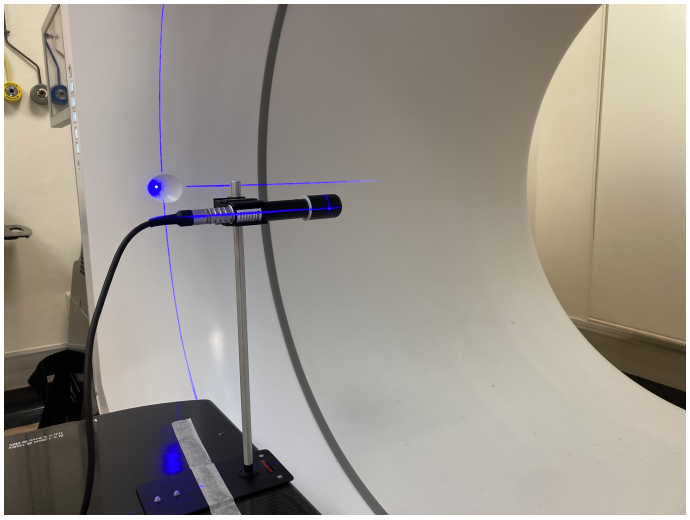

Figure 2.8: A Radcal 10X6-6 ionisation chamber positioned at the Halcyon virtual isocentre. The chamber height above the couchtop is meant to minimise the effect of backscatter on the Air Kerma measurement.

with the surface by using a pair of tweezers.

Each piece was digitised on the Epson scanner in reflection mode prior to x-ray irradiation. The scan image resolution used was 75 dpi (dots per inch) in 48 bit RGB mode (16 bit per channel) and saved in Tagged Image File Format (TIFF). The orientation and positioning of the RCF pieces during scanning were noted and reproduced throughout subsequent scans. A Matlab script was written to split each image into the constituent red, blue and green images, create a 5×5 pixel region of interest in the centre of each red image, extract the average Pixel Value (PV) and its standard deviation (σ), and save them to a text file. The values thus measured prior to irradiatiion in the reference air kerma were labelled with the subscript 'before', i.e., (PV^i_{before} and σ^i_{before}), where the superscript i refers to the $i-$th piece at each reference air kerma ($i = 1, 2, 3$). The PV from the control pieces were labelled PV_{before} and σ_{before}.

2.2.3 Irradiation of radiochromic film

For irradiation, an air-equivalent platform to hold the RCF pieces was constructed from a rectangular cardboard box. Its one end was cut out completely, and a piece of masking tape was run across the centre. During irradiation, the box was erected on its closed end so that the surface of the tape was at 100 cm SSD as illustrated in Figure (2.9). The RCF pieces were placed in the centre. At each beam

quality, the films were irradiated to the reference air kerma determined previously. Three RCF pieces were individually irradiated to each reference air kerma. After at least 24 hours, the films were again digitised and processed as before. This time the average and standard deviation of PV were labelled PV^i_{after} and σ^i_{after}. Those obtained from the control piece were labelled PV_{after} and σ_{after}.

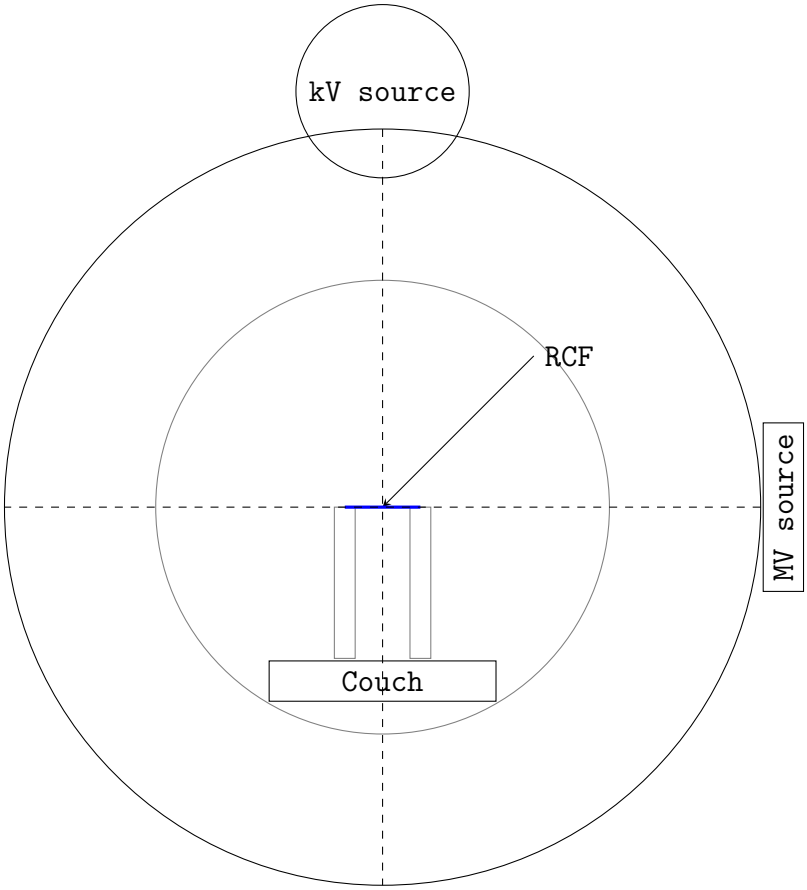

Figure 2.9: Experimental setup for irradiating RCF pieces. The pieces are placed on a platform made from masking tape atop air-equivalent supports made from cardboard. (Image by author.)

2.2.4 Characterisation of radiochromic film response

The reflectance (R) was then calculated as PV/2 [16]. For a film piece, the change in reflectance (ΔR^i) and corresponding standard deviations $\sigma_{\Delta R^i}$ over the region of interest is given in Equation (2.4)

$$\Delta R^i = {R^i}_{before} - {R^i}_{after} = \frac{1}{2^{16}}[{PV^i}_{before} - {PV^i}_{after}] \tag{2.4}$$

The uncertainty in ΔR^i is given by

$$\sigma_{\Delta R^i} = \frac{1}{2^{16}}\sqrt{(\sigma({PV^i}_{before}))^2 + (\sigma({PV^i}_{before}))^2} \tag{2.5}$$

For each air kerma point, the average change in reflectance ($\overline{\Delta R}$) was calculated in equation (2.6) below as a weighted mean.

$$\overline{\Delta R} = \sum_{i=1}^{3} (\omega^i \cdot \Delta R^i) \tag{2.6}$$

The corresponding weights, ω^i are given in equation (2.7).

$$\omega^i = \frac{1/(\sigma_{\Delta R^i})^2}{\sum_{i=1}^{3} \left(\frac{1}{\sigma_{\Delta R^i}}\right)^2} \tag{2.7}$$

Equation (2.8) below gives the standard deviation in $\overline{\Delta R}$.

$$\sigma_{\overline{\Delta R}} = \sqrt{\frac{1}{\sum_{i=1}^{3} \left(\frac{1}{\sigma_{\Delta R^i}}\right)^2}} \tag{2.8}$$

The final, net change in the reflectance ($net\Delta R$), was determined by subtracting the change in refletance of the control (unirradiated)strips from the irradiated strips (equation 2.9).

$$net\Delta R = \overline{\Delta R} - \overline{\Delta R}_{control} \tag{2.9}$$

The corresponding standard deviation of $net\Delta R$ is given in equation 2.10.

$$\sigma_{net\Delta R} = \sqrt{(\sigma_{\overline{\Delta R}})^2 + (\sigma_{\overline{\Delta R}_{control}})^2} \tag{2.10}$$

For each kVp, the air kerma based calibration curve was obtained by plotting measured ar kerma values (K_{air}) as a function of the final net reflectance, equation (2.9). Each calibration curve was fitted with three analytical functions of the forms:

$$(K_{air}^{film})^{air} = a\left(\frac{net\Delta R}{ln(net\Delta R)}\right) \tag{2.11}$$

$$(K_{air}^{film})^{air} = a{\cdot}net\Delta R{\cdot}e^{m{\cdot}net\Delta R} \tag{2.12}$$

$$(K_{air}^{film})^{air} = a{\cdot}net\Delta R + b{\cdot}net\Delta R^{n} \tag{2.13}$$

For each of these analytical models, the uncertainty in predicting an unknown air kerma was calculated using the expression of error propagation given by equation (2.14), while the absolute difference between the measured and model predicted air kerma is expressed by equation (2.15) as a fraction of the measured value.

$$\sigma_y^2 = \Sigma_i \left(\frac{\delta y}{\delta x_i}\right)^2 \cdot \sigma_{x_i}^2 \tag{2.14}$$

$$\Delta K_{air} = \left(\frac{K_{air}^{Exp} - K_{air}^{Mod}}{K_{air}^{Exp}}\right) \cdot 100\% \tag{2.15}$$

σ_y is the total estimated uncertainty for the air kerma determined using the analytical models, while σ_{x_i} $(i = 1, 2, 3)$ are the standard deviations of the $net\Delta R$ and the fitting parameters a, b, m, n. In equation (2.15), K_{air}^{Exp} and K_{air}^{Mod} are the measured and model-predicted air kerma, respectively. Thus, for the analytical forms given above, the expressions of experimental, fit, and total uncertainties are:

Logarithmic function

$$(\sigma_{K_{air}^{film}})^{Exp} = \frac{a\left(\frac{ln(net\Delta R-1)}{(ln(net\Delta R))^2}\right){\cdot}\sigma_{net\Delta R}}{K_{air}^{film}} \cdot 100\% \tag{2.16}$$

$$(\sigma_{K_{air}^{film}})^{Fit} = \frac{\left(\frac{net\Delta R}{ln(net\Delta R)}\right){\cdot}\sigma_a}{K_{air}^{film}} \cdot 100\% \tag{2.17}$$

$$(\sigma_{K_{air}^{film}})^{Tot} = \frac{\sqrt{\left(\frac{ln(net\Delta R-1)}{(ln(net\Delta R))^2}\right)^2{\cdot}\sigma_a^2 + a^2\left(\frac{ln(net\Delta R-1)}{(ln(net\Delta R))^2}\right)^2{\cdot}\sigma_{net\Delta R}^2}}{K_{air}^{film}} \tag{2.18}$$

Exponential function

$$(\sigma_{K_{air}^{film}})^{Exp} = \frac{\sqrt{\Sigma_1}}{K_{air}^{film}} \cdot 100\% \tag{2.19}$$

$$(\sigma_{K_{air}^{film}})^{Fit} = \frac{\sqrt{\Sigma_2}}{K_{air}^{film}} \cdot 100\% \tag{2.20}$$

$$(\sigma_{K_{air}^{film}})^{Tot} = \frac{\sqrt{\Sigma_1 + \Sigma_2}}{K_{air}^{film}} \cdot 100\% \tag{2.21}$$

Where,

$\Sigma_1 = a^2 \cdot (1 + m{\cdot}net\Delta R)^2{\cdot}e^{(2m{\cdot}net\Delta R)} \cdot \sigma^2_{net\Delta R}$

$\Sigma_2 = net\Delta R^2 \cdot \exp^{(2m{\cdot}net\Delta R)} {\cdot}\sigma_a^2 + a^2 \cdot net\Delta R^4 \cdot \exp^{(2m{\cdot}net\Delta R)} {\cdot}\sigma_m^2$

Power function

$$(\sigma_{K_{air}^{film}})^{Exp} = \frac{\sqrt{(a + n{\cdot}b{\cdot}net\Delta R^{n-1})^2{\cdot}\sigma^2_{net\Delta R}}}{K_{air}^{film}} \cdot 100\% \tag{2.22}$$

$$(\sigma_{K_{air}^{film}})^{Fit} = \frac{\sqrt{net\Delta R^2{\cdot}\sigma_a^2 + net\Delta R^{2{\cdot}n}{\cdot}\sigma_b^2}}{K_{air}^{film}} \cdot 100\% \tag{2.23}$$

$$(\sigma_{K_{air}^{film}})^{Tot} = \frac{\sqrt{net\Delta R^2{\cdot}\sigma_a^2 + net\Delta R^{2{\cdot}n}{\cdot}\sigma_b^2 + (a + n{\cdot}b{\cdot}net\Delta R^{n-1})^2{\cdot}\sigma^2_{net\Delta R}}}{K_{air}^{film}} \cdot 100\% \tag{2.24}$$

The analytical model with the lowest total uncertainty and absolute difference was selected for the calibration curves.

2.2.5 In-phantom dose profile measurements

$(K_{air}^{film})^{air}$ is the air kerma free in air as obtained from film dosimetry. For diagnostic photon energies, the dose to water (D_w) is equal to the air kerma in water (K_w). It is related to the air kerma measured by the film inside a phantom, $(K_{air}^{film})^{w}$ by equation (2.25) [66].

$$D_w = K_w = (K_{air}^{film})^{w} \cdot \left(\frac{\mu_{en}}{\rho}\right)_{air}^{w} \tag{2.25}$$

$(K_{air}^{film})^{w} \approx (K_{air}^{film})^{air}$ within 1%, and is derived from the net reflectance-to-air kerma calibration curve.

The body doses to the Alderson Rando anthropomorphic phantom (Radiology Support Devices, Long Beach, CA, USA) arising from the following kV CBCT acquisition protocols were measured: Breast, Pelvis, Pelvis Large, Pelvis Large Fast, Thorax and Thorax Fast. These imaging protocols are used for nearly all routine Halcyon kV CBCT imaging at Groote Schuur Hospital and use either 125 kV or 140 kV energy. For measurement of dose from the pelvis protocols, 2.4×30 cm^2 wide strips of film covered in Clingwrap® were sandwiched between slabs 6 and 7 of the pelvis phantom, horizontally along the second line of drill holes as shown in Figure (2.10). For the Breast and Thorax protocols, the strips were likewise sandwiched between slabs 6 and 7 of the thorax phantom.

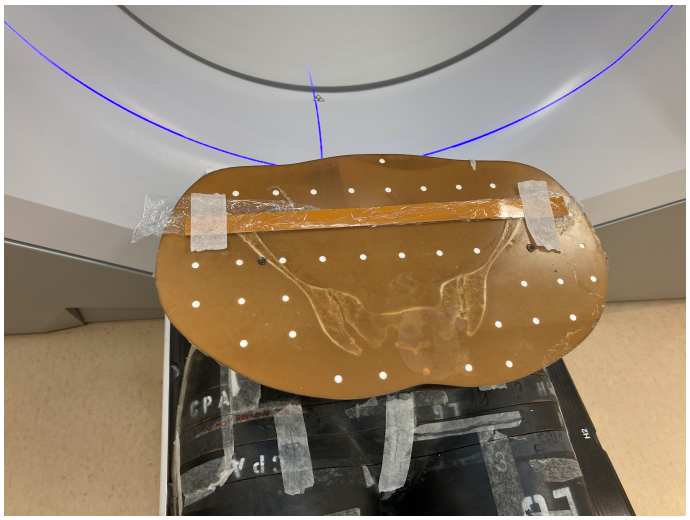

Figure 2.10: Phantom placement of a long film strip to measure the dose distribution horizontally.

The irradiated strips were scanned after 24 hours using the same scan parameters as for calibration.

ImageJ was used to split the TIFF images into Red, Blue and Green components and to draw line profiles through the centre of the red images in the long axis. PV vs spatial location were extracted. PVs were converted to dose to water using optical density calibration curves and Equation (2.25), in which the air-water mean mass absorption ratios were 1.0475 and 1.0507 for 125 kV and 140 kV, respectively. A Matlab script was written to resample the dose - location data every 5mm, apply a Savitzky-Golay filter to remove noise, and plot a dose distribution. The filter parameters - Window Length and Polynomial Order were set to values of 5 and 2, respectively.

2.3 Monte Carlo model of the X-ray source

GATE (GEANT4 Application for Tomographic Emmission) is a software toolkit, i.e., a collection of Object Oriented Programming classes written in C++ for monte carlo simulation based on the well-validated GEANT4 platform. GATE was developed for simulations in PET, SPECT, CT, optical imaging (Bioluminescence and Fluorescence) as well as radiotherapy dose calculation.

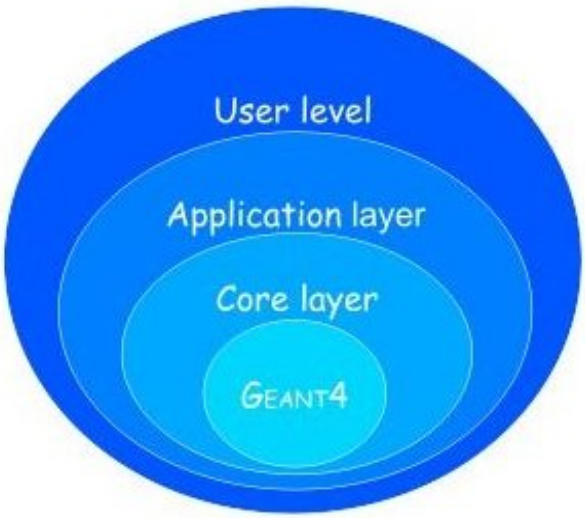

Figure 2.11: The architecture of GATE Monte Carlo toolkit. [34]

Figure (2.11) above illustrates GATE's architecture, showing that the toolkit is built around a GEANT4 kernel. The core layer consists of mechanisms for managing time, geometry, and radioactive sources, while the application layer modifies and extends basic GEANT4 for specific applications. These three inner layers comprise the so-called developer level, which the typical user does not usually need to access. The user level is where most operators build and interact with simulations by means of text commands created by combinations of predefined keywords arranged in a specific syntax. In practice, building and running a simulation involves writing ordered sequences of commands into a text file known as a macro. For a given application, the user completely defines the components of the simulation by means of a single macro or, for more complex applications, several macro files each defining a unique component of the simulation. In the latter case, a single Main macro file containing references to the individual macros would the input to GATE. A typical simulation in GATE requires definitions of geometry, physics processes, radiation sources,

data output, acquisition, verbosity and visualisation.

2.3.1 Geometry

Geometry definition specifies the shape and material composition of all the physical components that interact with radiation and therefore influence the final quantity under investigation, i.e., dose, fluence, image, etc. Physical components that play no significant role in radiation transport are omitted from the geometry to save on computational speed and memory. In the case of the Halcyon kV CBCT simulation, the collimator blades, half bowtie filter, phantom and patient volumes will comprise the geometry. As a rule, all such physical volumes must be daughter volumes of the World volume, which sets the experimental framework of the simulation [34].

The materials' chemical elements and compounds must be specified in a database file that is referenced in the geometry definition.

Material database

/gate/geometry/setMaterialDatabase data/GateMaterials.db

All the chemical elements and compounds from which the simulation's physical components are fabricated are specified in a materials database file, identified by a .db suffix. As an example, the element Hydrogen is specified in the database as:

Hydrogen: S= H ; Z= 1. ; A= 1.01 g/mole

S, Z, and A are the chemical symbol, proton number and mass number, respectively.

The entry for the liquid form of the compound Water appears in the database as:

Water: d=1.00 g/cm3; n=2 ; state=liquid

+el: name=Hydrogen ; n=2

+el: name=Oxygen; n=1

In this entry, d is the mass density in grams per cubic centimeters, the n immediately after is the number of

elements in the compound, $state$ is the physical material state, $= el$: denotes an element, and subsequent n the number of atoms of that element in a molecule. Mixtures may also be defined, with the specification of Polymethylmethacrelate (PMMA) provided as a case in point. f represents an element's mass fraction.

PMMA: d=1.195 g/cm3; n=3 ; state=Solid

+el: name=Hydrogen ; f=0.080541

+el: name=Carbon ; f=0.599846

+el: name=Oxygen; f=0.319613

In the GATE simulation of the Halcyon kV beamline, the geometry definition comprises the following volumes:

1. World
2. Gantry
3. Source capsule
4. Upper collimators
5. Lower collimators
6. Half bowtie filter
7. Water phantom
8. Rando phantom
9. ICRU 110 Adult Female computational phantom

World

The World volume is mandatory for GATE simulations and contains all of its components. It is a cuboid filled with Air by default, and is the only volume that is defined without explicitly specifying its shape:

one only needs to specify the dimensions and visibility. The World volume's centre also defines the origin of a cartesian coordinate system in which the Z- axis is along the superio-inferior direction, the X- axis in the left-right direction, and the Y- axis in the anterio-posterior direction as shown in Figure (2.12). In this simulation, it has sides of length 300 cm.

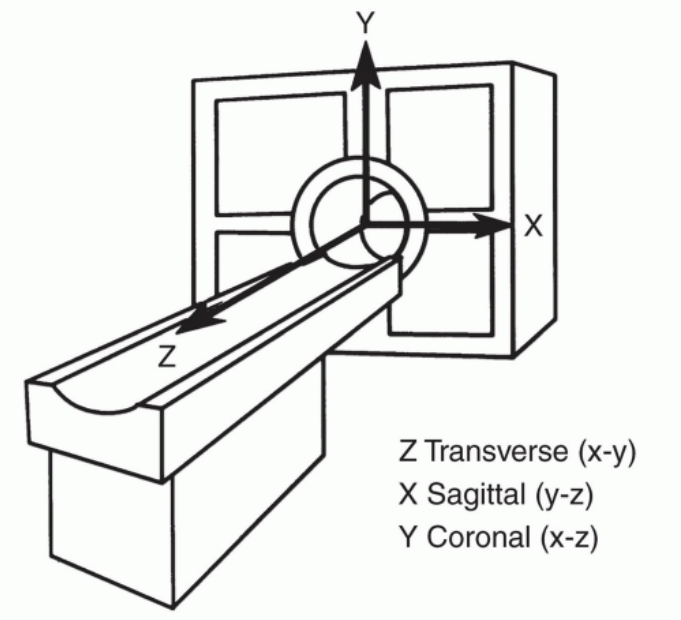

Figure 2.12: GATE corrdinate system [60].

Gantry

The gantry is a daughter volume of $World$. It's a cuboid filled with Air. The x, y, z dimensions are 2.60 m $\times$ 2.63 m $\times$ 2.82 m, respectively, representing the actual dimensions of the Halcyon gantry [65]. It has been assigned the colour white and is visualised as a wireframe as opposed to a solid.

Collimator box and Source capsule

The Collimator box is a daughter volume of the $Gantry$, has size 40 cm $\times$ 30 cm $\times$ 34 cm, and houses the x-ray source, collimator blades, and half bowtie filter. Its centre is translated 85 cm from the $Gantry$ origin along the y-axis. The source capsule houses the source. It is a cylindrical volume of length 10 mm and radius 5 mm, and made from Air. Its centre is positioned at 15 cm from the $xraybox$ centre along the y-axis, and 100 cm away from the $Gantry$ isocentre. It is rotated 270^o about its x-axis so that the

source emits radiation along the y-axis towards the gantry isocentre.

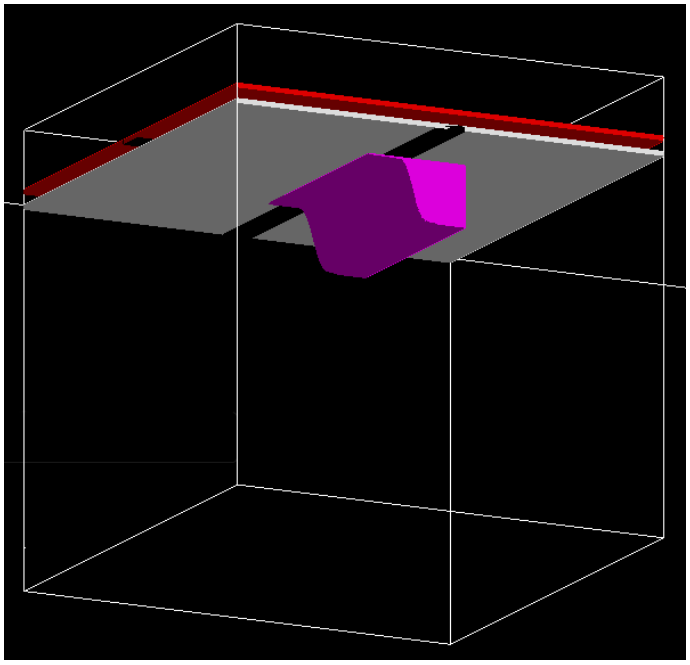

Figure 2.13: OpenGL visualisation of the collimator box (in white wireframe), half bowtie filter (magenta), and the lower and upper collimator blades (gray and red), respectively.

Source

The nominal kV CBCT energies, 100, 125, and 140 kV were each characterised by a discrete spectrum obtained from output measurements and SPEKTR 3.0 software, as described earlier in this thesis. The spectra are saved in individual text files, designated as $UserSpectrum$ in the source definition. Each polychromatic source is of the type General Particle Source (gps), emitting particles of the type $gamma$, where the relative contributions of particle energies are derived from the user spectrum file. It has the shape of a square plane of size 0.8 mm, whose centre is positioned at the centre of the volume $capsule$. The photon fluence is emitted isotropically at an emission angle of 14^o and azimuthal angle of 360^o.

Upper collimator blades

The upper collimator blades are two independent blades that displace in the positive (+ve) and negative (-ve) Z-directions, and define the field size in the inferio-superior direction. They are rectangular in shape with dimensions of 30 cm in X, 10 cm in Z, and 3 mm in Y. Both blades are made of lead and positioned

in a plane perpendicular to the Y-axis at a distance of 5.91 cm from the centre of the $xraybox$ mother volume. The +ve and -ve blades are displaced 5 cm and -5 cm, respectively, such that their edges abutt along the X-axis to define the zero collimator opening. Further displacement of either blade defines an open field in the Z-direction.

Lower collimator blades

The lower collimator blades are two independent blades that displace in the positive (+ve) and negative (-ve) X-directions, and define the field size in the lateral left-right direction. They are rectangular in shape with dimensions of 10 cm in X, and 30 cm in Z. The (+ve) lower blade is 1 mm thick and made from stainless steel (SS304), while the (-ve) blade is 3 mm thick and made from uranium. Both blades are positioned in a plane perpendicular to the Y-axis at a distance of 4.31 cm from the centre of the $xraybox$ mother volume. The +ve and -ve blades are displaced 5 cm and -5 cm, respectively, such that their edges abutt along the Z-axis to define the zero collimator opening. Further displacement of either blade defines an open field in the X-direction.

Half bow-tie filter

The half bowtie filter $(hbtf)$ is a tessellated volume created using the CAD software FreeCAD and saved in the stereolithography format (.stl). Its bounding box has x, y, z dimensions of 100.00 mm, 40.82 mm, and 90.00 mm, respectively. It is translated in the x, and z axes by -0.2mm and 45mm, respectively. The distance from the source to the proximal surface is 14.79cm. In the vertical orientation, the curved side is downstream of the source, while in the lateral orientation it is on the +ve X-axis. The filter is made of aluminium.

Mother Water phantom

The mother water phantom $(motherPhantom)$ is a water cuboid with x, y, and z dimensions of 60 cm, 40 cm, and 60 cm, respectively. It is a daughter volume of $Gantry$ and is centred at the isocentre. For

static acquisitions, the phantom is displaced -20 cm along the Y- axis so that the SSD is 100 cm.

Water phantom

The water phantom $(waterPhantom)$ is a daughter volume of $(motherPhantom)$ and is used for scoring the PDD and Crossline dose profiles, both normalised to 1.00 at maximum dose. It is a cuboid with y, and z dimensions of 40 cm and 40 cm, respectively. Its length in x is varied depending on the beam energy, so that the number of voxels in the x-axis is always equal to the number of ionisation chamber sampling points. In the present simulations, the x lengths for the 100 kV, 125 kV, and 140 kV energies were 32.8 cm, 31.2 cm, and 32.4 cm, respectively. A visualisation generated using DAWN and illustrating the components of the geometry are shown in Figure (2.14).

Water phantom output For each energy, the PDD and Crossline dose profiles are extracted from the $waterPhantom$ by means of dose actors named $depthdose$ and $doseprofile$. Both actors are attached to the $waterPhantom$, with the step hit type set to "Random". The resolution of the $depthdose$ actor in x, y, z is 1, 101, 1 voxels, respectively, where the value in the y-axis corresponds to the number of ionisation chamber sampling points in the depth direction. Each PDD is saved as a text file named "depth-pat.txt". The $doseprofile$ actor is positioned at a depth of 2 cm, with resolution in x, y, z of 164, 1, 1 voxels, 156, 1, 1 voxels, and 162, 1, 1 voxels for the 100kV, 125kV, and 140kV energies, respectively, corresponding to the number of ionisation chamber sampling points in the x-axis. Each crossline dose profile is saved as a text file name "profile-pat.txt".

RANDO phantom

kV CBCT images of RANDO pelvis and thorax phantoms were acquired on the Halcyon and saved as DICOM. The pelvis was imaged with protocols that used 125 kV and 140 kV beam energies, while the thorax was imaged with 125 kV protocols only. These are the protocols that were used for in-phantom exposure of the RCF. Using the software 3D Slicer [72], the DICOM sets were converted to Metaimage (mhd + raw), in which the pixel Hounsfield Units (HU) were saved in floating point. The metaimage

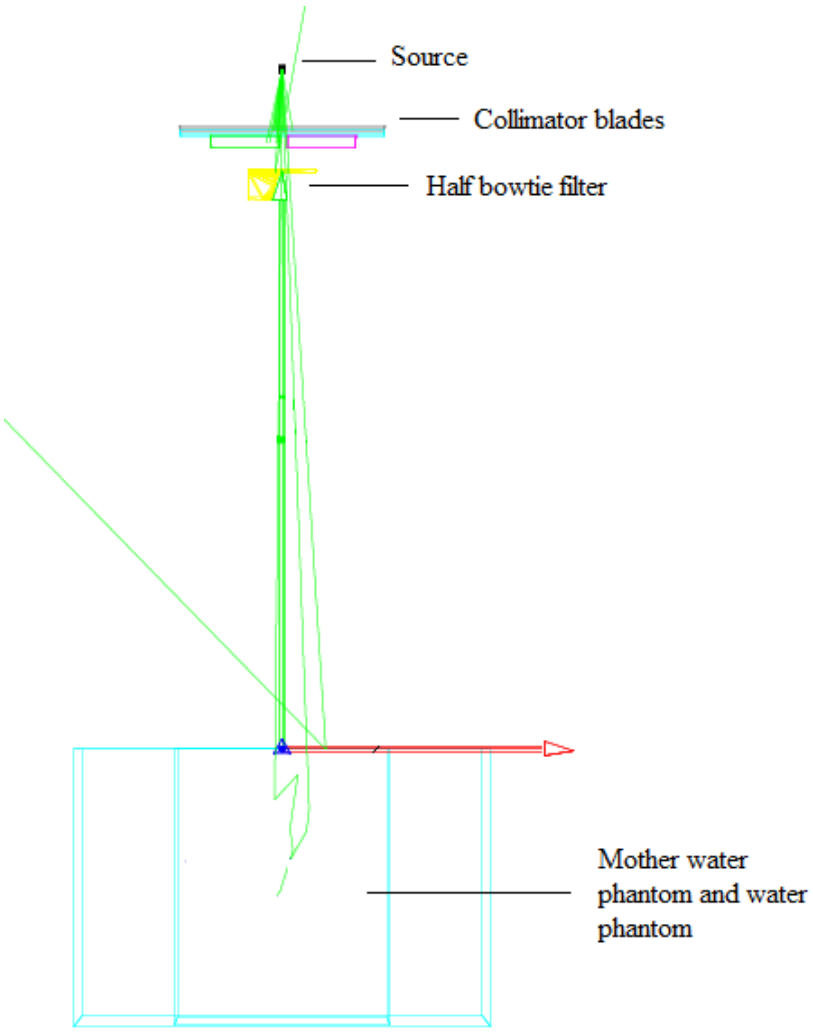

Figure 2.14: A DAWN visualisation of the source capsule, collimator blades, half bowtie filter, and water phantom in the simulation geometry.

datasets were imported to the simulation as "Nested Parameterised Volumes" for calculating the 3D dose distributions. Density and materials tables devised by Schneider et. al [34] were used to convert HU in the images to densities and materials that the Monte Carlo dose calculation engine required to compute the dose distributions. The macros "rando_pelvis.mac, rando_pelvis_fast.mac, rando_pelvis_large.mac, rando_pelvis_large_fast.mac, rando_thorax.mac, rando_thorax_fast.mac, rando_breast.mac" implement the importation of the Metaimage files, creation of the volumes, and conversion of HU to density and material.

FOV

To contain each imported RANDO volume, parent boxes named FOV (Field of View) were created. The x, y, z dimensions were equal to the x, y, z dimensions of the metaimage bounding boxes, which are 491.404 mm x 491.404 mm x 123.564 mm for the pelvis images, and 491.404 mm x 491.404 mm x 129.543 mm for the thorax images.

RANDO phantom output For each simulated CBCT imaging of the RANDO phantom, the 3D map of the dose-to-water is extracted via the Track Length Estimator Dose Actor $(TLEDoseActor)$ named $dose3D$, attached to the $rando\_volumes$, with a resolution equal to that of the image. The RANDO pelvis image sets have a resolution of 512 x 512 x 63 voxels, while the RANDO thorax image sets have a resolution of 512 x 512 x 66 voxels. The 3D dose distribution is computed using the $MassWeighting$ algorithm, and saved as a metaimage (mhd + raw) file for each simulation.

ICRP 110 Adult Female computational phantom

The ICRP 110 Adult Female (AF) computational phantom is a voxelised reference phantom of the average adult female, with an x, y, z resolution of 299 x 137 x 348 voxels. [31]. The phantom is anatomically realistic as it is generated from CT scans of a real patient subject of height 162 cm and weight 63 kg, physical characteristics which best resemble the RANDO adult phantom (height 163 cm, weight 60 kg [51]). A 3D rendering of the computational phantom is shown in Figure (2.15). The individual organs are presegmented and labelled, making it very convenient for use in radiation dose calculations. In addition, the phantom is delivered with data files to convert the segments to materials. The version used for the simulations was converted from ASCII format to labelled Metaimage, whose origin is at the midpoint of the hip joints. It is imported into the geometry as a $NestedParametrisedvolume$ named $icrp\_phantom$, and contained in a FOV volume whose x, y, z dimensions are 528.95 mm x 241.40 mm x 1679.48 mm, equal to the dimensions of the phantom's bounding box. The phantom is displaced along the Z- axis by -40 cm to the sternal notch for imaging the thorax, and by -73 cm to the centre of the Nasal and Maxillary

bones for imaging the head.

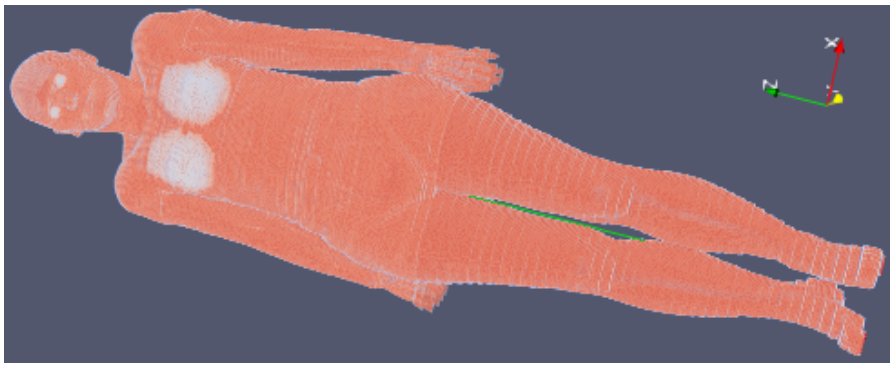

Figure 2.15: A 3D volumetric rendering of the ICRP AF computational phantom generated in ParaView from a Metaimage file.

ICRP 110 AF phantom output For each simulated CBCT imaging of the ICRP 110 AF phantom, the 3D map of the dose-to-water is extracted via the Dose Actor named $dose3D$, attached to the $icrp\_phantom$, with a resolution equal to that of the image. The $doseByRegions$ dose actor computes the absorbed dose in each segmented region and saves the result as a tab separated text file in which the region labels and the dosimetric quantities are arranged in columns. For the current study's purpose, the absorbed dose to the organs in Table (2.2) was determined.

2.3.2 Physics processes

The Physics processes define the mechanisms with which radiation interacts with the material media in the simulation. In these simulations, the $emstandard\_opt3$ process was used. It encompasses the Photoelectric Effect, Compton Scattering, Electron Ionisation, and Bremsstrahlung mechanisms which are the most relevant in the diagnostic photon energy range.

2.3.3 Simulating dynamic acquisitions

To simulate dynamic CBCT acquisitions, GATE's $TimeSlice$ mechanism was used to divide simulations into discrete time intervals. All CBCT protocols on the Halcyon use the full 360^o rotation of the x-ray tube, differing only in the number of projections and mAs. In the simulation, each protocol's $TimeSlice$

Table 2.2: ICRP organs and tissues of interest to the current study with their corresponding labels.

Pelvis		Thorax	
ID Label	Organ/tissue name	ID Label	Organ/tissue name
10	Blood vessels, trunk	7	Trachea
28	Femora, upper half, cortical	8	Bronchi
29	Femora, upper half, spongiosa	10	Blood vessels, trunk
30	Femora, upper half, medullary cavity	24	Clavicles, cortical
41	Pelvis, cortical	25	Clavicles, spongiosa
42	Pelvis, spongiosa	43	Ribs, cortical
51	Lumbar spine, cortical	44	Ribs, spongiosa
52	Lumbar spine, spongiosa	49	Thoracic spine, cortical
53	Sacrum, cortical	50	Thoracic spine, spongiosa
54	Sacrum, spongiosa	55	Sternum, cortical
86	Rectal	56	Sternum, spongiosa
123	Skin, trunk	62	Breast, left, adipose tissue
135	Left ureter	63	Breast, left, glandular tissue
136	Right ureter	64	Breast, right, adipose tissue
137	Urinary bladder wall	65	Breast, right, glandular tissue
139	Uterus/cervix	87	Heart wall
		89	Kidney, left, cortex
		90	Kidney, left, medulla
		92	Kidney, right, cortex
		93	Kidney, right, medulla

was fixed at 1 s, $TimeStart$ was 0, and $TimeStop$ was numerically equivalent to the total number of projections. The x-ray tube was orbited about the Z-axis at an angular speed obtained from dividing 360^o by the $TimeStop$.

Visualisation

Visualisation generates 3D rendering and videos of the simulation's geometry and particle trajectories. GATE uses several graphics systems for this purpose; for the current work, OpenGL (OGL) and DAWN were used.

Initialisation

The command $initialize$ prompts GATE to calculate the interaction cross section tables for the Physics processes defined. In the current work, $initialize$ is paired with the command specifying random number generator. Three such engines available in GATE: Ranlux64, James Random, and Mersenne Twister [34].

Starting the simulation

The simulation is started by first specifying the number of particles histories to be simulated with $setTotalNumberOfPrimaries$, and then invoking the $start$ command. A larger number of histories translates to lower uncertainty in the quantity under investigation, at the cost of computational speed. In this study, the simulations were run ona Geant4/GATE v9.3 Docker container hosted on Microsoft Azure. The Virtual Machine ran Ubuntu Linux 22.04.03 ("Jammy Jellyfish") using 2 virtual CPUs (64 Bit architecture) and 8 GB RAM. 8x10^8 particles histories were simulated for a typical run time of 12.5 Hours per simulation.

2.3.4 Analysis of output

Measurement to simulation normalisation factor

A normalisation factor (NF) is necessary to relate the results of dose measurement with RCF to the 3D dose map generated by GATE. For this purpose, the simulated 3D dose maps from the RANDO pelvis image set (imaged at 125kV) and RANDO pelvis large fast set (imaged at 140kV) were imported into 3D Slicer. The dose maps were registered to the corresponding original RANDO image sets, and line profiles drawn across the same locations where RCF strips had been placed to extract 1D dose distributions (Figure 2.16).

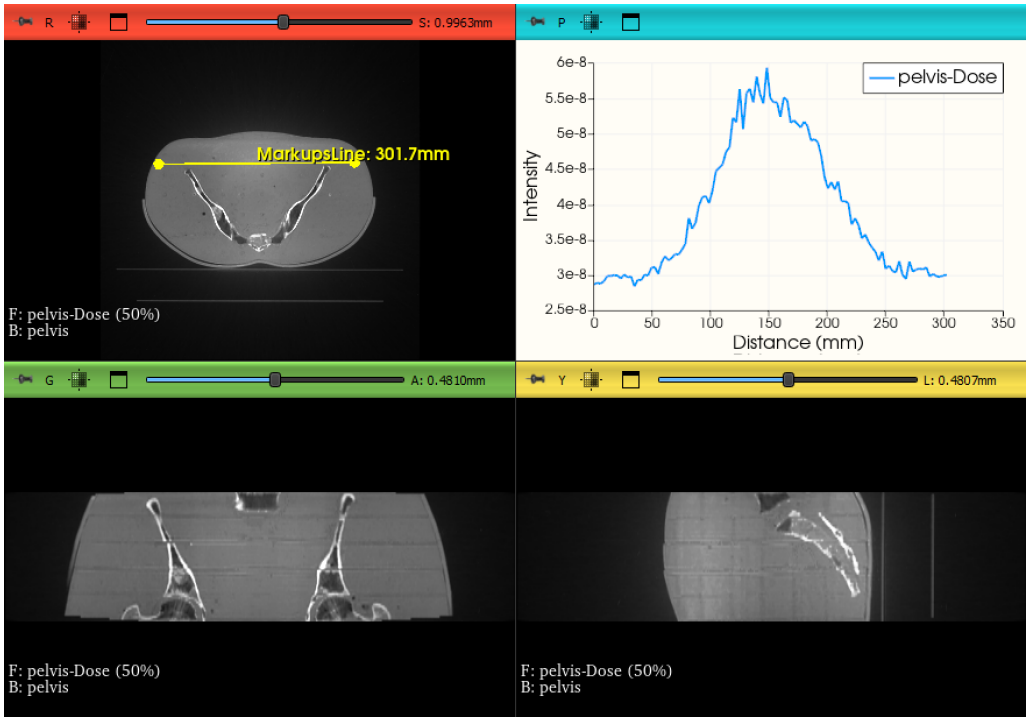

Figure 2.16: Extraction of line profiles from 3D dose maps co-registered to the input RANDO image set.

These were then resampled to match the sampling resolution of RCF measured dose distributions. At each sampled point, the relationship between the simulated (SD) and RCF measured dose (MD) was established using equation (2.26).

$$NF = \frac{MD(Dose(mGy)/mAs)}{SD(Dose(mGy)/photon_history)} \tag{2.26}$$

The number of particle histories was 8x10^8 in all simulations, while the mAs values were obtained from specifications of the imaging protocols obtained. Since it has been established that the RCF response is not significantly dependent of photon energy, it was expected that the NFs would not differ significantly. The average of the two NFs was obtained and used for the dose conversions in the output of the ICRP 110 AF phantom simulations. For each body region, i.e., pelvis, thorax, and head, the imaging protocol having the highest exposure technique factors was used in the estimation of imaging doses.

2.3.5 Conclusion

Since the precise source and filtration characteristics of the Halcyon kV CBCT system could not be obtained from the manufacturer, equivalent models were derived using semi-empirical methods were generated and used to create geometries for modeling in GATE. One dimensional dose distributions were determined from exposing strips of calibrated RCF film using breast, thorax, and pelvic imaging protocols, and a calibration factor relating the GATE output to the measured dose was established. The organ doses calculated by GATE in an ICRP 110 computational phantom were then derived.

Chapter 3

Results and discussion

The results of the dose measurements and simulations are presented in this section.

3.1 Equivalent spectra

Table (3.1) shows the measured HVLs, tube output normalised to the mAs and the calculated ripple for all the three x-ray beam qualities on Halcyon's kV beamline. These parameter values were the initial input to the SPEKTR software program to generate the spectra.

Table 3.1: Halcyon kV beamline HVL1, HVL2, and output

Tube potential (kV)	**HVL1 (mm Al)**	**HVL2 (mm Al)**	**Output (mGy/mAs)**	**Ripple (%)**
100	4.1	11.1	0.044	3.6
125	8.6	19.8	0.069	5.0
140	9.1	20.8	0.093	6.0

Figures (3.1, 3.2, 3.3) show the the three spectra corresponding to the 100, 125, and 140 kV beams generated by the SPEKTR program, with mean energies 56.78 keV, 69.75 keV, and 69.95 keV respectively.

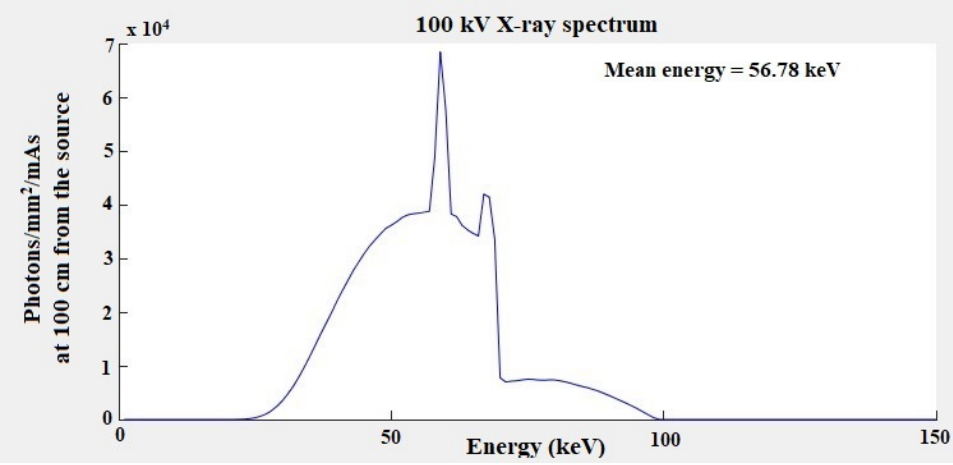

Figure 3.1: SPEKTR-derived energy spectra of the 100 kV beam used on Halcyon for kV CBCT imaging. The mean energy in each case is indicated in the top right corner.

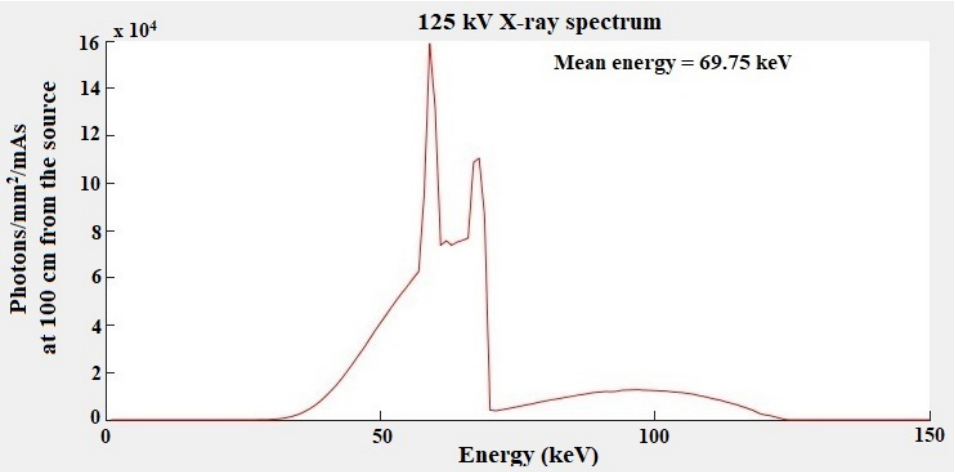

Figure 3.2: SPEKTR-derived energy spectra of the 125 kV beam used on Halcyon for kV CBCT imaging.

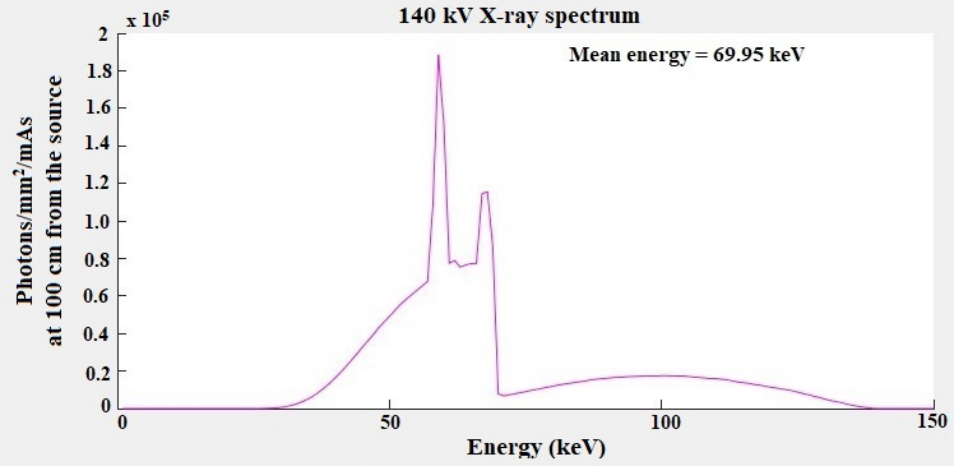

Figure 3.3: SPEKTR-derived energy spectra of the 140 kV beam used on Halcyon for kV CBCT imaging.

3.2 Bowtie filter

Figure (3.4) illustrates the bowtie filter profile derived from ionisation chamber measurements and analytical calculations using Equations (2.2) and (2.3). The 3-dimensional bowtie model created in FreeCAD with dimensions of $100mm \times 90mm \times 40mm$ and is rendered in Figure (3.5). The model was saved as a stereolithography (STL) file, imported into the Monte Carlo simulation and assigned material of pure Aluminium.

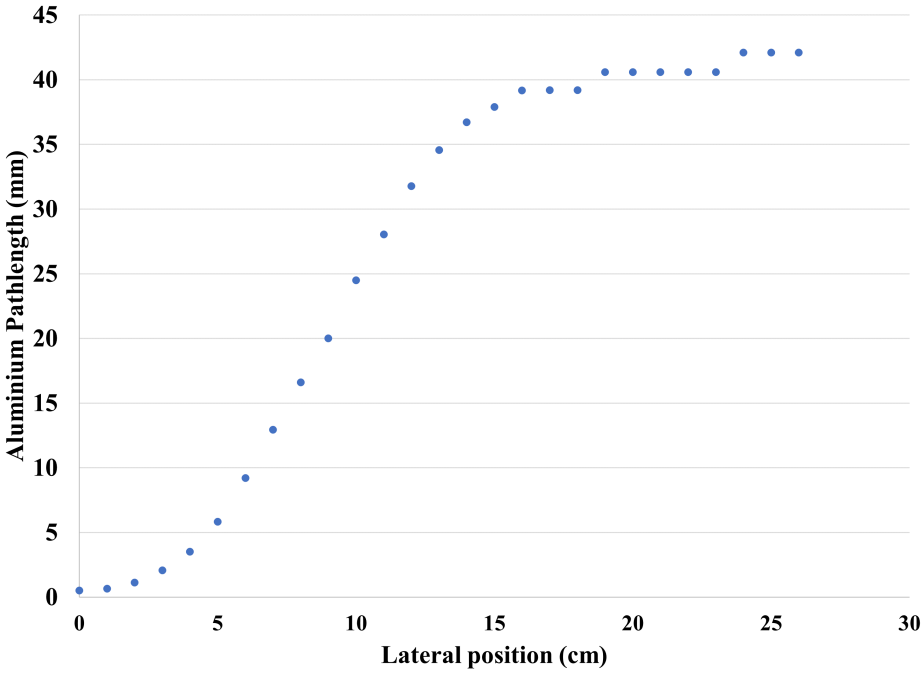

Figure 3.4: Profile of the curved portion of the bowtie filter in the Halcyon kV beamline. It was obatined from ionisation chamber measurements and analytical calculations.

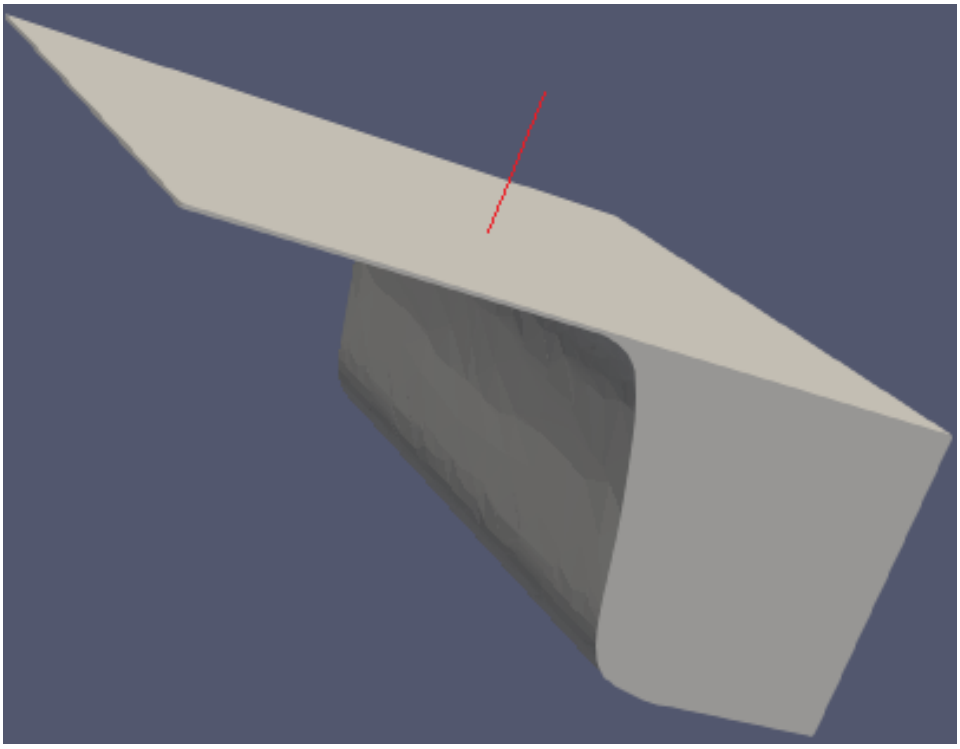

Figure 3.5: A 3 Dimensional rendering of the bowtie filter in the Halcyon kV beamline created in FreeCAD.

3.3 Percentage Depth Dose and off-axis profiles

Figure (3.6) shows the percentage depth dose curves measured in a water phantom for the x-ray beam energies of 100kV, 125 kV, and 140 kV. All the measurements were normalised to 100% at each beam's maximum dose.

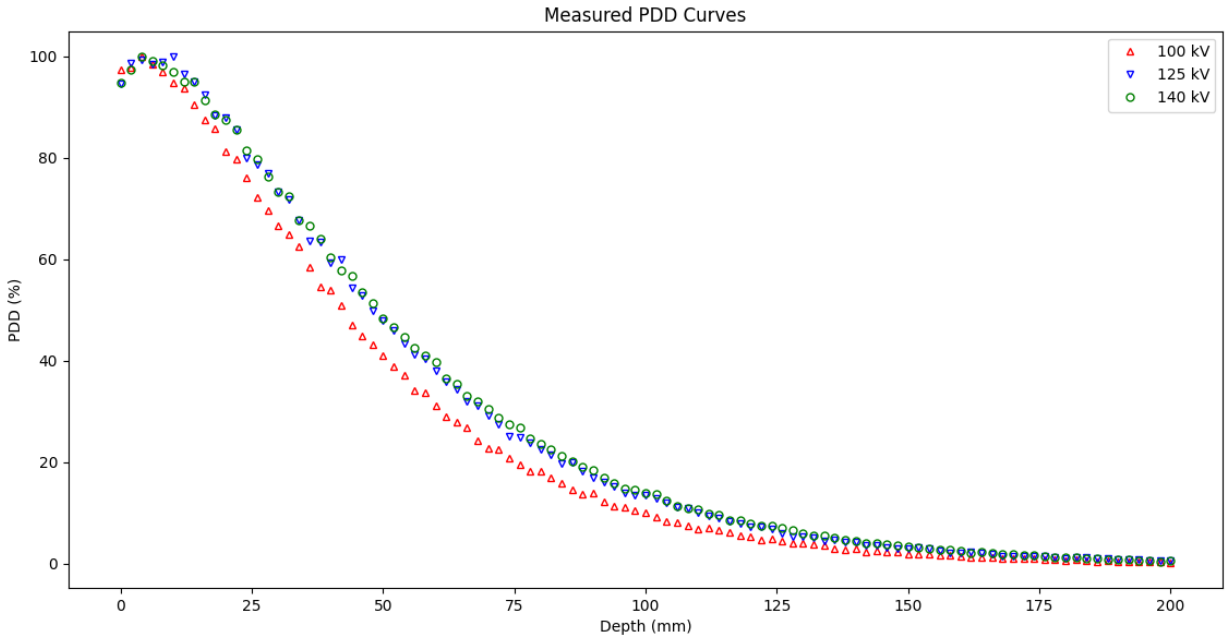

Figure 3.6: Percentage depth dose curves measured in water at 100 cm Source Surface Distance for 100 kV, 125 kV, and 140 kV. The curves were normalised to 100% at the maximum dose.

All the PDD curves have an identical depth of dose maximum close to the surface at around 4 mm. However, the PDDs at depth 10 cm are 9.99%, 13.44%, and 13.99% for the 100 kV, 125 kV, and 140 kV respectively, as the degree of penetration increases with beam energy. The kV potential difference to accelerate electrons from the tube cathode to anode is produced by a high frequency generator which attempts to rectify an input alternating current kV source to a constant potential. Due to inherent inefficiencies the generator design, there may be incomplete rectification of the input variable potential which manifests as ripples in the tube potential as measured in Table 3.1 and present in Figure 3.6. The PDD curves demonstrate shallow build up regions characteristic of kV beams in generally, and whose magnitude is proportional to the collimator field size. Smaller field sizes present less material in which secondary electrons may be scattered laterally therefore reducing the depth of dose buildup. The converse

is true for larger collimator sizes.

Figures (3.7) illustrate the crossline dose profiles also measured in a water phantom for the beam energies 100 kV, 125 kV, and 140 kV. As with the PDD curves, the crossline curves are normalised to 100% at the maximum dose.

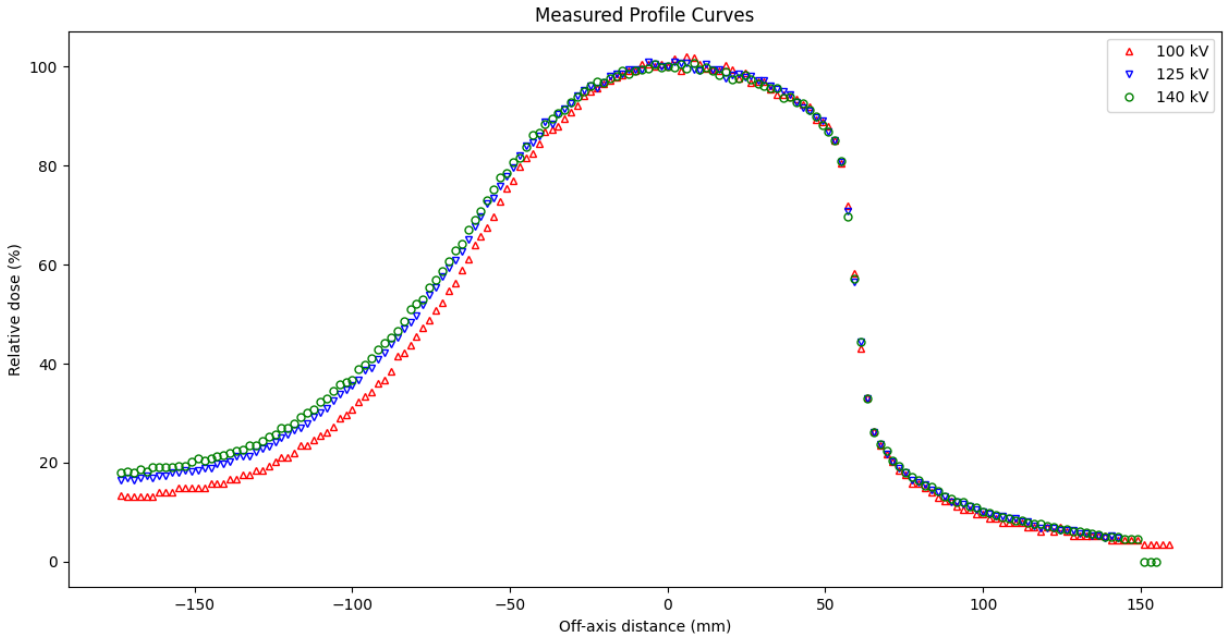

Figure 3.7: Crossline dose profiles for 100, 125, and 140 kV beams. The curves are normalised to 100% at the maximum dose.

These profiles display the lopsided, asymmetrical shape characteristic of a half bowtie filter. In the case of the Halcyon, the filter is permanently in the kV beamline and may not be retracted as is common with the more conventional kV CBCT systems on C-arm linear accelerators.

3.4 Reference air kerma

The measured reference air kerma in air $(K_{air})^{air}$ for each beam quality and the mAs values used are shown in tables (3.2) to (3.4).

Table 3.2: Exposure parameters and reference air kerma measured on the Haclyon kV beamline at 100 kV.

mA	**ms**	**mAs**	**Air Kerma (mGy)**
160	6000	960	36.99
160	5000	800	30.87
160	4000	640	24.71
160	3000	480	18.54
160	2000	320	12.36
160	1000	160	6.18
160	800	128	4.94

Table 3.3: Exposure parameters and reference air kerma measured on the Haclyon kV beamline at 125 kV.

mA	**ms**	**mAs**	**Air Kerma (mGy)**
160	6000	960	65.95
160	5000	800	55.01
160	4000	640	43.97
160	3000	480	32.93
160	2000	320	21.95
160	1000	160	10.98
160	800	128	8.78

Table 3.4: Exposure parameters and reference air kerma measured on the Haclyon kV beamline at 140 kV.

mA	ms	mAs	Air Kerma (mGy)
100	6000	600	86.21
100	5000	500	71.83
100	4000	400	57.38
100	3000	300	43.06
100	2000	200	28.71
100	1000	100	14.36
100	800	80	11.49

3.5 Radiochromic film response

Table 3.5 shows the values and corresponding uncertainties of the fitting parameters used in the analytical models. By utilising the error propagation - Equation (2.5), the total uncertainty associated with fitting analytical functions to film response data may be decomposed into fit and experimental uncertainties. Fit uncertainties arise purely from the mathematical method used to generate the fitting function, e.g., Least Squares Regression, Maximum Likelihood Regression, etc, while experimental uncertainties are caused by the measurement of netΔR which is in turn affected by reproducibility of the measurement, uncertainties in x-ray tube calibration, temporal and thermal mismatch of the film pieces, differences in mean response from one film piece to another, etc [67]. In this study, relative fitting uncertainties were well moderated across the three analytical models tested. The largest contributor to the total uncertainty stems from experimental components, chief of which is possibly temporal mismatches in film pieces owing to the absence of reliable image registration facilities in the film processing software used. More expensive commercial software solutions equipped with robust image registration capabilities could have mitigated the experimental and, consequently total uncertainties thereby improving the dosimetric accuracy. Since

uncertainties were determined for each data point for in the analytical fit models, it was more economical to illustrate them on figures as opposed to listing them in tabular form. In this regard, the fitting uncertainties are expressed as percentages of the absolute value of the fit parameters, majority of which are small compared to the total uncertainties. As such, their magnitude may not be obvious on the figures.

Table 3.5: Values of the fitting parameters and associated uncertainties for the Exponential, Logarithmic, and Power analytical functions.

	Exponential $(y = axe^{mx})$	**Logarithmic** $(y = ax/lnx)$	**Power function** $(y = ax + bx^n)$
100 kV	a = 187.58 ± 18.42 m = 6.81 ± 6.81	a = -830.73 ± 16.36	a = 180.38 ± 90.72 b = 2980.98 ± 5024 n = 2.20 ± 0.92
125 kV	a = 285.86 ± 13.76 m = 3.26 ± 0.39	a = -890.71 ± 12.89	a = 262.18 ± 71.93 b = 1282.77 ± 972.1 n = 1.99 ± 0.57
140 kV	a = 269.26 ± 10.05 m = 3.34 ± 0.24	a = -847.17 ± 10.12	a = 308.05 ± 22.66 b = 3773.23 ± 2204 n = 2.76 ± 0.40

Figures (3.8) to (3.33) are plots of the measured film response and the analytical models, i.e. netΔR vs $(K_{air})^{air}$ as well as the relative uncertainties and absolute errors for the three beam qualities and three fitting functions. Of the three analytical functions, the exponential models yielded the lowest total uncertainties for the majority of data points and were hence used for the air kerma calibration curves.

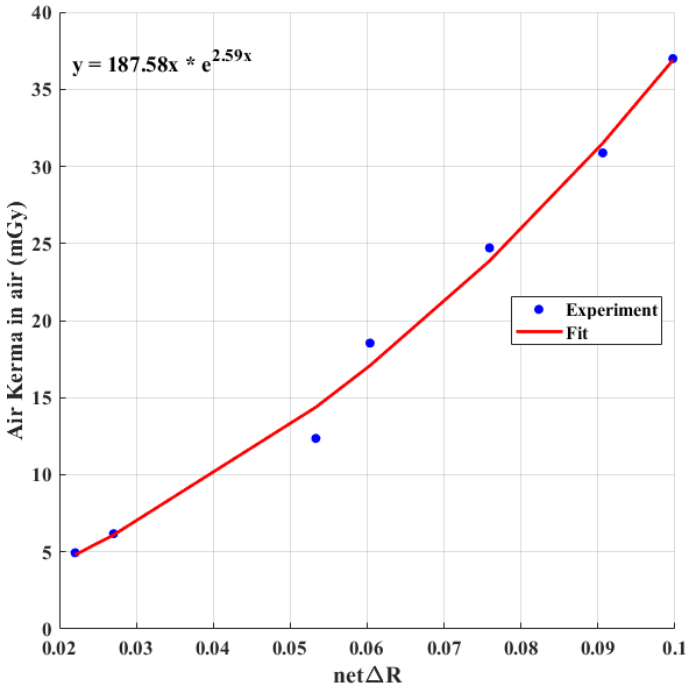

Figure 3.8: An exponential analytical function fit to RCF net reflectance - reference air kerma at 100 kV.

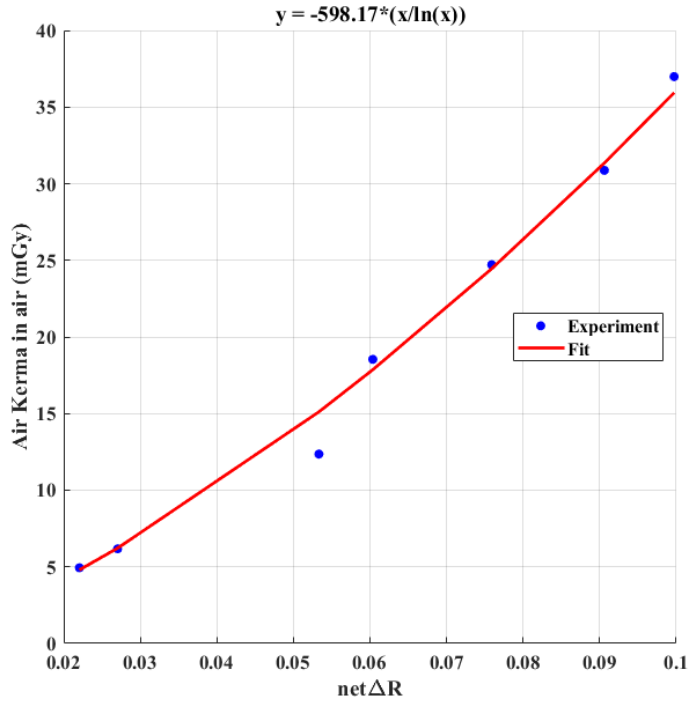

Figure 3.9: A logarithmic analytical function fit to RCF net reflectance - reference air kerma at 100 kV.

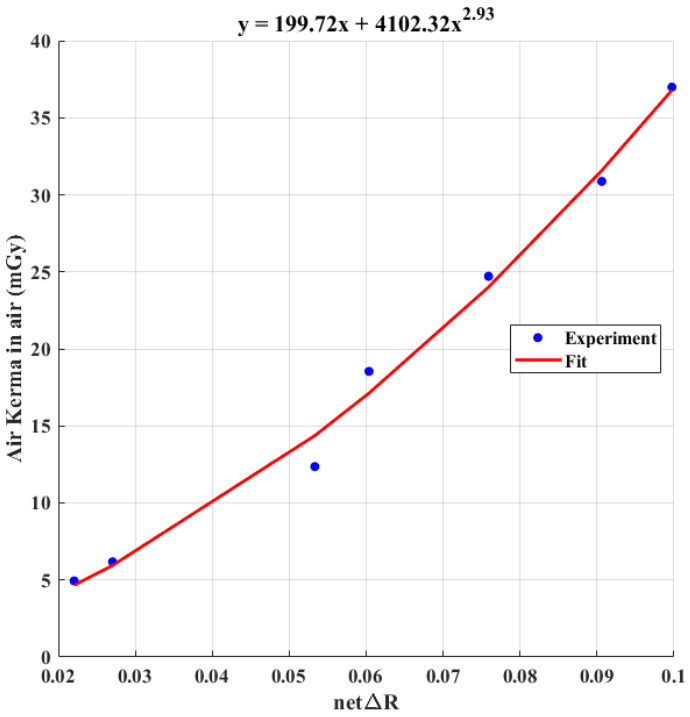

Figure 3.10: A power analytical function fit to RCF net reflectance - reference air kerma at 100 kV.

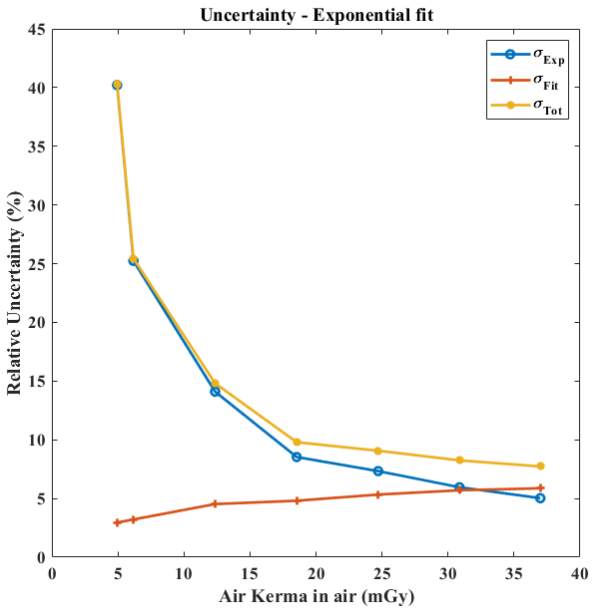

Figure 3.11: Uncertainty analysis of the exponential analytical model fit at 100kV.

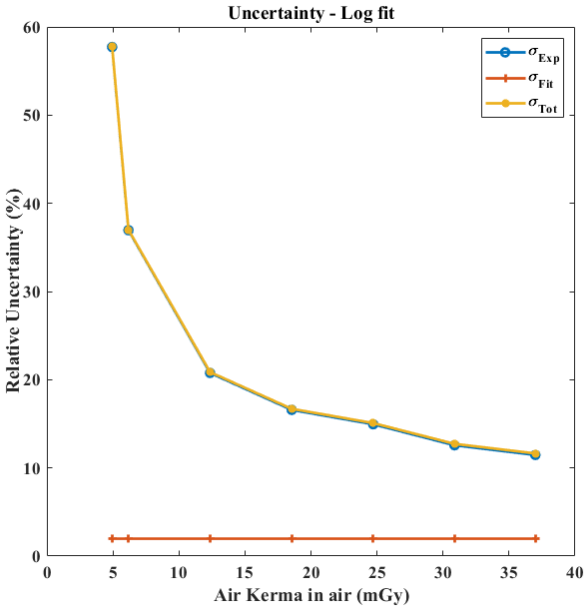

Figure 3.12: Uncertainty analysis of the logarithmic analytical model fit at 100kV.

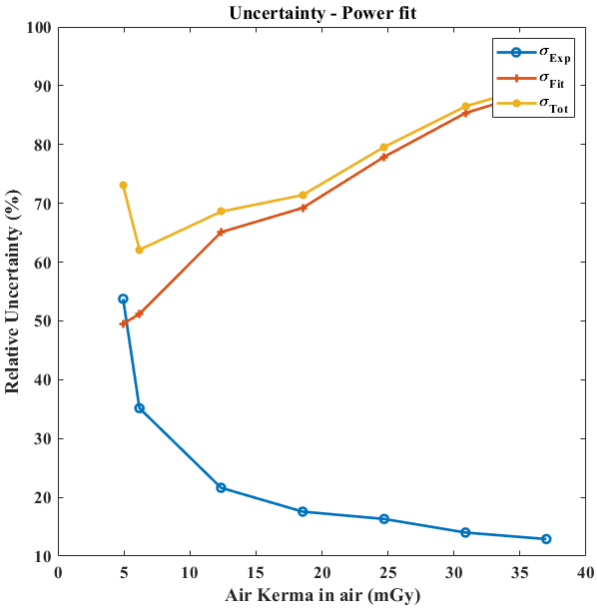

Figure 3.13: Uncertainty analysis of the power analytical model fit at 100kV.

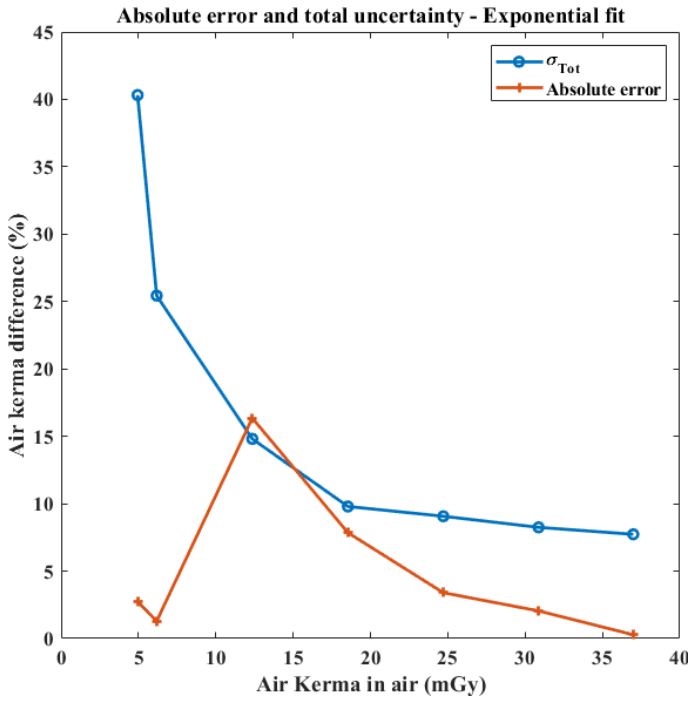

Figure 3.14: (%) difference between measured and exponential fit derived air kerma at 100 kV.

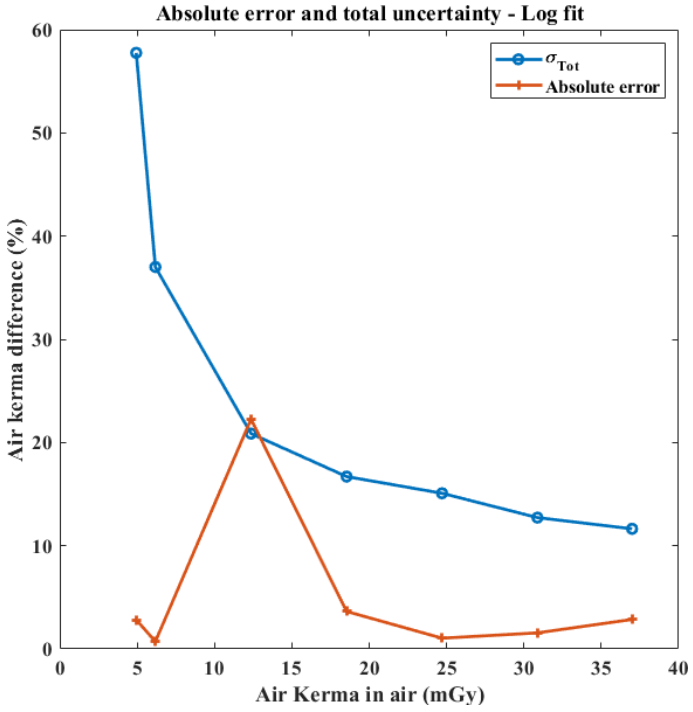

Figure 3.15: (%) difference between measured and logarithmic fit derived air kerma at 100 kV.

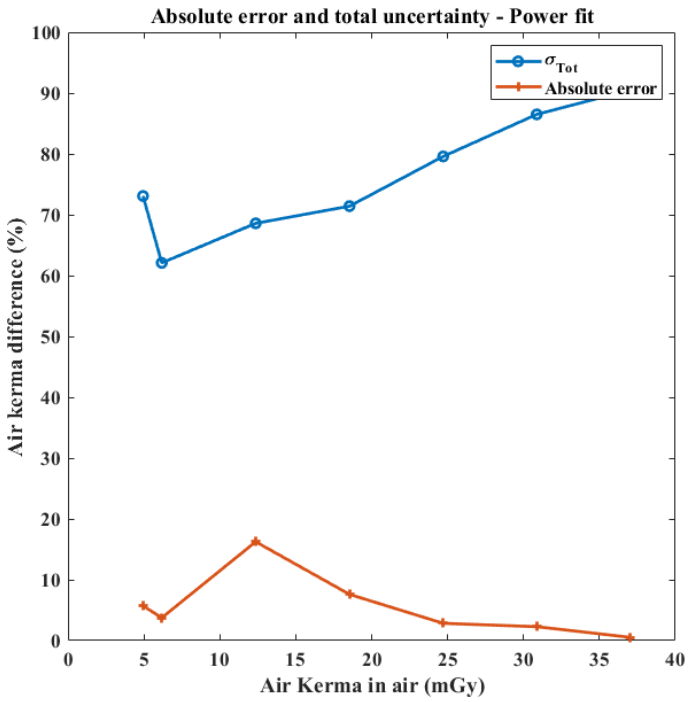

Figure 3.16: (%) difference between measured and power fit derived air kerma at 100 kV.

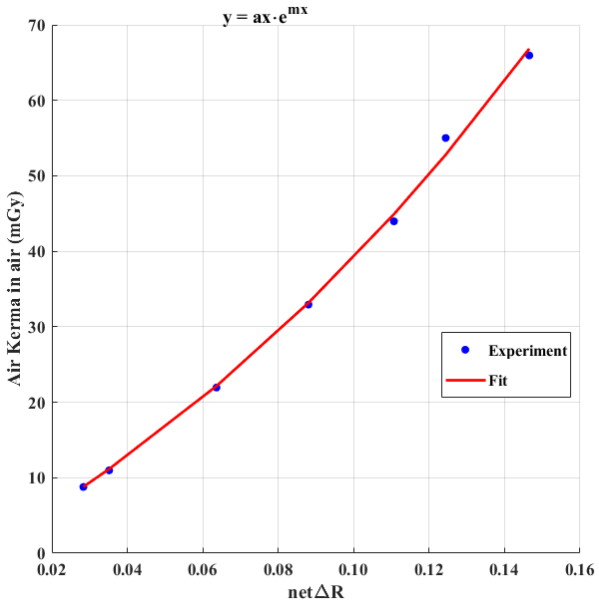

Figure 3.17: An exponential analytical function fit to RCF net reflectance - reference air kerma at 125kV.

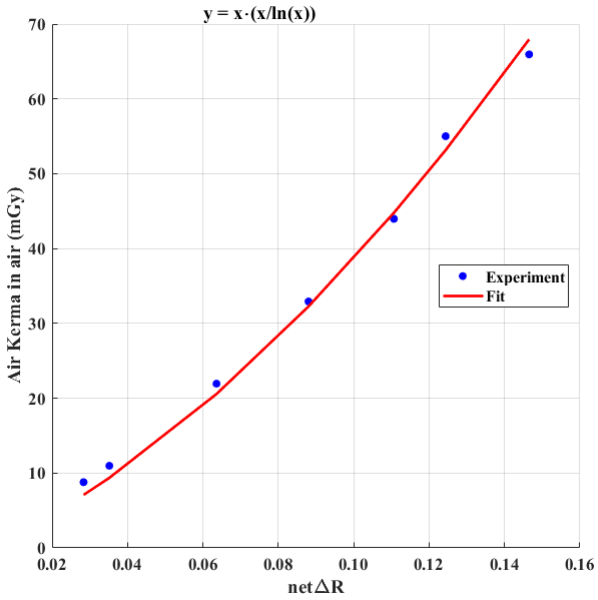

Figure 3.18: A logarithmic analytical function fit to RCF net reflectance - reference air kerma at 125 kV.

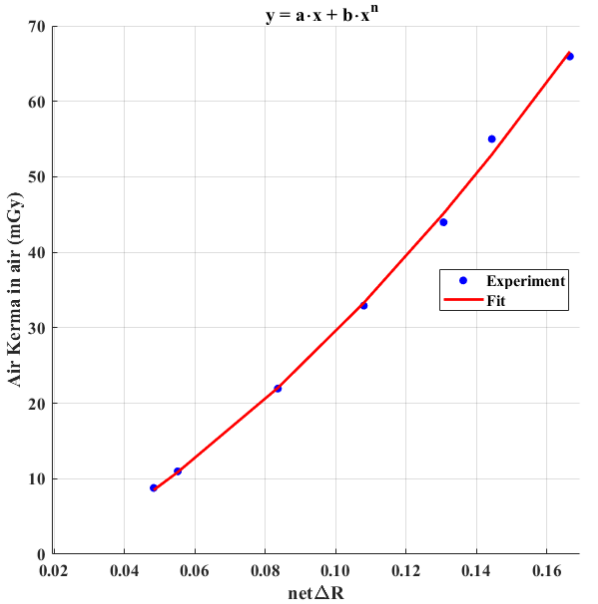

Figure 3.19: A power analytical function fit to RCF net reflectance - reference air kerma at 125 kV.

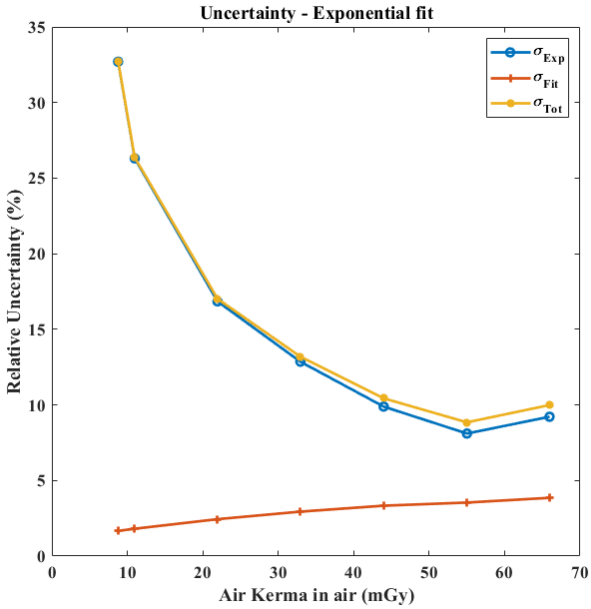

Figure 3.20: Uncertainty analysis of the exponential analytical model fit at 125 kV.

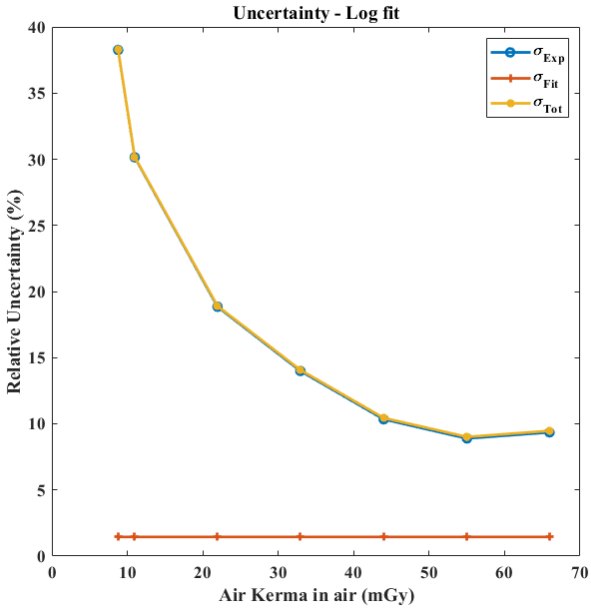

Figure 3.21: Uncertainty analysis of the logarithmic analytical model fit at 125 kV.

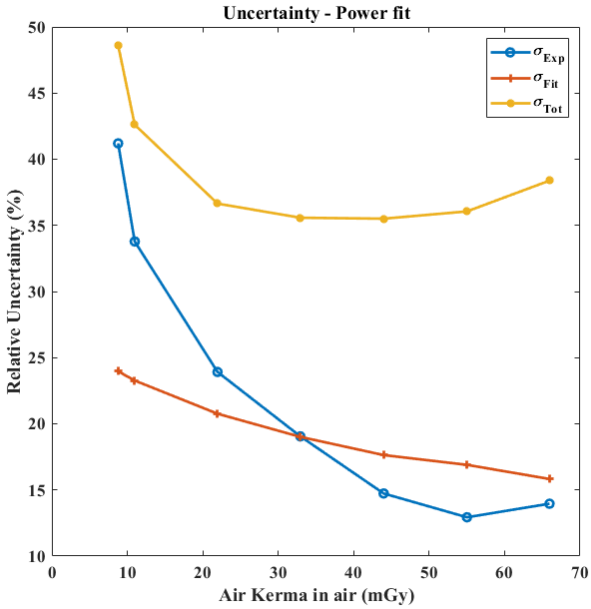

Figure 3.22: Uncertainty analysis of the power analytical model fit at 125 kV.

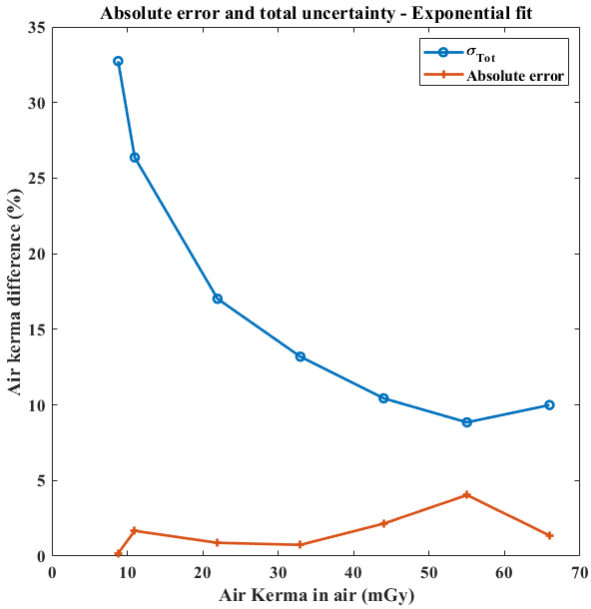

Figure 3.23: (%) difference between measured and exponential fit derived air kerma at 125 kV.

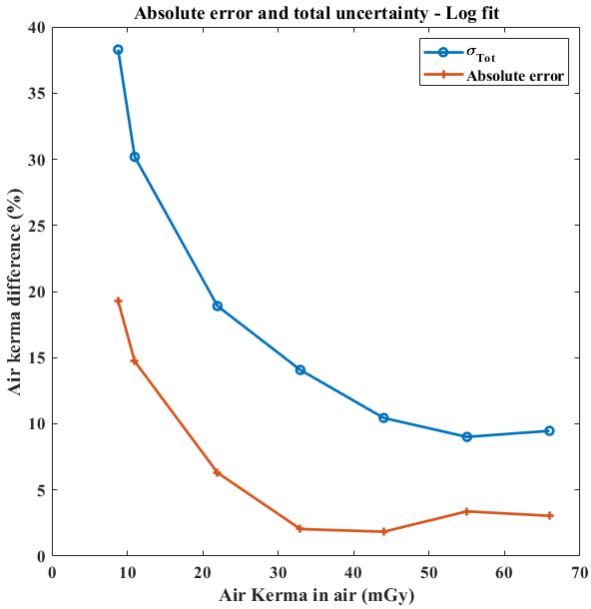

Figure 3.24: (%) difference between measured and logarithmic fit derived air kerma at 125 kV.

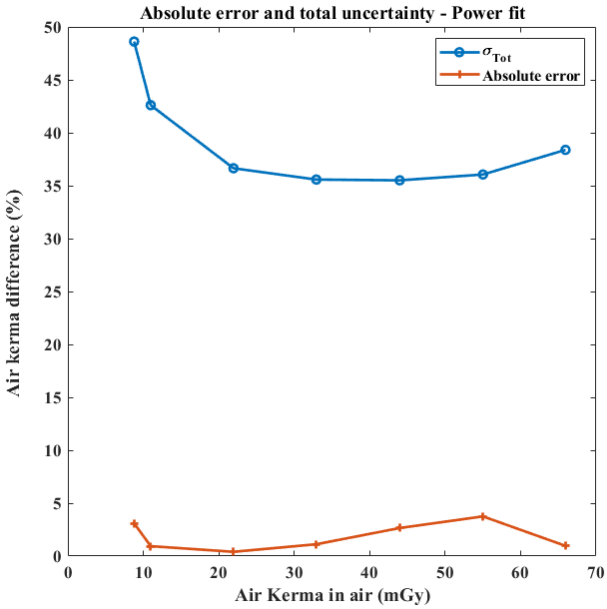

Figure 3.25: (%) difference between measured and power fit derived air kerma at 125 kV.

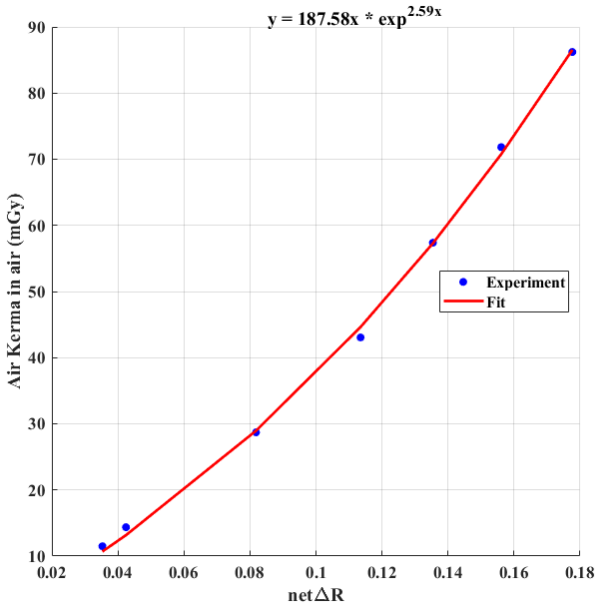

Figure 3.26: 140 kV exponential fit

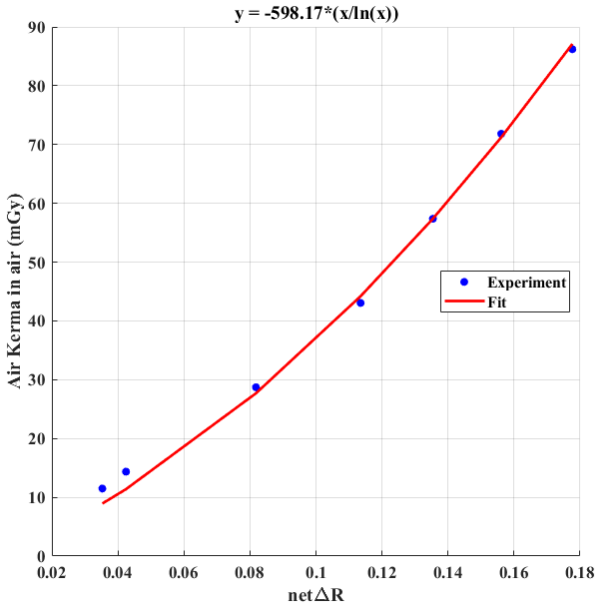

Figure 3.27: 140 kV logarithmic fit

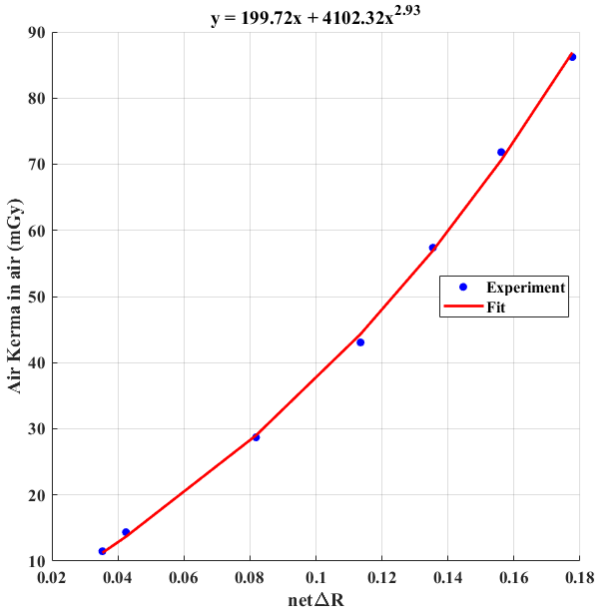

Figure 3.28: 140 kV power fit

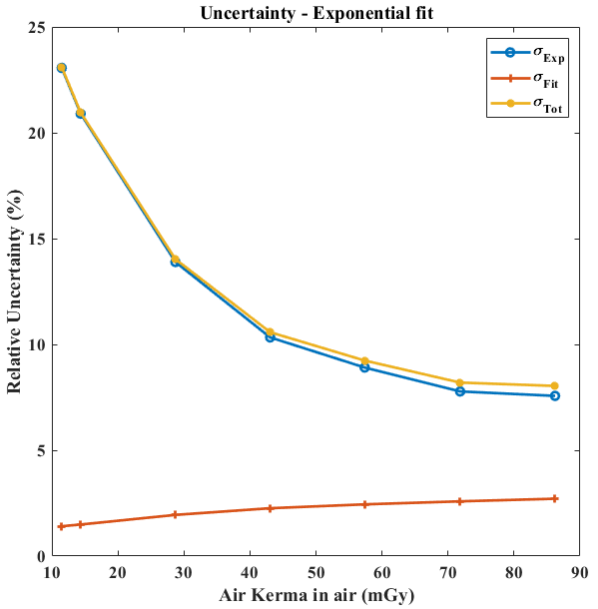

Figure 3.29: Uncertainty analysis of the exponential analytical model fit at 140 kV.

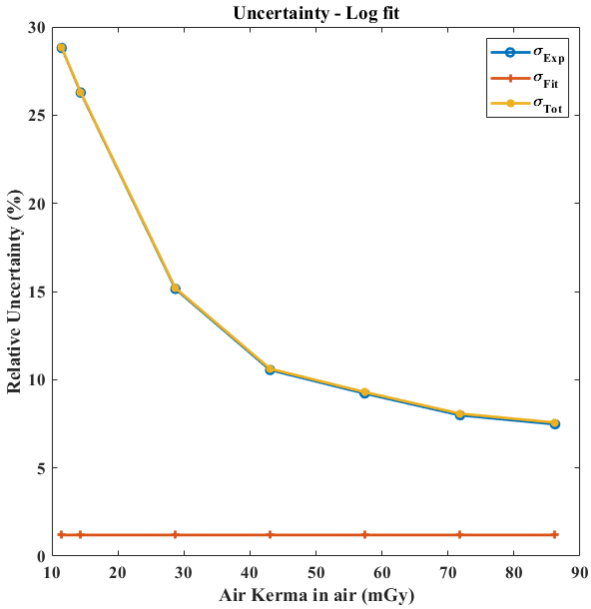

Figure 3.30: Uncertainty analysis of the logarithmic analytical model fit at 140 kV.

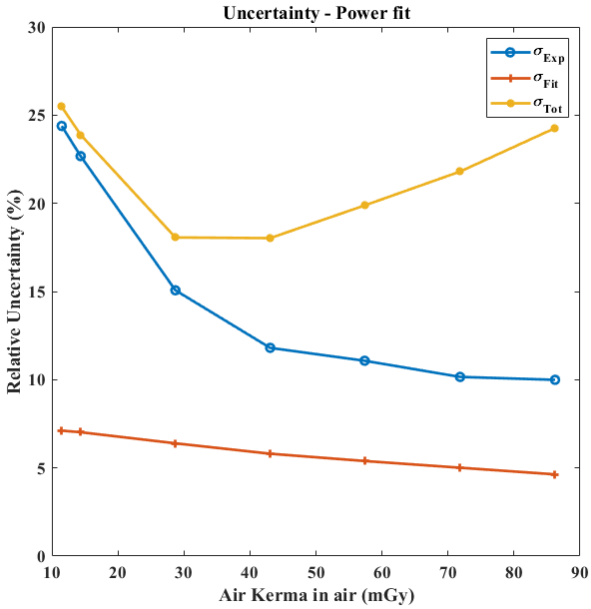

Figure 3.31: Uncertainty analysis of the power analytical model fit at 140 kV.

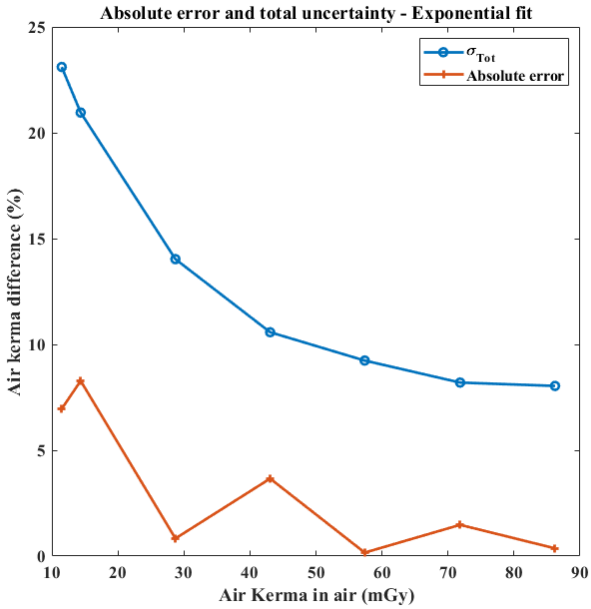

Figure 3.32: (%) difference between measured and exponential fit derived air kerma at 140 kV.

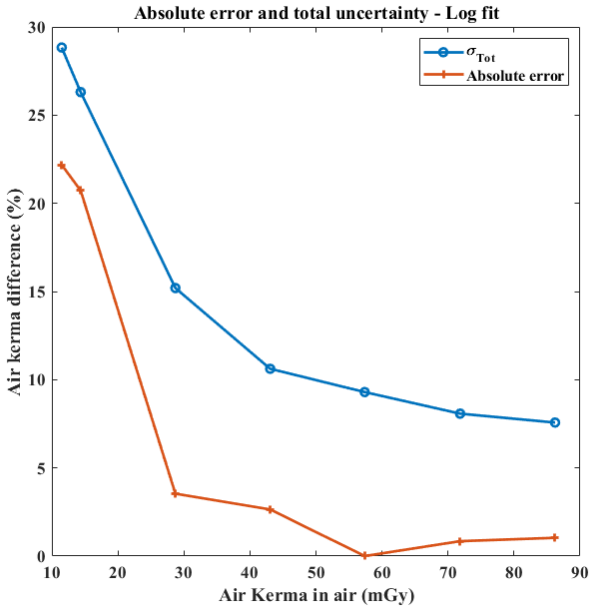

Figure 3.33: (%) difference between measured and logarithmic fit derived air kerma at 140 kV.

3.6 In-phantom dose profile measurements

Figures (3.34) to (3.38) are plots of dose-to-water vs spatial location as measured in-phantom using 30 cm long strips of Gafchromic LD-V1 RCF film. The films were scanned at a spatial resolution of 75 dpi but downsampled to 5mm per dot for better visualisation. Table (3.6) summarises the maximum doses from the six kV CBCT body protocols investigated with RCF. The Thorax Fast, Thorax, and Pelvis protocols use a kVp of 125 kV and default mAs of 295, 301, and 1074, respectively, while Pelvis Large Fast and Pelvis Large use a kVp of 140 kV and default mAs of 698 and 1456, respectively. The effect of these technique factors on the dose distributions is apparent: the Thorax protocol has the lowest mAs as well as the distribution with the lowest and lowest maximum dose. The maximum dose was higher in those dose distributions from protocols with higher mAs values (Figures 3.38, 3.36, 3.37). Collectively, the Thorax protocols have lower maximum doses due to the higher proportion of soft lung tissue in the thoracic area.

Table 3.6: Maximum dose-to-water measured in-phantom from Halcyon kV CBCT body imaging protocols.

Protocol	Breast	Pelvis	Thorax	Thorax Fast	Pelvis Large	Pelvis Large Fast
Max dose (mGy)	3.6	67.2	23.3	23.7	113.5	56.3

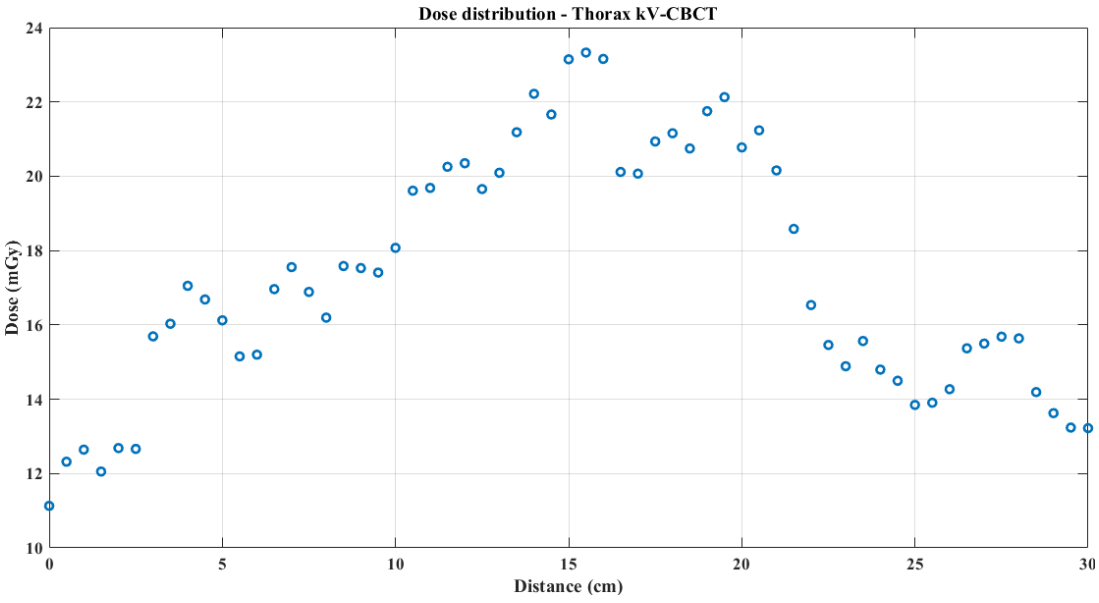

Figure 3.34: Dose distribution from Halcyon Thorax kV CBCT protocol.

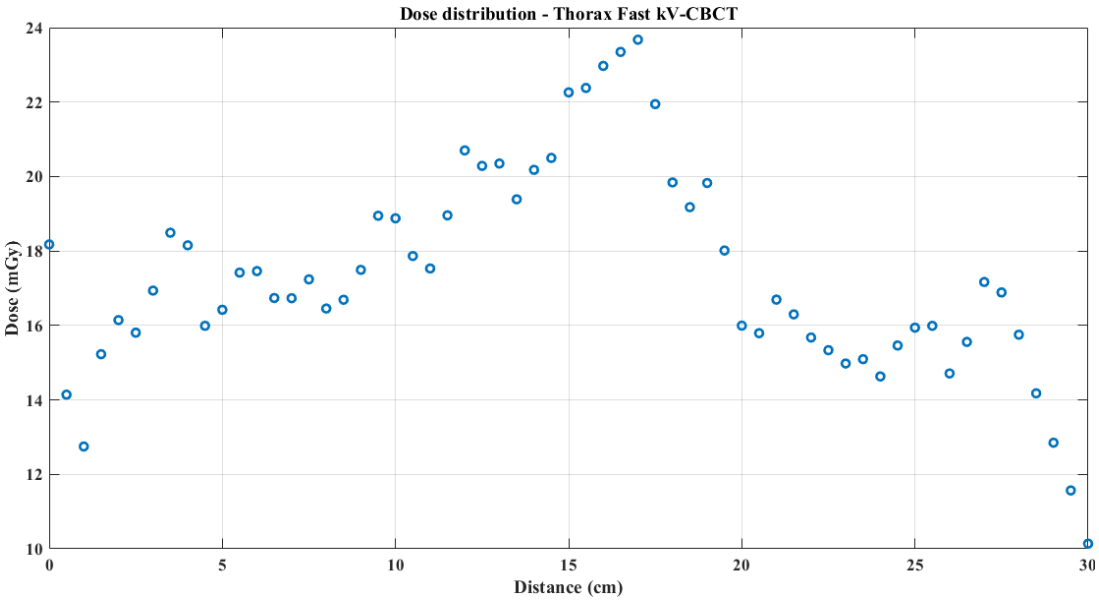

Figure 3.35: Dose distribution from Halcyon Thorax Fast kV CBCT protocol.

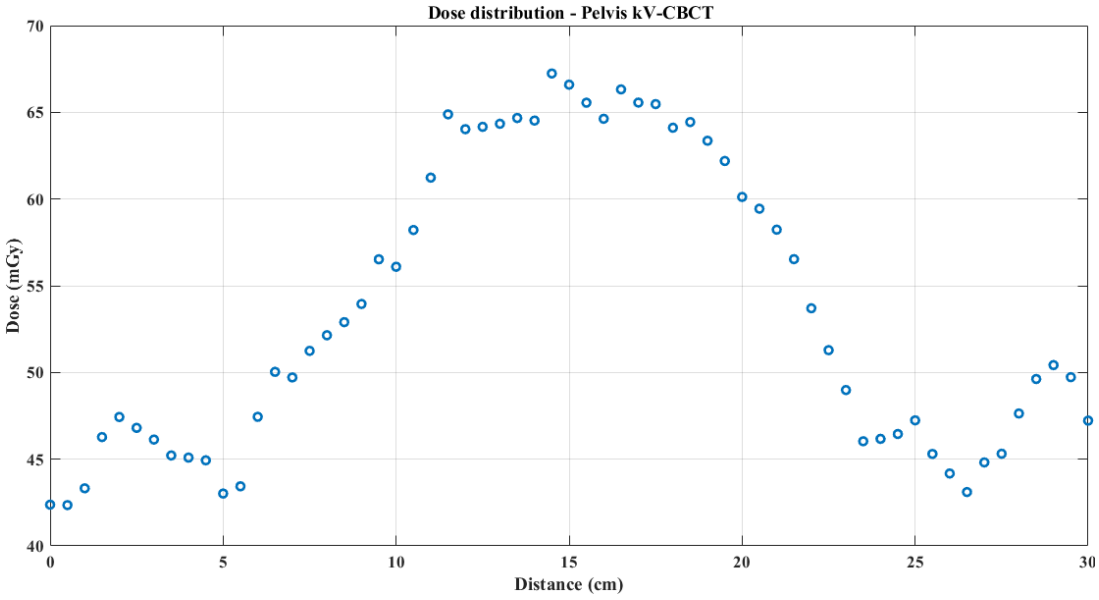

Figure 3.36: Dose distribution from Halcyon Pelvis kV CBCT protocol.

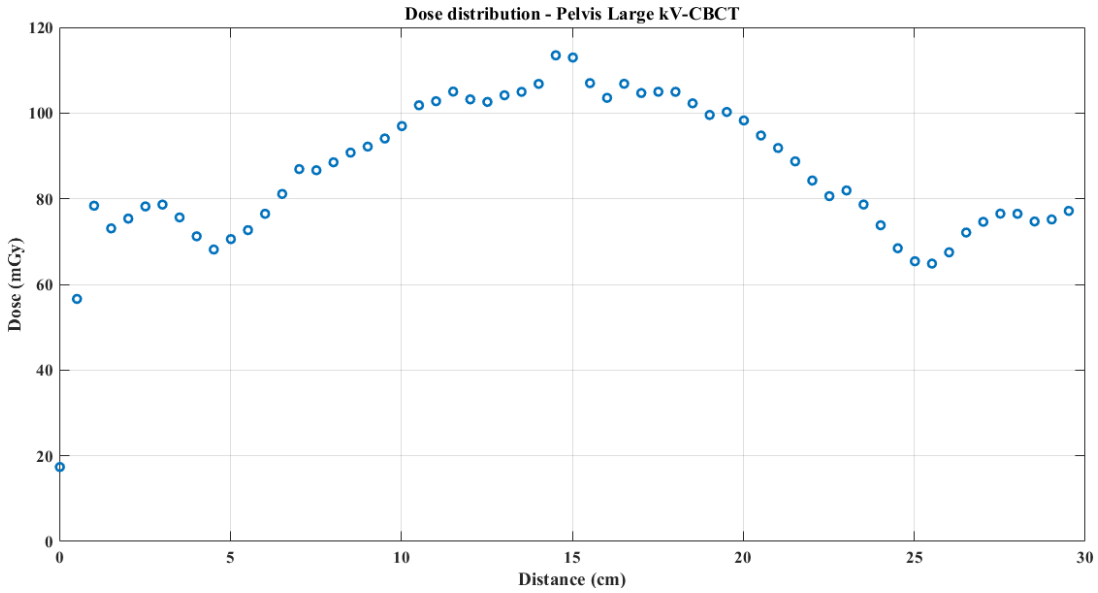

Figure 3.37: Dose distribution from Halcyon Pelvis Large kV CBCT protocol.

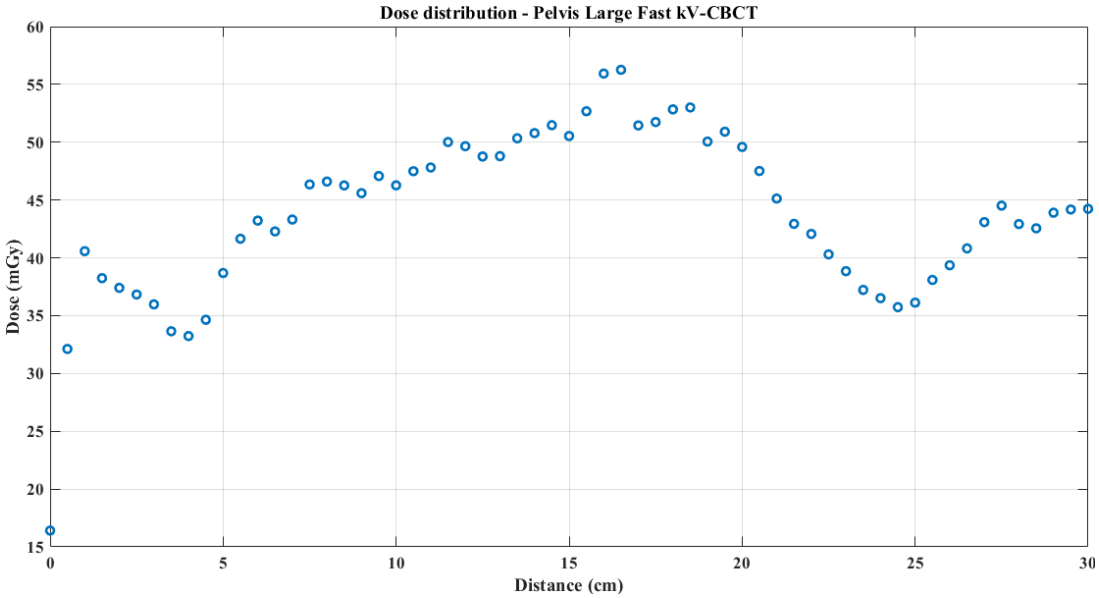

Figure 3.38: Dose distribution from Halcyon Pelvis Large Fast kV CBCT protocol.

3.7 Validation of the Monte Carlo model

The Monte Carlo models were tested by comparing model computations of percentage depth dose and crossline profiles in water, to ionisation chamber measurements. Across the beam energies tested, the maximum differences were 3.47% for the 100 kV, 3.65% for the 125 kV, and 3.27% for the 140 kV beams, as shown in Figures (3.39), (3.40), and (3.41). In all cases, the differences occurred within the dose fall-off region where GATE predicted the higher percentage dose. The good agreement between the depth dose profiles indicates that the spectral modeling was acceptable [17].

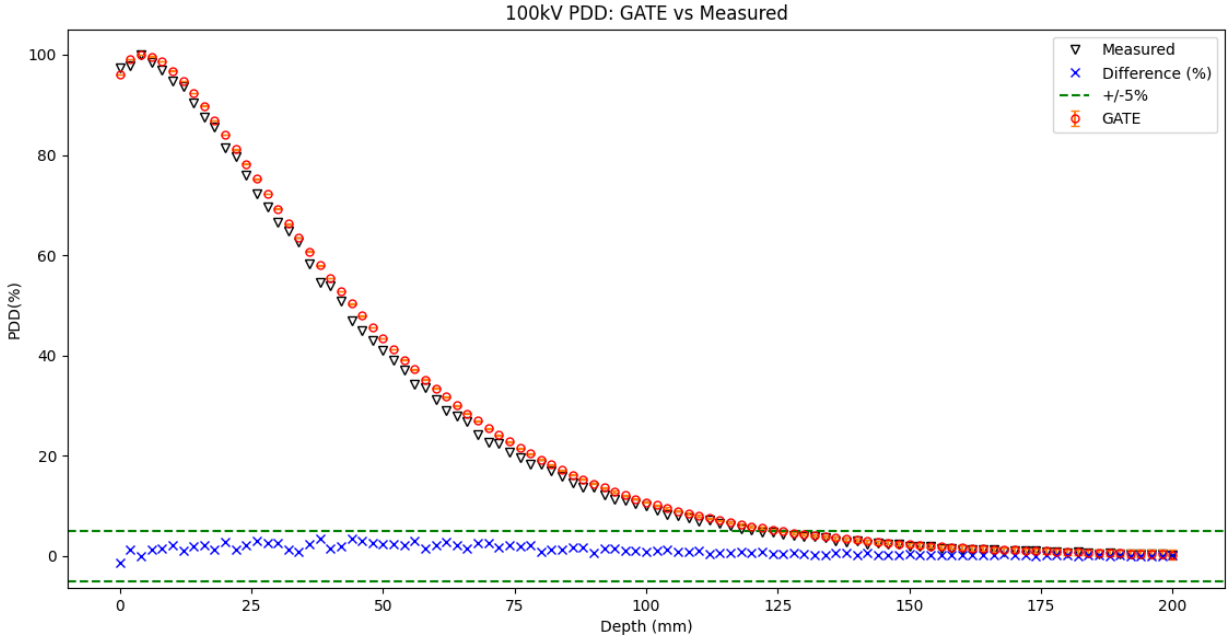

Figure 3.39: Comparison of measured and GATE Monte Carlo computed percentage depth dose profiles of the 100kV beam.

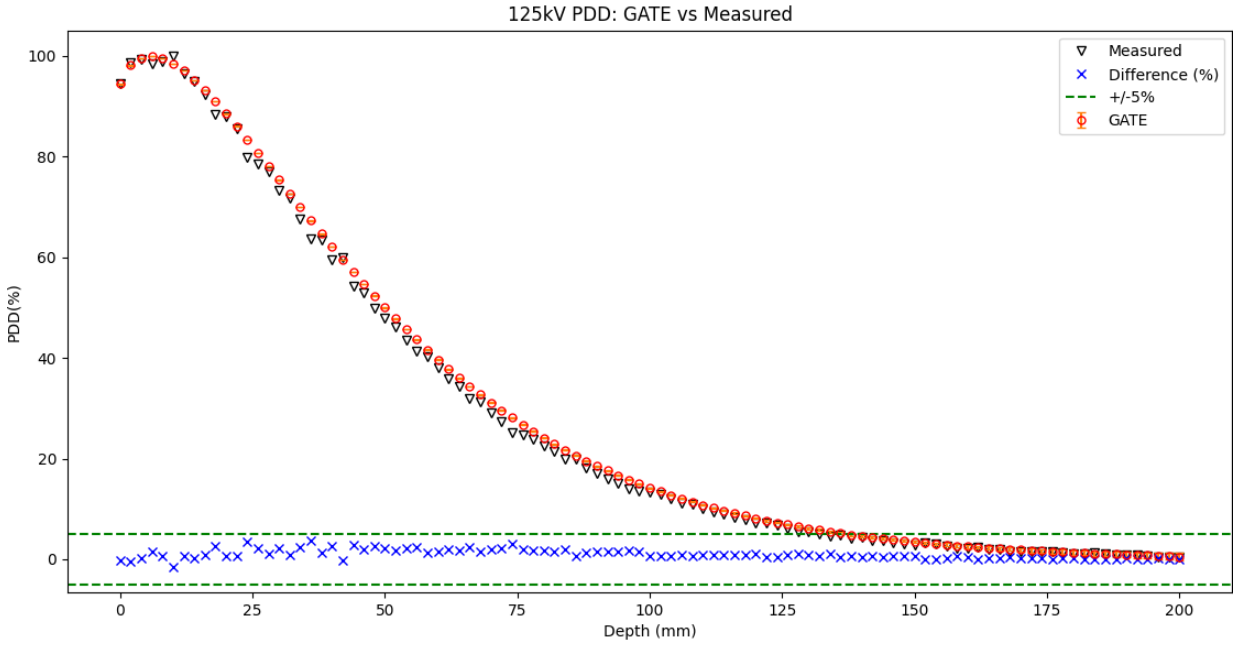

Figure 3.40: Comparison of measured and GATE Monte Carlo computed percentage depth dose profiles of the 125 kV beam.

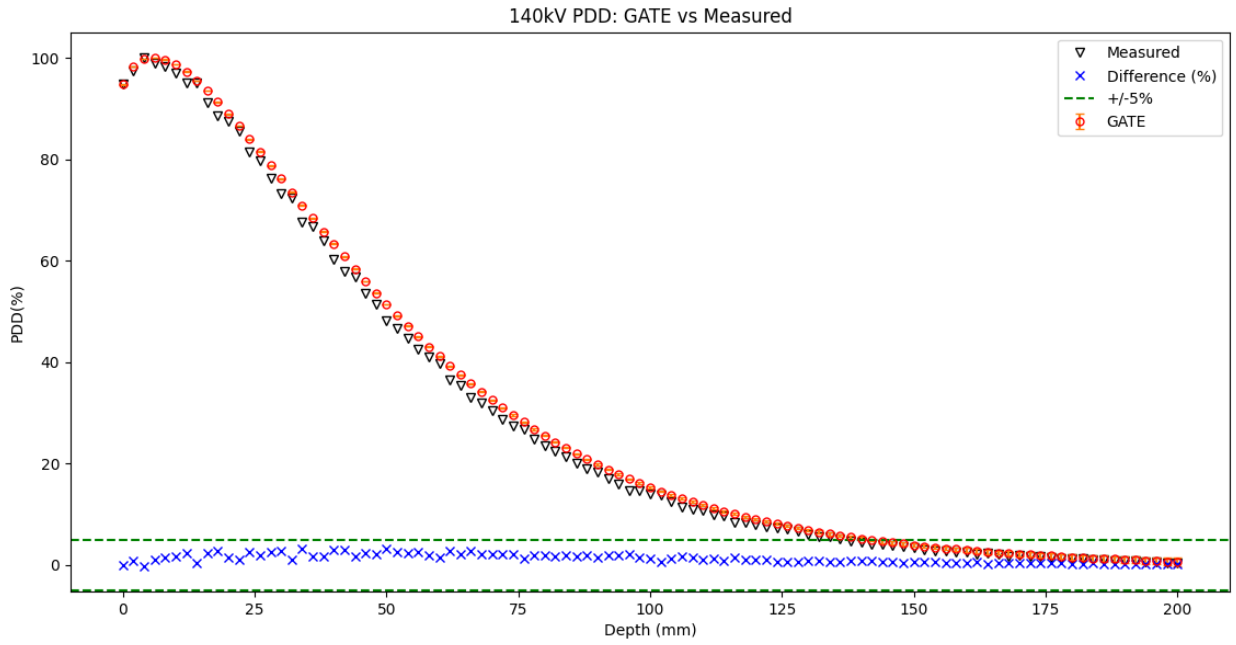

Figure 3.41: Comparison of measured and GATE Monte Carlo computed percentage depth dose profiles of the 140 kV beam.

The crossline dose profiles tested the quality of filtration modeling - in particular the quality of the bowtie filter model. The results are shown in Figures (3.42), (3.43), and (3.44). Across the beam energies, the maximum differences were 3.73% for 100 kV, 6.84% for 125 kV, and 4.44% for 140 kV when assessing

differences within central beam and below the curved portion of the bowtie filter. The majority of the data points were well within 3%. This good agreement is indicative of the acceptable quality of the bowtie filter model.

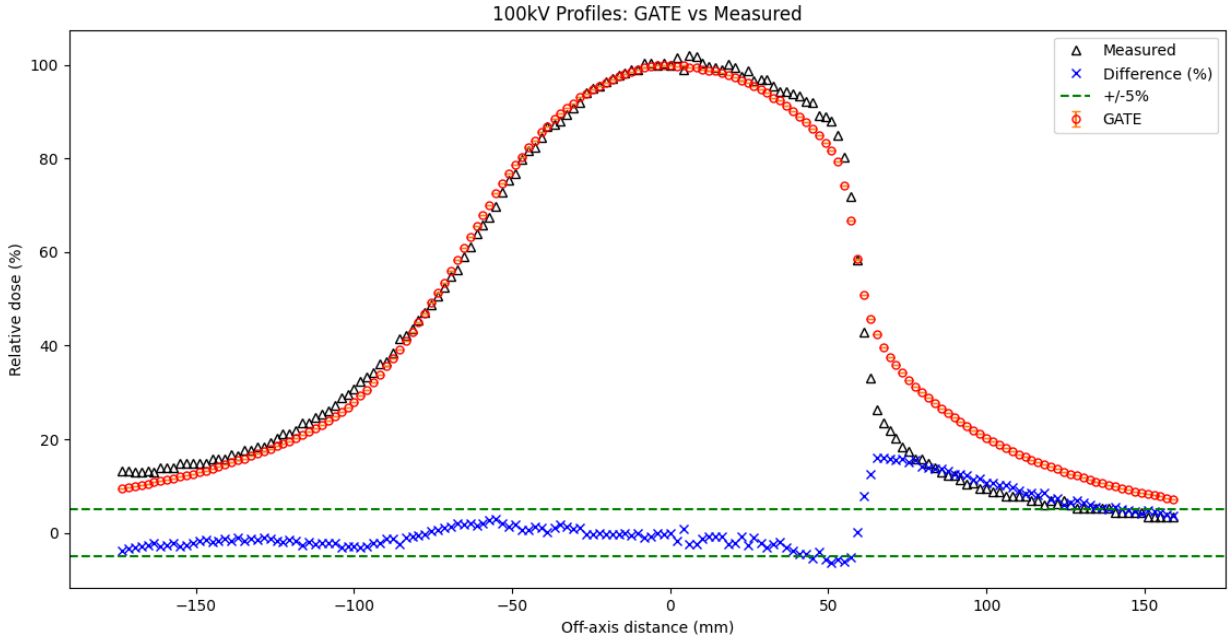

Figure 3.42: Comparison of measured and GATE Monte Carlo computed crossline dose profiles of the 100kV beam.

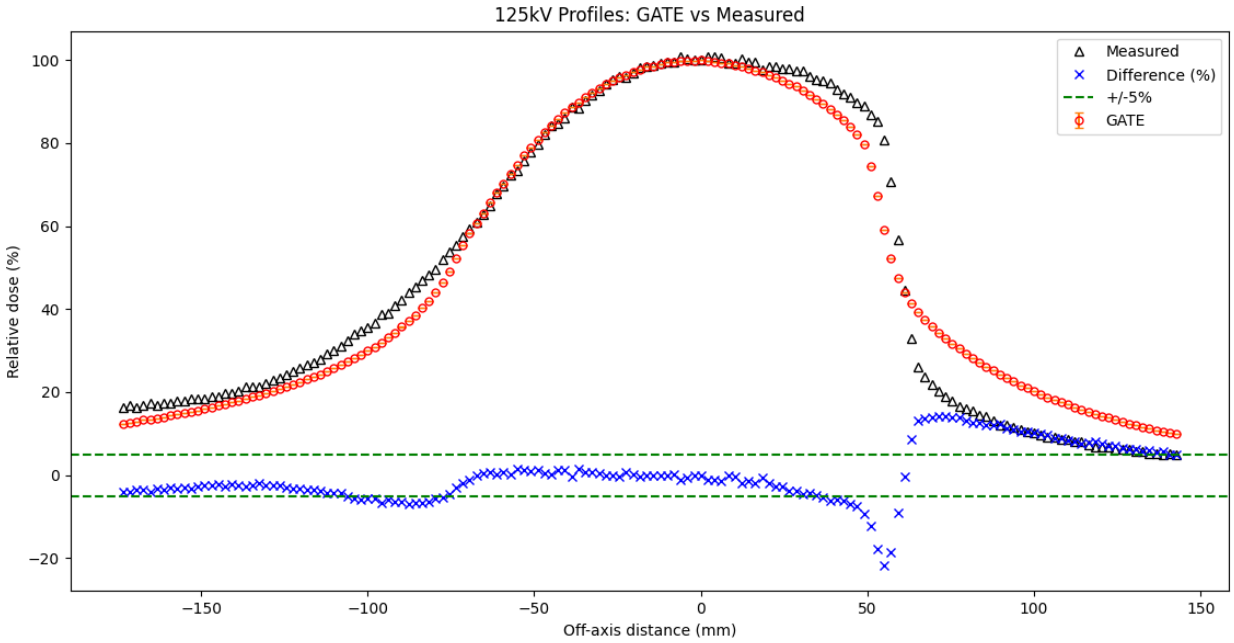

Figure 3.43: Comparison of measured and GATE Monte Carlo computed crossline dose profiles of the 125 kV beam.

The differences got accentuated rather dramatically when assessed in the penumbra towards the 'flat' side

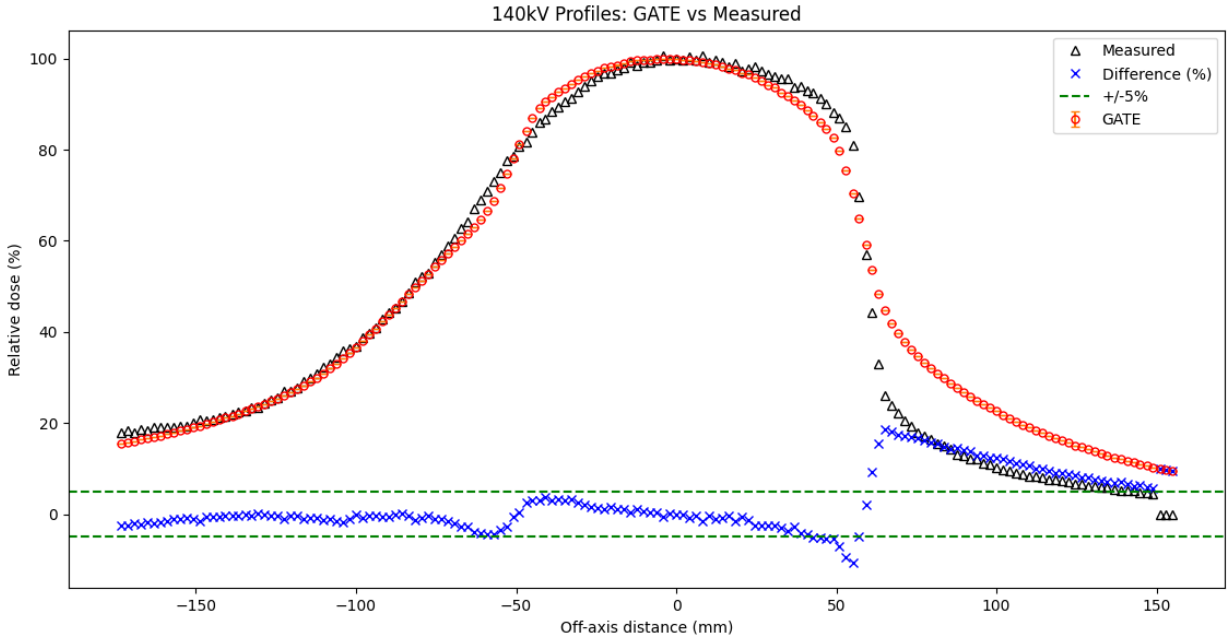

Figure 3.44: Comparison of measured and GATE Monte Carlo computed crossline dose profiles of the 140 kV beam.

of the bowtie filter, however. Maximum differences were 15.95% for 100 kV, 21.72% for 125 kV, and 18.57% for 140 kV. In an attempt to reduce these discrepancies, the material composition, thickness, and shape of the collimator blade in that portion of the bowtie filter were iterated. However, no satisfactory resolution could be attained, and the current blade configuration was selected because it yielded the least differences. To the author's best efforts, no explanation could be found in the literature for these differences, except to postulate that the blade construction is novel. It is worth noting that of all the references in the literature that used this methodology for spectral and filtration modeling there's no evidence that their models were validated by direct comparison of depth and crossline dose profiles, but rather opted to compare $CTDI_w$ values. We argue that this approach may mask significant and otherwise resolvable inaccuracies in the model. Indeed, the current models were arrived at by an iterative process of tuning.

3.8 RANDO phantom: GATE dose output

Figures (3.45), (3.46), and (3.47) illustrate the dose distribution calculated by GATE on the RANDO phantoms. Since the absolute voxel values are typically in the order of x10^{-8}, the image sets were renormalised to permit the use of colour maps for visualisation. In these images, the colours represent absorbed dose. The numbers representing colour intensity on the color scale are directly proportional to the absorbed dose in the region.

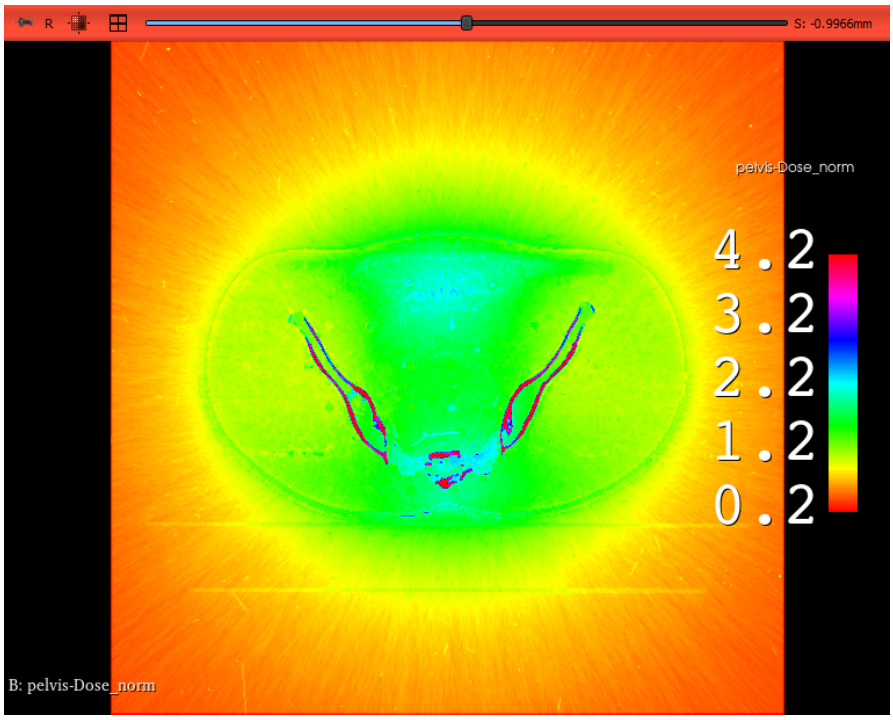

Figure 3.45: The normalised dose distribution computed by GATE Monte Carlo through the central slice of RANDO pelvis, using the Pelvis protocol with 125 kV. Voxel values were renormalised to allow visualisation using a colour map.

3.9 Normalisation factor

The average Normalisation Factor to convert the simulated dose (SD, mGy/photon history) to Measured Dose (MD, mGy/mAs) was 1.0352 x 10^{12} photon histories/mAs.

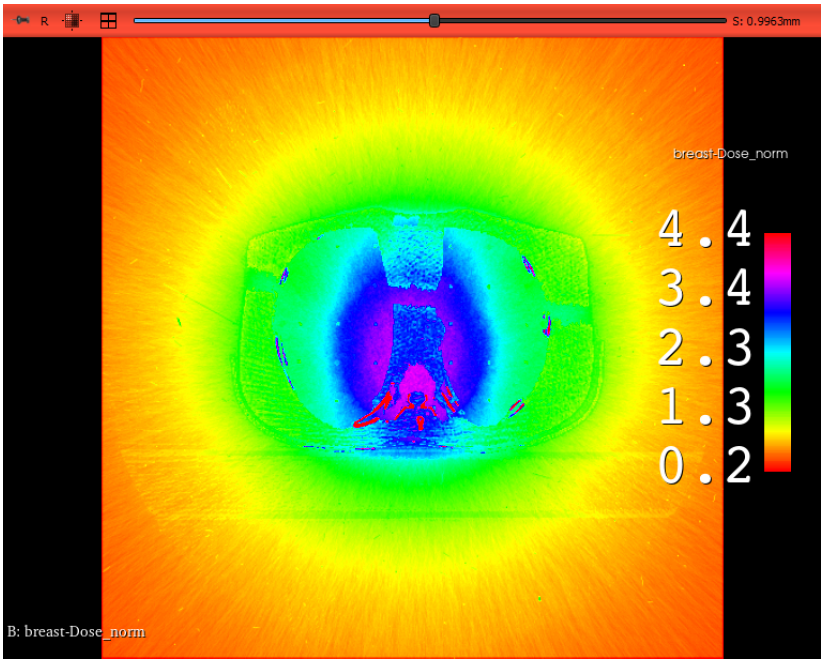

Figure 3.46: The normalised dose distribution computed by GATE Monte Carlo through the central slice of RANDO pelvis, using the Breast protocol with 125 kV. Voxel values were renormalised to allow visualisation using a colour map.

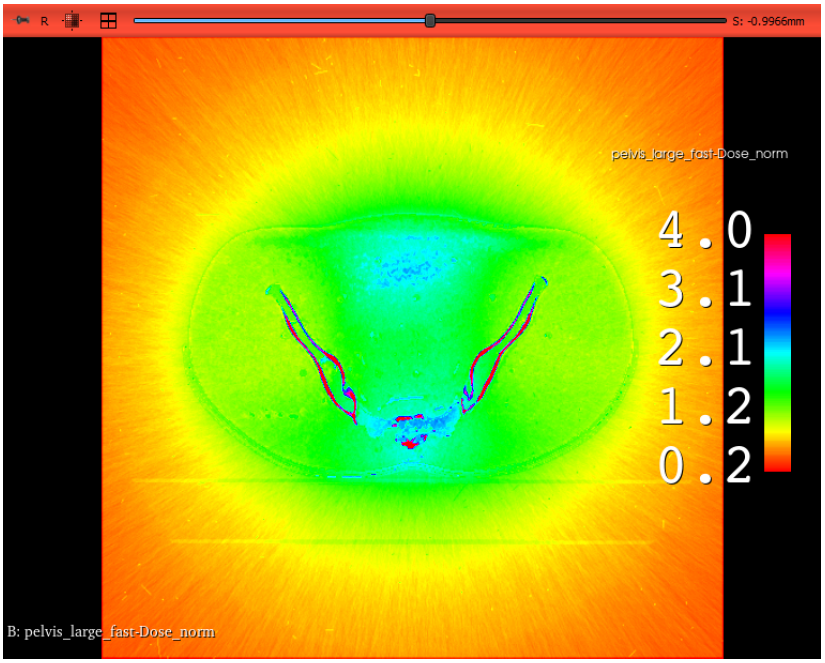

Figure 3.47: The normalised dose distribution computed by GATE Monte Carlo through the central slice of RANDO pelvis, using the Pelvis Large Fast protocol with 140 kV. Voxel values were renormalised to allow visualisation using a colour map.

3.10 Organ doses

Tables (3.7) and (3.8) show the protocol specific doses to organs and tissues in the [1]pelvic and [2]thoracic regions, respectively. Protocols that use higher mAs result in higher organ doses.

Table 3.7: Protocol-specific doses to organs in the pelvic region.

Organ/tissue	Protocol		
	Pelvis large (mGy)	**Pelvis (mGy)**	**Pelvis large fast (mGy)**
Blood vessels, trunk	18.16	13.39	8.70
Femora, upper half, cortical	183.44	135.31	87.94
Femora, upper half, spongiosa	62.09	45.80	29.77
Femora, upper half, medullary cavity	28.95	21.36	13.88
Pelvis, cortical	174.96	129.06	83.88
Pelvis, spongiosa	57.16	42.16	27.40
Lumbar spine, cortical	11.73	8.65	5.62
Lumbar spine, spongiosa	5.11	3.77	2.45
Sacrum, spongiosa	24.99	18.43	11.98
Rectum wall	107.10	79.00	51.35
Skin, trunk	15.16	11.20	7.28
Left ureter	21.17	15.62	10.15
Right ureter	20.00	14.75	9.59
Urinary bladder wall	123.26	90.92	59.09
Uterus/cervix	95.61	70.53	45.84

[1]Pelvis: kVp = 125 kV, mAs = 1074; Pelvis large: kVp = 140 kV, mAs = 1456; Pelvis large fast: 140 kV, mAs = 698

[2]Thorax: kVp = 125 kV, mAs = 301; Thorax fast: kVp = 125 kV, mAs = 295; Breast: kVp = 125 kV, mAs = 49

Table 3.8: Protocol-specific doses to organs in the thoracic region.

Organ/tissue	Protocol		
	Thorax (mGy)	**Thorax fast (mGy)**	**Breast (mGy)**
Trachea, trunk	2.75	2.69	0.45
Bronchi	15.60	15.29	2.54
Blood vessels, trunk	7.40	7.25	1.20
Clavicles, cortical	7.07	6.92	1.15
Clavicles, sporangiosa	3.01	2.95	0.49
Ribs, cortical	42.17	41.33	6.87
Ribs, spongiosa	16.06	15.74	2.61
Thoracic spine, cortical	54.63	53.54	8.89
Sternum, cortical	20.24	19.84	3.29
Sternum, sporangiosa	26.04	25.52	4.24
Breast, left, adipose tissue	12.03	11.79	1.96
Breast, left, glandular tissue	15.58	15.27	2.54
Breast, right, adipose tissue	13.20	12.94	2.15
Breast, right, glandular tissue	16.46	16.13	2.68
Heart wall	22.19	21.74	3.61
Kidney, left cortex	11.03	10.81	1.80
kidney, left medulla	6.75	6.62	1.10
Kidney, right cortex	6.20	6.07	1.01
kidney, right medulla	4.54	4.45	0.74
Lung, left, tissue	12.49	12.24	2.03
Lung, right, tissue	16.15	15.85	2.63
Spinal cord	8.16	8.00	1.33

In calculating the organ doses to the ICRP 110 computational phantom, the $doseToRegions$ Dose Actor used in the GATE Monte Carlo utilises first principles: since individual organs and tissues in the phantom are segmented, their physical properties such as volume, mass, density, and shape are known. In addition, the Monte Carlo method accurately computes the radiation energy deposited in the organs and tissues, so that the organ absorbed dose is determined from its basic definition. Therefore, the 3D organ doses are reported as opposed to point doses measured using dosimeters such as TLDs and OSLDs. The underlying assumption in point dosimetry is that the dose measured at a single location is homogeneously distributed throughout the organ volume. Provided the model has been well validated, Monte Carlo computed organ doses are more accurate.

The highest organ doses across all imaging protocols were doses to the cortical bones. The upper half femoral cortical bone received the highest dose at 183.44 mGy, 135.31 mGy, and 87.94 mGy per fraction from the Pelvis Large, Pelvis, and Pelvis Large Fast CBCT protocols. For a 30 fraction radiotherapy course, it may be necessary to incorporate these doses into the treatment plan in cases where this organ is considered at risk. The bladder and rectal walls are often contoured as organs-at-risk in radiotherapy of the pelvis. The dose to these organ were elevated, peaking at 123.26 mGy and 107.1 mGy in the Pelvis Large protocol. These doses may also need to be incoporated into treatment plans for hyperfractionated treatments.

As more centres incorporate the Halcyon system with kV CBCT imaging, this study has provided a Monte Carlo based method that centres may use to estimate organ doses in reference patients arising from kV CBCT pretreatment imaging. This tool could be especially useful since the accurate source and filtration characteristics of the kV CBCT system remain confidential.

Chapter 4

Conclusion and Future Work

4.1 Conclusion and Future Work

This study aimed to quantify, using GATE Monte Carlo models, doses to the organs in the thorax and pelvis arising from kV-CBCT imaging performed on the Halcyon 2.0 kV-CBCT system. The Monte Carlo models were developed using Geant4/GATE and validated against depth dose and crossline dose profiles measured in water. The maximum differences between the measured and GATE computed PDDs did not exceed 4%, while those in crossline profiles were within 5% within the central beam axis, but rose to approximately 20% in the penumbral regions. A normalisation factor of 1.0352 x 10^{12} photon histories/mAs was established between physical dose measurements which are influenced by mAs, and simulated doses influenced by the number of particles. Finally, organ doses to the thoracic and pelvic regions were computed on an ICRP 110 voxelised computational phantom using the $doseByRegions$ Dose Actor in the Geant4/GATE Monte Carlo toolkit. For the conventional 25 and 30 fraction radiotherapy courses, it was found that the femoral cortical bone, bladder and rectal walls may receive imaging doses that exceed the 5% threshold recommended by AAPM TG 180 for imaging doses to added to the treatment plan.

Since the present study was limited to estimating organ doses the thoracic and pelvis regions of the reference adult, future work could be extended to the head-and-neck region of the reference adult, as well as all body regions of weight stratified reference paediatrics. A follow-on study could estimate the risk of cancer induction in paediatric patients from exposure to kV-CBCT.

4.2 Strengths and limitations

By using Monte Carlo calculations of imaging dose in a reference computational phantom, this study yielded results that were more robust than those generated from point dose measurements using TLDs and OSLDs. The 3-dimensional nature of the computational reference phantom enabled doses to whole organs to be determined. An important limitation was compromised accuracy of GafChromic film dosimetry attributed to the absence of robust image registration facilities in the film processing software. This was evidenced by the elevated experimental uncertainties that were attributed to mismatch in temporal registration of

the calibration film pieces. The major limitation lay in the absence of accurate spectral and geometric data characterising the x-ray source and the beamline. It goes without saying that the precision of the final organ doses could be improved by using Monte Carlo models created from accurate information as opposed to measurements and model tuning.

Chapter 5

Bibliography

[1] Agostinelli S., et al., 2003, Nuclear instruments and Methods in Physics Research Section A: Accelerators, Spectrometers, Detectors and Associated Equipment, 506, 250

[2] Alaei P., Gerbi B. J., Geise R. A., 1999, Generation and use of photon energy deposition kernels for diagnostic quality x rays, Medical Physics, 26, 1687

[3] Anam C., Fujibuchi T., Haryanto F., Widita R., Arif I., Dougherty G., 2019, An evaluation of computed tomography dose index measurements using a pencil ionisation chamber and small detectors, Journal of Radiological Protection, 39, 112

[4] Andreo P., 1991, Monte Carlo Techniques in Medical Radiation Physics, Physics in Medicine & Biology, 36, 861

[5] Battista J. J., Rider W. D., Van Dyk J., 1980, Computed tomography for radiotherapy planning, International Journal of Radiation Oncology* Biology* Physics, 6, 99

[6] Bauhs J. A., Vrieze T. J., Primak A. N., Bruesewitz M. R., McCollough C. H., 2008, CT dosimetry: comparison of measurement techniques and devices, Radiographics, 28, 245

[7] Biggs P. J., Goitein M., Russell M. D., 1985, A diagnostic X ray field verification device for a 10 MV linear accelerator, International Journal of Radiation Oncology* Biology* Physics, 11, 635

[8] Boone J., Strauss K., Cody D., McCollough C., McNitt-Gray M., Toth T., 2011, Report of AAPM TG 204: size-specific dose estimates (SSDE) in pediatric and adult body CT examinations, J Appl Clin Med Phys

[9] Boone J. M., et al., 2012, ICRU Report No. 87: Radiation dose and image-quality assessment in computed tomography, Journal of the ICRU, 12, 9

[10] Buckley J. G., Wilkinson D., Malaroda A., Metcalfe P., 2018, Investigation of the radiation dose from cone-beam CT for image-guided radiotherapy: A comparison of methodologies, Journal of Applied Clinical Medical Physics, 19, 174

[11] Chamberlain D., Carter J., Kuang Y., 2023, Varian Halcyon, Principles and Practice of Image-Guided Abdominal Radiation Therapy. IOP Publishing Bristol, UK, pp 10–1

[12] Cho P. S., Lindsley K. L., Douglas J. G., Stelzer K. J., Griffin T. W., 1998, Digital radiotherapy simulator, Computerized Medical Imaging and Graphics, 22, 1

[13] Commission N. R., 2019, Thermoluminescent dosimeters, https://www.nrc.gov/docs/ML1122/ML11229A698.pdf, note = Online; accessed 19-December-2022

[14] Commission I., et al., 2009, Technical report, Particular requirements for the basic safety and essential performance of X-ray equipment for computed tomography. IEC 60601-2-44: 2009

[15] Descamps C., Gonzalez M., Garrigo E., Germanier A., Venencia D., 2012, Measurements of the dose delivered during CT exams using AAPM Task Group Report No. 111, Journal of Applied Clinical Medical Physics, 13, 293

[16] Devic S., Seuntjens J., Sham E., Podgorsak E. B., Schmidtlein C. R., Kirov A. S., Soares C. G., 2005, Precise radiochromic film dosimetry using a flat-bed document scanner, Medical Physics, 32, 2245

[17] Ding G. X., Duggan D. M., Coffey C. W., 2007, Characteristics of kilovoltage x-ray beams used for cone-beam computed tomography in radiation therapy, Physics in Medicine & Biology, 52, 1595

[18] Dixon R. L., Boone J. M., 2010, Cone beam CT dosimetry: A unified and self-consistent approach including all scan modalities—With or without phantom motion, Medical Physics, 37, 2703

[19] Donovan M. Bakalyar Erin Angel K. L. B., 2020, The Design and Use of the ICRU/AAPM CT Radiation Dosimetry Phantom: An Implementation of AAPM Report 111, Medical Physics, pp e84–e99

[20] Giacometti V., Hounsell A. H., McGarry C. K., 2020, A review of dose calculation approaches with cone beam CT in photon and proton therapy, Physica Medica, 76, 243

[21] Giaddui T., Cui Y., Galvin J., Yu Y., Xiao Y., 2013, Comparative dose evaluations between XVI and OBI cone beam CT systems using Gafchromic XRQA2 film and nanoDot optical stimulated luminescence dosimeters, Medical Physics, 40, 062102

[22] Gilling L., Ali O., 2022, Organ dose from Varian XI and Varian OBI systems are clinically comparable for pelvic CBCT imaging, Physical and Engineering Sciences in Medicine, 45, 279

[23] Greene L., Srinivas S., Park S., Hatami N., Nobashi T., Baratto L., Toriihara A., Gambhir S. S., 2018, in Kummar S., Takimoto C., eds, , Novel Designs of Early Phase Trials for Cancer Therapeutics. Academic Press, pp 129–149, https://www.sciencedirect.com/science/article/pii/B9780128125120000105

[24] Gregory K. J., Bibbo G., Pattison J. E., 2008, On the uncertainties in effective dose estimates of adult CT head scans, Medical Physics, 35, 3501

[25] Haba T., Yasui K., Saito Y., Kobayashi M., Koyama S., 2021, A new cone-beam computed tomography dosimetry method providing optimal measurement positions: A Monte Carlo study, Physica Medica, 81, 130

[26] Hammoudah M. M., Henschke U. K., 1977, Supervoltage beam films, International Journal of Radiation Oncology* Biology* Physics, 2, 571

[27] Hernandez A. M., Boone J. M., 2014, Tungsten anode spectral model using interpolating cubic splines: unfiltered x-ray spectra from 20 kV to 640 kV, Medical Physics, 41, 042101

[28] Hu N., McLean D., 2014, Measurement of radiotherapy CBCT dose in a phantom using different methods, Australasian physical & engineering sciences in medicine, 37, 779

[29] Huda W., Magill D., He W., 2011, CT effective dose per dose length product using ICRP 103 weighting factors, Medical Physics, 38, 1261

[30] (IAEA) I. A. E. A., 2011, Status of computed tomography dosimetry for wide cone beam scanners. International Atomic Energy Agency

[31] ICRP 2009, ICRP Publication 110: Adult Reference Computational Phantoms, Annals of the ICRP, 39

[32] Jaffray D. A., Drake D. G., Moreau M., Martinez A. A., Wong J. W., 1999, A radiographic and tomographic imaging system integrated into a medical linear accelerator for localization of bone and soft-tissue targets, International Journal of Radiation Oncology* Biology* Physics, 45, 773

[33] Jaffray D. A., Siewerdsen J. H., Wong J. W., Martinez A. A., 2002, Flat-panel cone-beam computed tomography for image-guided radiation therapy, International Journal of Radiation Oncology* Biology* Physics, 53, 1337

[34] Jan S., et al., 2004, GATE: a simulation toolkit for PET and SPECT, Physics in Medicine & Biology, 49, 4543

[35] Jin J.-Y., Yin F.-F., Tenn S. E., Medin P. M., Solberg T. D., 2008, Medical Dosimetry, 33, 124

[36] Jung B., Larsson B., Rosengren B., Ståhl K., Wretlind W., 1968, Use of the BrainLAB ExacTrac X-Ray 6D system in image-guided radiotherapy, Acta Radiologica: Therapy, Physics, Biology, 7, 282

[37] Jurgen Riegel Werner Mayer Y. v. H., 2002, FreeCAD: Your own 3D parametric modeler, `https://www.freecadweb.org/`

[38] Khong P., Ringertz H., Donoghue V., Frush D., Rehani M., Appelgate K., Sanchez R., et al., 2013,

ICRP publication 121: radiological protection in paediatric diagnostic and interventional radiology, Annals of the ICRP, 42, 1

[39] Kry S. F., et al., 2020, AAPM TG 191: Clinical use of luminescent dosimeters: TLDs and OSLDs, Medical Physics, 47, e19

[40] Landry G., Hua C.-h., 2018, Current state and future applications of radiological image guidance for particle therapy, Medical Physics, 45, e1086

[41] Li X., Marschall T. A., Yang K., Liu B., 2022, Advancing size-specific dose estimates in CT examinations: Dose estimates at longitudinal positions of scans, Medical Physics, 49, 1303

[42] Marchant T. E., Joshi K. D., 2016, Comprehensive Monte Carlo study of patient doses from cone-beam CT imaging in radiotherapy, Journal of radiological protection, 37, 13

[43] Marinello G., 1996, Thermoluminescence dosimetry applied to quality assurance in radiotherapy, brachytherapy and radiodiagnostic,IAEA

[44] Martin C. J., Harrison J. D., Rehani M. M., 2020, Effective dose from radiation exposure in medicine: past, present, and future, Physica Medica, 79, 87

[45] Mbewe J., 2023, Energy Dependence of GafChromic LD-V1 Film Dose Response to X-ray Photons in the 60 to 180 kV Range, `https://www.researchsquare.com/article/rs-3451210/v1`

[46] McKeever S., 2011, Optically stimulated luminescence: a brief overview, Radiation Measurements, 46, 1336

[47] McMillan K., McNitt-Gray M., Ruan D., 2013, Development and validation of a measurement-based source model for kilovoltage cone-beam CT Monte Carlo dosimetry simulations, Medical Physics, 40, 111907

[48] Murphy M., Isaksson M., Jalden J., Ozhasoglu C., 2001, Realtime compensation of breathing motion during radiotherapy, International Journal of Radiation Oncology• Biology• Physics, 51, 388

[49] Nakajima E., Sato H., 2023, Characterization of a New Radiochromic Film (LD-V1) Using Mammographic Beam Qualities, Zeitschrift für Medizinische Physik

[50] Nasir M., Pratama D., Anam C., Haryanto F., 2016, Calculation of size specific dose estimates (SSDE) value at cylindrical phantom from CBCT Varian OBI v1. 4 X-ray tube EGSnrc Monte Carlo simulation based, Journal of Physics: Conference Series. p. 012040

[51] Ng K.-H., Yeong C.-H., 2013, in , The Phantoms of Medical and Health Physics: Devices for Research and Development. Springer, pp 91–122

[52] Nielsen J., Jensen S. H., 1942, Some Experimental and Clinical Lights on the Rotation Therapy, its Bases and Possibilities, Acta Radiologica, 23, 51

[53] Niroomand-Rad A., et al., 2020, Report of AAPM task group 235 radiochromic film dosimetry: an update to TG-55, Medical Physics, 47, 5986

[54] Osei E. K., Schaly B., Fleck A., Charland P., Barnett R., 2009, Dose assessment from an online kilovoltage imaging system in radiation therapy, Journal of Radiological Protection, 29, 37

[55] Papalazarou C., Klop G. J., Milder M. T., Marijnissen J. P., Gupta V., Heijmen B. J., Nuyttens J. J., Hoogeman M. S., 2017, CyberKnife with integrated CT-on-rails: System description and first clinical application for pancreas SBRT, Medical Physics, 44, 4816

[56] Pisani L., Lockman D., Jaffray D., Yan D., Martinez A., Wong J., 2000, Setup error in radiotherapy: on-line correction using electronic kilovoltage and megavoltage radiographs, International Journal of Radiation Oncology* Biology* Physics, 47, 825

[57] Protection R., 2007, ICRP publication 103, Annals of the ICRP, 37, 2

[58] Punnoose J., Xu J., Sisniega A., Zbijewski W., Siewerdsen J., 2016, Spektr 3.0—A computational tool for x-ray spectrum modeling and analysis, Medical Physics, 43, 4711

[59] Rampado O., Garelli E., Deagostini S., Ropolo R., 2006, Dose and energy dependence of response of Gafchromic® XR-QA film for kilovoltage x-ray beams, Physics in Medicine & Biology, 51, 2871

[60] Robert Pooley Joel Felmlee R. M., 2019, Basic Principles and Terminology of Magnetic Resonance Imaging, https://musculoskeletalkey.com/basic-principles-and-terminology-of-magnetic-resonance-imaging/

[61] Sherouse G. W., Novins K., Chaney E. L., 1990, Computation of digitally reconstructed radiographs for use in radiotherapy treatment design, International Journal of Radiation Oncology* Biology* Physics, 18, 651

[62] Sontag M. R., Cunningham J., 1978, Clinical application of a CT based treatment planning system, Computerized Tomography, 2, 117

[63] Swain R. W., Steckel R. J., 1966, Beam localization in cobalt and megavoltage therapy during treatment, Radiology, 87, 529

[64] Sykes J., Lindsay R., Iball G., Thwaites D., 2013, Dosimetry of CBCT: methods, doses and clinical consequences, Journal of Physics: Conference Series. p. 012017

[65] Systems V. M., 2018, Halcyon Product Planning Guide, https://imlive.s3.amazonaws.com/Federal%20Government/ID333658238046585449321839190588795370231/Halcyon%20DDR.pdf

[66] Tomic N., Devic S., DeBlois F., Seuntjens J., 2010, Reference radiochromic film dosimetry in kilovoltage photon beams during CBCT image acquisition, Medical Physics, 37, 1083

[67] Tomic N., et al., 2014, Characterization of calibration curves and energy dependence GafChromicTM XR-QA2 model based radiochromic film dosimetry system, Medical Physics, 41, 062105

[68] Turner A. C., et al., 2009, A method to generate equivalent energy spectra and filtration models based on measurement for multidetector CT Monte Carlo dosimetry simulations, Medical Physics, 36, 2154

[69] Uematsu M., Fukui T., Shioda A., Tokumitsu H., Takai K., Kojima T., Asai Y., Kusano S., 1996, A dual computed tomography linear accelerator unit for stereotactic radiation therapy: a new approach without cranially fixated stereotactic frames, International Journal of Radiation Oncology* Biology* Physics, 35, 587

[70] Vañó E., et al., 2017, ICRP publication 135: diagnostic reference levels in medical imaging, Annals of the ICRP, 46, 1

[71] Velbeck K., Luo L., Streetz K., 2006, Type testing the model 6600 plus automatic TLD reader, Radiation protection dosimetry, 120, 303

[72] Wiki S., 2019, Main Page — Slicer Wiki,, https://www.slicer.org/w/index.php?title=Main_Page&oldid=62645

[73] Yuasa Y., Shiinoki T., Onizuka R., Fujimoto K., 2019, Estimation of effective imaging dose and excess absolute risk of secondary cancer incidence for four-dimensional cone-beam computed tomography acquisition, Journal of Applied Clinical Medical Physics, 20, 57

[74] Zhang G., Marshall N., Jacobs R., Liu Q., Bosmans H., 2013, Bowtie filtration for dedicated cone beam CT of the head and neck: a simulation study, The British journal of radiology, 86, 20130002

Chapter 6

Appendices

6.1 GATE macros

Listing 6.1: Main macro

```
#================================================================

# VERBOSITY

#================================================================


/control/execute verbose.mac


#================================================================

# PROTOCOL SPECIFIC TIMESLICES AND ROTATION SPEEDS

#================================================================


#/control/alias PROTOCOL "protocols/static.mac"

#/control/alias PROTOCOL "protocols/pelvis.mac"

#/control/alias PROTOCOL "protocols/image_gently.mac"

#/control/alias PROTOCOL "protocols/image_gently_large.mac"

/control/alias PROTOCOL "protocols/head.mac"

#/control/alias PROTOCOL "protocols/head_ld.mac"

#/control/alias PROTOCOL "protocols/breast.mac"

#/control/alias PROTOCOL "protocols/thorax_fast.mac"

#/control/alias PROTOCOL "protocols/pelvis_fast.mac"

#/control/alias PROTOCOL "protocols/thorax.mac"

#/control/alias PROTOCOL "protocols/pelvis_large_fast.mac"

#/control/alias PROTOCOL "protocols/pelvis_large.mac"


#================================================================
```

```
# GEOMETRY
#=======================================================

/control/execute geometry.mac

#=======================================================
# HALF BOWTIE FILTER
#=======================================================

/control/execute bowtie.mac

#=======================================================
# WATER PHANTOM
#=======================================================

#/control/execute phantom.mac

#=======================================================
# CTDI PHANTOM
#=======================================================

#/control/execute body_ctdi.mac
/control/execute head_ctdi.mac

#=======================================================
```

```
# VOXELISED RANDO PHANTOM
#=====================================================

#/control/execute rando_breast.mac
#/control/execute rando_pelvis.mac
#/control/execute rando_pelvis_large.mac
#/control/execute rando_pelvis_large_fast.mac
#/control/execute rando_thorax.mac
#/control/execute rando_thorax_fast.mac

#=====================================================
# ICRP PHANTOM DOSE DISTRIBUTION
#=====================================================

#/control/execute icrp_phantom.mac
#/control/execute mesh_phantom.mac

#=====================================================
# PHYSICS
#=====================================================

/gate/physics/addPhysicsList              emstandard_opt3

/gate/physics/Gamma/SetCutInRegion        world 10 mm
/gate/physics/Electron/SetCutInRegion     world 10 mm
```

```
/gate/physics/Gamma/SetCutInRegion      CTDIPhantom 0.1 mm
/gate/physics/Electron/SetCutInRegion   CTDIPhantom 0.1 mm

#=====================================================
# PHANTOM DOSE DISTRIBUTION
#=====================================================

#/control/execute phantom_output.mac

#=====================================================
# CTDI PHANTOM OUTPUT
#=====================================================

#/control/execute body_ctdi_output.mac
/control/execute head_ctdi_output.mac

#=====================================================
# RANDO PHANTOM DOSE DISTRIBUTION
#=====================================================

#/control/execute rando_pelvis_output.mac
#/control/execute rando_breast_output.mac
#/control/execute rando_pelvis_large_output.mac
```

```
#=====================================================

# ICRP PHANTOM DOSE DISTRIBUTION

#=====================================================


#/control/execute icrp_phantom_output.mac

#/control/execute mesh_phantom_output.mac

#=====================================================

# INITIALISE THE SIMULATION

#=====================================================


/gate/run/initialize


#=====================================================

# ADD THE SOURCE

#=====================================================


#/control/execute source_80kV.mac

/control/execute source_100kV.mac

#/control/execute source_125kV.mac

#/control/execute source_140kV.mac


#=====================================================


#=====================================================

# VISUALISATION
```

```
#/control/execute visu.mac

#=====================================================

# START BEAMS

#=====================================================

/gate/random/setEngineName MersenneTwister

/gate/random/setEngineSeed auto

/control/execute {PROTOCOL}

/gate/application/setTotalNumberOfPrimaries 10e11

#=====================================================

# START THE SIMULATION

#=====================================================

/gate/application/start
```

Listing 6.2: Definition of the pelvis kV CBCT protocol

```
# Timeslice

/gate/application/setTimeSlice          1 s

/gate/application/setTimeStart          0. s

/gate/application/setTimeStop           895 s

#

# Tube rotation

/gate/xraybox/moves/insert                                      orbiting
```

```
/gate/xraybox/orbiting/setSpeed                    0.40223463687 deg/s
/gate/xraybox/orbiting/setPoint1                   0 0 0 cm
/gate/xraybox/orbiting/setPoint2                   0 0 1 cm
/gate/xraybox/orbiting/enableAutoRotation          true
```

Listing 6.3: Definition of the pelvis_large kV CBCT protocol

```
# Timeslice
/gate/application/setTimeSlice          1 s
/gate/application/setTimeStart          0. s
/gate/application/setTimeStop           809 s

# Tube rotation
/gate/xraybox/moves/insert              orbiting
/gate/xraybox/orbiting/setSpeed         0.44499382 deg/s
/gate/xraybox/orbiting/setPoint1        0 0 0 cm
/gate/xraybox/orbiting/setPoint2        0 0 1 cm
/gate/geometry/rebuild
```

Listing 6.4: Definition of the pelvis_large_fast kV CBCT protocol

```
# Timeslice
/gate/application/setTimeSlice          0.035816619 s
/gate/application/setTimeStart          0. s
/gate/application/setTimeStop           25 s

# Tube rotation
/gate/xraybox/moves/insert              orbiting
/gate/xraybox/orbiting/setSpeed         14.4 deg/s
```

```
/gate/xraybox/orbiting/setPoint1         0 0 0 cm
/gate/xraybox/orbiting/setPoint2         1 0 0 cm
/gate/geometry/rebuild
```

Listing 6.5: Definition of the thorax kV CBCT protocol

```
# Timeslice
/gate/application/setTimeSlice           1 s
/gate/application/setTimeStart           0. s
/gate/application/setTimeStop            859 s

# Tube rotation
/gate/xraybox/moves/insert                   orbiting
/gate/xraybox/orbiting/setSpeed          0.41909197 deg/s
/gate/xraybox/orbiting/setPoint1         0 0 0 cm
/gate/xraybox/orbiting/setPoint2         0 0 1 cm
/gate/xraybox/orbiting/enableAutoRotation        true
```

Listing 6.6: Definition of the thorax_fast kV CBCT protocol

```
# Timeslice
/gate/application/setTimeSlice           1 s
/gate/application/setTimeStart           0. s
/gate/application/setTimeStop            491 s

# Tube rotation
/gate/xraybox/moves/insert                   orbiting
/gate/xraybox/orbiting/setSpeed          0.73319756 deg/s
/gate/xraybox/orbiting/setPoint1         0 0 0 cm
```

```
/gate/xraybox/orbiting/setPoint2          0 0 1 cm
/gate/xraybox/orbiting/enableAutoRotation        true
```

Listing 6.7: Definition of the breast kV CBCT protocol

```
# Timeslice
/gate/application/setTimeSlice            1 s
/gate/application/setTimeStart            0. s
/gate/application/setTimeStop             491 s


# Tube rotation
/gate/xraybox/moves/insert                orbiting
/gate/xraybox/orbiting/setSpeed           0.73319756 deg/s
/gate/xraybox/orbiting/setPoint1          0 0 0 cm
/gate/xraybox/orbiting/setPoint2          0 0 1 cm
/gate/xraybox/orbiting/enableAutoRotation        true
```

Listing 6.8: Definition of the static kV CBCT protocol

```
# Timeslice
/gate/application/setTimeSlice            1. s
/gate/application/setTimeStart            0. s
/gate/application/setTimeStop             1. s
```

Listing 6.9: Definition of the half bowtie filter volume

```
#=====================================================
# HALF BOWTIE FILTER [Size (x,y,z) = (100, 40.82, 90)]
#=====================================================
## Half bow-tie filter
```

```
/gate/xraybox/daughters/name                    hbtf
/gate/xraybox/daughters/insert                  tessellated
/gate/hbtf/geometry/setPathToSTLFile    data/newhbtf.stl
/gate/hbtf/setMaterial                                  Aluminium
/gate/hbtf/placement/setRotationAxis    0 1 0
/gate/hbtf/placement/setRotationAngle   180 deg
/gate/hbtf/placement/setTranslation             -0.2 -14.79 4.5 cm # 0.1 -11.79
/gate/hbtf/vis/setColor                                 yellow
/gate/hbtf/vis/forceSolid
```

Listing 6.10: Definition of the water phantom

```
##############################
# Mother water phantom       #
##############################

/gate/Gantry/daughters/name                             motherPhantom
/gate/Gantry/daughters/insert                           box
/gate/motherPhantom/setMaterial                 Water
/gate/motherPhantom/geometry/setXLength         60 cm
/gate/motherPhantom/geometry/setYLength         40 cm
/gate/motherPhantom/geometry/setZLength         60 cm
/gate/motherPhantom/placement/setRotationAxis   0 1 0
/gate/motherPhantom/placement/setRotationAngle  0 deg
#
##################################
# Water phantom for scoring #
```

```
#################################

#

/gate/motherPhantom/daughters/name              waterPhantom

/gate/motherPhantom/daughters/insert            box

/gate/waterPhantom/setMaterial                  Water

#/gate/waterPhantom/geometry/setXLength         34.2 cm # For 80 kV

#/gate/waterPhantom/geometry/setXLength         32.8 cm # For 100 kV

/gate/waterPhantom/geometry/setXLength          31.2 cm # For 125 kV

#/gate/waterPhantom/geometry/setXLength         32.4 cm # For 140 kV

/gate/waterPhantom/geometry/setYLength          40 cm

/gate/waterPhantom/geometry/setZLength          40 cm

/gate/waterPhantom/placement/setRotationAxis    0 1 0

/gate/waterPhantom/placement/setRotationAngle   0 deg

#############################

# For static acquisition #

#############################

#

/gate/motherPhantom/placement/setTranslation            0 -20 0 cm
```

Listing 6.11: Definition of the RANDO Breast volume

```
#=================

# INSERT FOV BOX #

#=================

/gate/Gantry/daughters/name                              FOV

/gate/Gantry/daughters/insert                        box

/gate/FOV/setMaterial                                    Air

/gate/FOV/geometry/setXLength                        491.404 mm

/gate/FOV/geometry/setYLength                        491.404 mm

/gate/FOV/geometry/setZLength                        129.543 mm

/gate/FOV/vis/setColor                                   white

/gate/FOV/vis/setVisible                                 1

/gate/FOV/vis/forceWireframe

#=======================================================

# GENERATE MATERIALS FROM HOUNSFIELD UNITS

#=======================================================

# Generate materials from Hounsfield units
```

```
/gate/HounsfieldMaterialGenerator/SetMaterialTable                    data/Schneider2000MaterialsTable.txt
/gate/HounsfieldMaterialGenerator/SetDensityTable                     data/Schneider2000DensitiesTable.txt
/gate/HounsfieldMaterialGenerator/SetDensityTolerance                 0.1 g/cm3
/gate/HounsfieldMaterialGenerator/SetOutputMaterialDatabaseFilename   data/rando/patient-HUmaterials.db
/gate/HounsfieldMaterialGenerator/SetOutputHUMaterialFilename         data/rando/patient-HU2mat.txt
/gate/HounsfieldMaterialGenerator/Generate

#=====================================================

# IMPORT PELVIS .MHD FILE

#=====================================================

/gate/FOV/daughters/name                                    rando_breast
/gate/FOV/daughters/insert                                  ImageNestedParametrisedVolume
/gate/rando_breast/geometry/setImage                 data/rando/mhd/breast/breast.mhd
/gate/geometry/setMaterialDatabase                        data/rando/patient-HUmaterials.db
/gate/rando_breast/geometry/setHUToMaterialFile      data/rando/patient-HU2mat.txt
/gate/rando_breast/vis/setColor                             blue
/gate/rando_breast/vis/forceWireframe
```

Listing 6.12: Definition of the RANDO Pelvis volume

```
#=================

# INSERT FOV BOX #

#=================

/gate/Gantry/daughters/name                                  FOV

/gate/Gantry/daughters/insert                          box

/gate/FOV/setMaterial                                        Air

/gate/FOV/geometry/setXLength                          491.404 mm

/gate/FOV/geometry/setYLength                          491.404 mm

/gate/FOV/geometry/setZLength                          123.564 mm

#/gate/FOV/placement/setRotationAxis                  0 0 1

#/gate/FOV/placement/setRotationAngle                 180 deg

/gate/FOV/vis/setColor                                       white

/gate/FOV/vis/setVisible                                     1

/gate/FOV/vis/forceWireframe

#=====================================================

# GENERATE MATERIALS FROM HOUNSFIELD UNITS

#=====================================================
```

```
# Generate materials from Hounsfield units
/gate/HounsfieldMaterialGenerator/SetMaterialTable                    data/Schneider2000MaterialsTable.txt
/gate/HounsfieldMaterialGenerator/SetDensityTable                     data/Schneider2000DensitiesTable.txt
/gate/HounsfieldMaterialGenerator/SetDensityTolerance                 0.1 g/cm3
/gate/HounsfieldMaterialGenerator/SetOutputMaterialDatabaseFilename   data/rando/patient-HUmaterials.db
/gate/HounsfieldMaterialGenerator/SetOutputHUMaterialFilename         data/rando/patient-HU2mat.txt
/gate/HounsfieldMaterialGenerator/Generate
#=====================================================
# IMPORT PELVIS .MHD FILE
#=====================================================
/gate/FOV/daughters/name                                    rando_pelvis
/gate/FOV/daughters/insert                                                ImageNestedParametrisedV
/gate/rando_pelvis/geometry/setImage                  data/rando/mhd/pelvis/pelvis.mhd
/gate/geometry/setMaterialDatabase                          data/rando/patient-HUmaterials.db
/gate/rando_pelvis/geometry/setHUToMaterialFile       data/rando/patient-HU2mat.txt
/gate/rando_pelvis/vis/setColor                                       blue
/gate/rando_pelvis/vis/forceWireframe
```

Listing 6.13: Definition of the RANDO Pelvis Large volume

```
#=================

# INSERT FOV BOX #

#=================

/gate/Gantry/daughters/name                                  FOV

/gate/Gantry/daughters/insert                            box

/gate/FOV/setMaterial                                     Air

/gate/FOV/geometry/setXLength                          491.404 mm

/gate/FOV/geometry/setYLength                          491.404 mm

/gate/FOV/geometry/setZLength                          123.564 mm

#/gate/FOV/placement/setRotationAxis                  0 0 1

#/gate/FOV/placement/setRotationAngle                 180 deg

/gate/FOV/vis/setColor                                    white

/gate/FOV/vis/setVisible                                  1

/gate/FOV/vis/forceWireframe

#=====================================================

# GENERATE MATERIALS FROM HOUNSFIELD UNITS
```

```
#=====================================================

# Generate materials from Hounsfield units

/gate/HounsfieldMaterialGenerator/SetMaterialTable                    data/Schneider2000MaterialsTable.txt

/gate/HounsfieldMaterialGenerator/SetDensityTable                     data/Schneider2000DensitiesTable.txt

/gate/HounsfieldMaterialGenerator/SetDensityTolerance                 0.1 g/cm3

/gate/HounsfieldMaterialGenerator/SetOutputMaterialDatabaseFilename   data/rando/patient-HUmaterials.db

/gate/HounsfieldMaterialGenerator/SetOutputHUMaterialFilename         data/rando/patient-HU2mat.txt

/gate/HounsfieldMaterialGenerator/Generate

#=====================================================

# IMPORT pelvis_large .MHD FILE

#=====================================================

/gate/FOV/daughters/name                                        rando_pelvis_large

/gate/FOV/daughters/insert                                                  ImageNestedParametrisedV

/gate/rando_pelvis_large/geometry/setImage                  data/rando/mhd/pelvis_large/pelvis_large.mhd

/gate/geometry/setMaterialDatabase                              data/rando/patient-HUmaterials.db

/gate/rando_pelvis_large/geometry/setHUToMaterialFile           data/rando/patient-HU2mat.txt

/gate/rando_pelvis_large/vis/setColor                                       blue
```

```
/gate/rando_pelvis_large/vis/forceWireframe
```

Listing 6.14: Definition of the RANDO Pelvis Large Fast volume

```
#=====================================================

# Voxelised rando_pelvis_large_fast

#=====================================================

/gate/Gantry/daughters/name                                    rando_breast

#/gate/Gantry/daughters/insert                                      ImageNestedParametrisedVolume

/gate/Gantry/daughters/insert                                      ImageRegionalizedVolume

/gate/rando_pelvis_large_fast/geometry/setImage                data/rando/mhd/pelvis_large_fast/pelvis_large_fa

/gate/rando_pelvis_large_fast/vis/setColor                                                  blue

/gate/rando_pelvis_large_fast/vis/forceWireframe

#/gate/rando_pelvis_large_fast/placement/setRotationAxis              1 0 0

#/gate/rando_pelvis_large_fast/placement/setRotationAngle             90 deg


#=====================================================

# HU to Materials conversion

#=====================================================
```

```
/gate/geometry/setMaterialDatabase                                  data/image-HUmaterials.db
/gate/rando_pelvis_large_fast/geometry/setHUToMaterialFile          data/image-HUmat.dat
/gate/rando_pelvis_large_fast/geometry/setRangeToMaterialFile       data/image-HUmat.dat


#=============================================================

# Generate and use the dose map

#=============================================================

/gate/rando_pelvis_large_fast/geometry/buildAndDumpDistanceTransfo  output/pelvis_large_fast.mhd
/gate/rando_pelvis_large_fast/geometry/distanceMap                  output/pelvis_large_fast
```


Listing 6.15: Definition of the RANDO Thorax volume

```
#================

# INSERT FOV BOX #

#================

/gate/Gantry/daughters/name                                         FOV
/gate/Gantry/daughters/insert                                       box
/gate/FOV/setMaterial                                               Air
/gate/FOV/geometry/setXLength                                       491.404 mm
```

```
/gate/FOV/geometry/setYLength                                   491.404 mm
/gate/FOV/geometry/setZLength                                   129.543 mm
/gate/FOV/vis/setColor                                          white
/gate/FOV/vis/setVisible                                        1
/gate/FOV/vis/forceWireframe
#=====================================================
# GENERATE MATERIALS FROM HOUNSFIELD UNITS
#=====================================================
# Generate materials from Hounsfield units
/gate/HounsfieldMaterialGenerator/SetMaterialTable              data/Schneider2000MaterialsTable.txt
/gate/HounsfieldMaterialGenerator/SetDensityTable               data/Schneider2000DensitiesTable.txt
/gate/HounsfieldMaterialGenerator/SetDensityTolerance           0.1 g/cm3
/gate/HounsfieldMaterialGenerator/SetOutputMaterialDatabaseFilename data/rando/patient-HUmaterials.db
/gate/HounsfieldMaterialGenerator/SetOutputHUMaterialFilename   data/rando/patient-HU2mat.txt
/gate/HounsfieldMaterialGenerator/Generate
#=====================================================
# IMPORT PELVIS .MHD FILE
```

```
#=====================================================

/gate/FOV/daughters/name                                    rando_thorax

/gate/FOV/daughters/insert                                  ImageNestedParam

/gate/rando_thorax/geometry/setImage                        data/rando/mhd/thorax_fast/thorax_fast.mhd

/gate/geometry/setMaterialDatabase                          data/rando/patient-HUmaterials.d

/gate/rando_thorax/geometry/setHUToMaterialFile             data/rando/patient-HU2mat.txt

/gate/rando_thorax/vis/setColor                             blue

/gate/rando_thorax/vis/forceWireframe
```


Listing 6.16: Definition of the RANDO Thorax Fast volume

```
#=================

# INSERT FOV BOX #

#=================

/gate/Gantry/daughters/name                                 FOV

/gate/Gantry/daughters/insert                               box

/gate/FOV/setMaterial                                       Air

/gate/FOV/geometry/setXLength                               491.404 mm

/gate/FOV/geometry/setYLength                               491.404 mm
```

```
/gate/FOV/geometry/setZLength                                    129.543 mm
/gate/FOV/vis/setColor                                           white
/gate/FOV/vis/setVisible                                         1
/gate/FOV/vis/forceWireframe
#=====================================================
# GENERATE MATERIALS FROM HOUNSFIELD UNITS
#=====================================================
# Generate materials from Hounsfield units
/gate/HounsfieldMaterialGenerator/SetMaterialTable               data/Schneider2000MaterialsTable.txt
/gate/HounsfieldMaterialGenerator/SetDensityTable                data/Schneider2000DensitiesTable.txt
/gate/HounsfieldMaterialGenerator/SetDensityTolerance            0.1 g/cm3
/gate/HounsfieldMaterialGenerator/SetOutputMaterialDatabaseFilename data/rando/patient-HUmaterials.db
/gate/HounsfieldMaterialGenerator/SetOutputHUMaterialFilename    data/rando/patient-HU2mat.txt
/gate/HounsfieldMaterialGenerator/Generate
#=====================================================
# IMPORT PELVIS .MHD FILE
#=====================================================
```

```
/gate/FOV/daughters/name                                    rando_thorax_fast
/gate/FOV/daughters/insert                                  ImageNestedParam
/gate/rando_thorax_fast/geometry/setImage                   data/rando/mhd/thorax_fast/thorax_fast.mhd
/gate/geometry/setMaterialDatabase                          data/rando/patient-HUmaterials.d
/gate/rando_thorax_fast/geometry/setHUToMaterialFile        data/rando/patient-HU2mat.txt
/gate/rando_thorax_fast/vis/setColor                        blue
/gate/rando_thorax_fast/vis/forceWireframe
```

Listing 6.17: Definition of the ICRP-110 AF volume


```
#=================
# INSERT FOV BOX #
#=================
/gate/Gantry/daughters/name                                 FOV
/gate/Gantry/daughters/insert                               box
/gate/FOV/setMaterial                                       Air
/gate/FOV/geometry/setXLength                               528.95 mm
/gate/FOV/geometry/setYLength                               241.4 mm
/gate/FOV/geometry/setZLength                               1679.48 mm
```

```
/gate/FOV/vis/setColor                                          white
/gate/FOV/vis/setVisible                                        1
/gate/FOV/vis/forceWireframe
#=============================================================
# Voxelised patient
#=============================================================
/gate/FOV/daughters/name                                icrp_phantom
/gate/FOV/daughters/insert                                      ImageNestedParametrisedVolume
/gate/geometry/setMaterialDatabase          data/patient/AF_GateMaterials.db
/gate/icrp_phantom/geometry/setHUToMaterialFile  data/patient/AF_LabelsToMaterials.txt
/gate/icrp_phantom/geometry/setImage        data/patient/AF_UINT16_299_137_348.mhd
/gate/icrp_phantom/placement/setTranslation             0. 0. 0. cm # Pelvis
#/gate/icrp_phantom/placement/setTranslation            0. 0. -40. cm # Thorax
#/gate/icrp_phantom/placement/setTranslation            0. 0. -85. cm # Head
/gate/icrp_phantom/vis/forceWireframe
/gate/icrp_phantom/vis/setColor                                 blue
```

Listing 6.18: Definition of the ICRP-110 AF dose output

```
#=====================================================

# Voxelised icrp_phantom

#=====================================================

/gate/actor/addActor                                    DoseActor  dose3D

/gate/actor/dose3D/attachTo                             icrp_phantom

/gate/actor/dose3D/stepHitType                                                  random

/gate/actor/dose3D/setResolution                        299 137 348

/gate/actor/dose3D/enableDose                           true

/gate/actor/dose3D/save                                 output/patient/pelvis/icru_phantom_pelvis.mhd

/gate/actor/dose3D/save                                 output/patient/thorax/icru_phantom_thorax.mhd

/gate/actor/dose3D/save                                 output/patient/head/icru_phantom_head.mhd

/gate/actor/dose3D/inputDoseByRegions                   data/patient/AF_UINT16_299_137_348.mhd

/gate/actor/dose3D/outputDoseByRegions                  output/patient/pelvis/pelvis_DoseByRegions.txt

#/gate/actor/dose3D/outputDoseByRegions                  output/patient/thorax/thorax_DoseByRegions.tx

#/gate/actor/dose3D/outputDoseByRegions                  output/patient/head/head_DoseByRegions.txt #

/gate/actor/dose3D/saveEveryNSeconds                                            60

#
```

```
/gate/actor/addActor                                    SimulationStatisticAct
/gate/actor/stat/save                                   output/patient
#/gate/actor/stat/save                                  output/patient
#/gate/actor/stat/save                                  output/patient
/gate/actor/stat/saveEveryNSeconds 60
```

Listing 6.19: Definition of the RANDO Pelvis dose output

```
#=====================================================
# VOXELISED RANDO_PELVIS DOSE OTPUT
#=====================================================
/gate/actor/addActor                    TLEDoseActor   dose3D
/gate/actor/dose3D/attachTo             rando_pelvis
/gate/actor/dose3D/stepHitType          random
/gate/actor/dose3D/setPosition                  0 0 0 cm
/gate/actor/dose3D/setResolution                512 512 63
/gate/actor/dose3D/enableDose                   true
/gate/actor/dose3D/enableUncertaintyDose  true
/gate/actor/dose3D/setDoseAlgorithm       MassWeighting
```

```
/gate/actor/dose3D/saveEveryNSeconds        60

/gate/actor/dose3D/save                     output/rando/pelvis/pelvis.mhd


#=====================================================

# SIMULATION STATISTICS

#=====================================================

/gate/actor/addActor                        SimulationStatisticActor stat

/gate/actor/stat/save                       output/rando/pelvis/stat-pat.txt

/gate/actor/stat/saveEveryNSeconds          60
```


Listing 6.20: Definition of the RANDO Pelvis Large dose output

```
#=====================================================

# VOXELISED RANDO_pelvis_large DOSE OTPUT

#=====================================================

/gate/actor/addActor                        TLEDoseActor  dose3D

/gate/actor/dose3D/attachTo                 rando_pelvis_large

/gate/actor/dose3D/stepHitType              random

/gate/actor/dose3D/setPosition                    0 0 0 cm
```

```
/gate/actor/dose3D/setResolution                    512 512 63
/gate/actor/dose3D/enableDose                       true
/gate/actor/dose3D/enableUncertaintyDose   true
/gate/actor/dose3D/setDoseAlgorithm        MassWeighting
/gate/actor/dose3D/saveEveryNSeconds       60
/gate/actor/dose3D/save                    output/rando/pelvis_large/pelvis_large.mhd


#=====================================================
# SIMULATION STATISTICS
#=====================================================
/gate/actor/addActor                                SimulationStatisticActor stat
/gate/actor/stat/save                               output/rando/pelvis_large/stat-pat.txt
/gate/actor/stat/saveEveryNSeconds                  60
```

Listing 6.21: Definition of the RANDO Pelvis Large Fast dose output

```
#=====================================================
# VOXELISED RANDO_PELVIS DOSE OTPUT
#=====================================================
```

```
/gate/actor/addActor                    TLEDoseActor   dose3D
/gate/actor/dose3D/attachTo             rando_pelvis
/gate/actor/dose3D/stepHitType          random
/gate/actor/dose3D/setPosition                  0 0 0 cm
/gate/actor/dose3D/setResolution                512 512 63
/gate/actor/dose3D/enableDose                   true
/gate/actor/dose3D/enableUncertaintyDose  true
/gate/actor/dose3D/setDoseAlgorithm     MassWeighting
/gate/actor/dose3D/saveEveryNSeconds    60
/gate/actor/dose3D/save                 output/rando/pelvis_large_fast/pelvis_large_fast.mhd


#=====================================================
# SIMULATION STATISTICS
#=====================================================
/gate/actor/addActor                            SimulationStatisticActor stat
/gate/actor/stat/save                           output/rando/pelvis_large_fast/stat-pat.txt
/gate/actor/stat/saveEveryNSeconds              60
```

Listing 6.22: Definition of the RANDO Thorax dose output

```
#=====================================================

# VOXELISED RANDO_BREAST DOSE OTPUT

#=====================================================

/gate/actor/addActor                    TLEDoseActor   dose3D

/gate/actor/dose3D/attachTo             rando_thorax

/gate/actor/dose3D/stepHitType          random

/gate/actor/dose3D/setPosition                  0 0 0 cm

/gate/actor/dose3D/setResolution                512 512 66

/gate/actor/dose3D/enableDose                   true

/gate/actor/dose3D/enableUncertaintyDose  true

/gate/actor/dose3D/setDoseAlgorithm       MassWeighting

/gate/actor/dose3D/saveEveryNSeconds      60

/gate/actor/dose3D/save                   output/rando/thorax/thorax.mhd


#=====================================================

# SIMULATION STATISTICS
```

```
#=====================================================

/gate/actor/addActor                    SimulationStatisticActor stat

/gate/actor/stat/save                   output/rando/thorax/stat-pat.txt

/gate/actor/stat/saveEveryNSeconds      60
```

Listing 6.23: Definition of the RANDO Thorax Fast dose output

```
#=====================================================

# VOXELISED RANDO_BREAST DOSE OTPUT

#=====================================================

/gate/actor/addActor                    TLEDoseActor   dose3D

/gate/actor/dose3D/attachTo             rando_thorax_fast

/gate/actor/dose3D/stepHitType          random

/gate/actor/dose3D/setPosition                  0 0 0 cm

/gate/actor/dose3D/setResolution                512 512 66

/gate/actor/dose3D/enableDose                   true

/gate/actor/dose3D/enableUncertaintyDose  true

/gate/actor/dose3D/setDoseAlgorithm     MassWeighting

/gate/actor/dose3D/saveEveryNSeconds    60
```

```
/gate/actor/dose3D/save                    output/rando/thorax_fast/thorax_fast.mhd


#=====================================================

# SIMULATION STATISTICS

#=====================================================

/gate/actor/addActor                       SimulationStatisticActor stat

/gate/actor/stat/save                      output/rando/thorax_fast/stat-pat.txt

/gate/actor/stat/saveEveryNSeconds         60
```

Listing 6.24: Definition of the Water phantom dose output

```
/gate/actor/addActor                       DoseActor  depthdose
/gate/actor/depthdose/normaliseDoseToMax       true
/gate/actor/depthdose/attachTo                 waterPhantom
/gate/actor/depthdose/stepHitType          random
/gate/actor/depthdose/setPosition          0 0 0 cm
/gate/actor/depthdose/setResolution            1 101 1
/gate/actor/depthdose/saveEveryNSeconds    60
/gate/actor/depthdose/enableEdep           false
/gate/actor/depthdose/enableUncertaintyEdep false
/gate/actor/depthdose/enableDose           true
/gate/actor/depthdose/enableUncertaintyDose true
/gate/actor/depthdose/enableNumberOfHits   false
/gate/actor/depthdose/save                 output/depth-pat.txt
#
/gate/actor/addActor                         DoseActor  doseprofile
/gate/actor/doseprofile/normaliseDoseToMax       true
/gate/actor/doseprofile/attachTo               waterPhantom
/gate/actor/doseprofile/stepHitType          random
/gate/actor/doseprofile/setPosition          0 -2 0 cm
#/gate/actor/doseprofile/setResolution         171 1 1 # for 80 kV
#/gate/actor/doseprofile/setResolution         164 1 1 # for 100 kV
#/gate/actor/doseprofile/setResolution         156 1 1 # for 125 kV
/gate/actor/doseprofile/setResolution         162 1 1 # for 140 kV
#/gate/actor/doseprofile/setSize                2 400 400 mm
```

```
/gate/actor/doseprofile/saveEveryNSeconds      60
/gate/actor/doseprofile/enableEdep             false
/gate/actor/doseprofile/enableUncertaintyEdep  false
/gate/actor/doseprofile/enableDose             true
/gate/actor/doseprofile/enableUncertaintyDose  true
/gate/actor/doseprofile/enableNumberOfHits     false
/gate/actor/doseprofile/save                   output/profile-pat.txt
#
/gate/actor/addActor                SimulationStatisticActor stat
/gate/actor/stat/save               output/stat-pat.txt
/gate/actor/stat/saveEveryNSeconds 60
```

Listing 6.25: Definition of the 100 kV source

```
/gate/source/addSource spectra                                  gps
/gate/source/spectra/gps/particle                               gamma
/gate/source/spectra/gps/energytype                    UserSpectrum
/gate/source/spectra/gps/setSpectrumFile               data/normSpectra/100kV.
/gate/source/spectra/attachTo                                   capsule
/gate/source/spectra/gps/position                               0 0 0 mm
/gate/source/spectra/gps/pos/type                               Plane
/gate/source/spectra/gps/shape                                  Rectangle
/gate/source/spectra/gps/halfx                                  0.4 mm
/gate/source/spectra/gps/halfy                                  0.4 mm
/gate/source/spectra/gps/pos/centre                    0. 0. 0. cm


#Set the angular distribution of emission
```

```
/gate/source/spectra/gps/ang/type                    iso


#Set min and max emission angles
/gate/source/spectra/gps/mintheta                    0. deg
/gate/source/spectra/gps/maxtheta                    14. deg
/gate/source/spectra/gps/minphi                      0. deg
/gate/source/spectra/gps/maxphi                      360. deg
#/gate/source/spectra/setIntensity                  1
```

Listing 6.26: Definition of the 125 kV source

```
/gate/source/addSource spectra                       gps
/gate/source/spectra/gps/particle                    gamma
/gate/source/spectra/gps/energytype                  UserSpectrum
/gate/source/spectra/gps/setSpectrumFile             data/normSpectra/125kV.
/gate/source/spectra/attachTo                        capsule
/gate/source/spectra/gps/position                    0 0 0 mm
/gate/source/spectra/gps/pos/type                    Plane
/gate/source/spectra/gps/shape                       Rectangle
/gate/source/spectra/gps/halfx                       0.4 mm
/gate/source/spectra/gps/halfy                       0.4 mm
/gate/source/spectra/gps/pos/centre                  0. 0. 0. cm


#Set the angular distribution of emission
/gate/source/spectra/gps/ang/type                    iso


#Set min and max emission angles
```

```
/gate/source/spectra/gps/mintheta                    0. deg
/gate/source/spectra/gps/maxtheta                    14. deg
/gate/source/spectra/gps/minphi                      0. deg
/gate/source/spectra/gps/maxphi                      360. deg
#/gate/source/spectra/setIntensity                  1
```

Listing 6.27: Definition of the 140 kV source

```
/gate/source/addSource spectra                       gps
/gate/source/spectra/gps/particle                    gamma
/gate/source/spectra/gps/energytype                  UserSpectrum
/gate/source/spectra/gps/setSpectrumFile             data/normSpectra/140kV.
/gate/source/spectra/attachTo                        capsule
/gate/source/spectra/gps/position                    0 0 0 mm
/gate/source/spectra/gps/pos/type                    Plane
/gate/source/spectra/gps/shape                       Rectangle
/gate/source/spectra/gps/halfx                       0.75 mm
/gate/source/spectra/gps/halfy                       0.9 mm
/gate/source/spectra/gps/pos/centre                  0. 0. 0. cm

#Set the angular distribution of emission
/gate/source/spectra/gps/ang/type                    iso

#Set min and max emission angles
/gate/source/spectra/gps/mintheta                    0. deg
/gate/source/spectra/gps/maxtheta                    14. deg
/gate/source/spectra/gps/minphi                      0. deg
```

```
/gate/source/spectra/gps/maxphi                    360. deg

#/gate/source/spectra/setIntensity                 1
```

6.2 Energy spectrum files

Listing 6.28: 100 kV spectrum file

```
1       0

0.001   0

0.002   0

0.003   1.0382E-192

0.004   8.9197E-101

0.005   1.98519E-59

0.006   4.28612E-38

0.007   5.98542E-26

0.008   2.3403E-18

0.009   1.56037E-13

0.01    7.86641E-20

0.011   9.82956E-16

0.012   1.32571E-18

0.013   2.31261E-15

0.014   7.99679E-13

0.015   8.32301E-11

0.016   3.50605E-09

0.017   6.92466E-08

0.018   7.81668E-07

0.019   5.6829E-06
```

0.02	2.96817E−05
0.021	0.000119002
0.022	0.000381284
0.023	0.001020359
0.024	0.002359139
0.025	0.004817225
0.026	0.008875609
0.027	0.015080371
0.028	0.023879081
0.029	0.035674916
0.03	0.050779241
0.031	0.069015408
0.032	0.090325555
0.033	0.114607411
0.034	0.141317296
0.035	0.169861588
0.036	0.200055649
0.037	0.231176045
0.038	0.260401748
0.039	0.289880616
0.04	0.321246365
0.041	0.349924892
0.042	0.376802294
0.043	0.404040876
0.044	0.42819952

0.045	0.450779313
0.046	0.471550881
0.047	0.488340005
0.048	0.504728529
0.049	0.520159968
0.05	0.529010599
0.051	0.538370986
0.052	0.549698695
0.053	0.556869878
0.054	0.560126394
0.055	0.561535089
0.056	0.564115616
0.057	0.56675536
0.058	0.715349001
0.059	1
0.06	0.845348862
0.061	0.559036251
0.062	0.552282433
0.063	0.528198343
0.064	0.5163302
0.065	0.506683723
0.066	0.499489709
0.067	0.613235173
0.068	0.604905713
0.069	0.491141343

0.07	0.113396661
0.071	0.102460633
0.072	0.104553307
0.073	0.105153456
0.074	0.107782534
0.075	0.109676478
0.076	0.109046864
0.077	0.107566431
0.078	0.106958149
0.079	0.107949622
0.08	0.107705553
0.081	0.105483674
0.082	0.102158775
0.083	0.098477938
0.084	0.094023942
0.085	0.090178835
0.086	0.086702579
0.087	0.082089949
0.088	0.077382181
0.089	0.071431486
0.09	0.06525966
0.091	0.058617959
0.092	0.051819336
0.093	0.045274128
0.094	0.038208927

0.095	0.030562376
0.096	0.0222524
0.097	0.014278717
0.098	0.006147901
0.099	0.00058635
0.1	0
0.101	0
0.102	0
0.103	0
0.104	0
0.105	0
0.106	0
0.107	0
0.108	0
0.109	0
0.11	0
0.111	0
0.112	0
0.113	0
0.114	0
0.115	0
0.116	0
0.117	0
0.118	0
0.119	0

0.12 0

0.121 0

0.122 0

0.123 0

0.124 0

0.125 0

0.126 0

0.127 0

0.128 0

0.129 0

0.13 0

0.131 0

0.132 0

0.133 0

0.134 0

0.135 0

0.136 0

0.137 0

0.138 0

0.139 0

0.14 0

0.141 0

0.142 0

0.143 0

0.144 0

```
0.145    0
0.146    0
0.147    0
0.148    0
0.149    0
0.15     0
```

Listing 6.29: 125 kV spectrum file

```
1        0
0.001    0
0.002    0
0.003    7.2824E-300
0.004    4.2556E-159
0.005    5.78278E-95
0.006    1.67444E-61
0.007    2.73434E-42
0.008    2.91661E-30
0.009    1.64553E-22
0.01     1.76162E-37
0.011    1.21259E-29
0.012    1.68472E-36
0.013    4.09414E-30
0.014    3.73993E-25
0.015    3.36773E-21
0.016    5.27411E-18
0.017    1.87876E-15
```

0.018	2.2536E−13
0.019	1.14349E−11
0.02	3.04666E−10
0.021	4.83531E−09
0.022	4.94679E−08
0.023	3.55882E−07
0.024	1.92071E−06
0.025	8.15669E−06
0.026	2.84336E−05
0.027	8.43197E−05
0.028	0.000217369
0.029	0.000498648
0.03	0.001038688
0.031	0.001999185
0.032	0.00355757
0.033	0.005929846
0.034	0.009389982
0.035	0.014123953
0.036	0.020164699
0.037	0.027928778
0.038	0.037593198
0.039	0.048690756
0.04	0.061677562
0.041	0.07663833
0.042	0.092661405

0.043	0.110489985
0.044	0.129616069
0.045	0.149755974
0.046	0.170312656
0.047	0.191043163
0.048	0.213475101
0.049	0.235798984
0.05	0.256683194
0.051	0.277290406
0.052	0.298796734
0.053	0.319390301
0.054	0.338031933
0.055	0.356467012
0.056	0.37621944
0.057	0.394271024
0.058	0.599723557
0.059	1
0.06	0.830429675
0.061	0.464369923
0.062	0.476305261
0.063	0.464546206
0.064	0.472789285
0.065	0.477482101
0.066	0.483563368
0.067	0.685068048

0.068	0.695795375
0.069	0.541583893
0.07	0.026237134
0.071	0.023857388
0.072	0.026511624
0.073	0.029161229
0.074	0.032055814
0.075	0.034997707
0.076	0.03806345
0.077	0.040821025
0.078	0.043722293
0.079	0.047099459
0.08	0.050228822
0.081	0.052882116
0.082	0.055276873
0.083	0.057826959
0.084	0.060497882
0.085	0.063175662
0.086	0.065855
0.087	0.067785115
0.088	0.070627646
0.089	0.072778826
0.09	0.073868217
0.091	0.075463879
0.092	0.07508312

0.093	0.076028818
0.094	0.078697731
0.095	0.079304888
0.096	0.079717579
0.097	0.079945224
0.098	0.078859157
0.099	0.078383607
0.1	0.077962327
0.101	0.077306372
0.102	0.076664686
0.103	0.074459339
0.104	0.073268507
0.105	0.072299986
0.106	0.070140078
0.107	0.068042684
0.108	0.064583472
0.109	0.061701044
0.11	0.058146002
0.111	0.054650771
0.112	0.051931085
0.113	0.047418882
0.114	0.043681287
0.115	0.039751236
0.116	0.034640326
0.117	0.029941165

0.118	0.024358161
0.119	0.017135114
0.12	0.013328215
0.121	0.011108367
0.122	0.007317849
0.123	0.003544462
0.124	0.000471737
0.125	0
0.126	0
0.127	0
0.128	0
0.129	0
0.13	0
0.131	0
0.132	0
0.133	0
0.134	0
0.135	0
0.136	0
0.137	0
0.138	0
0.139	0
0.14	0
0.141	0
0.142	0

```
0.143    0
0.144    0
0.145    0
0.146    0
0.147    0
0.148    0
0.149    0
0.15     0
```

Listing 6.30: 140 kV spectrum file

```
1        0
0.001    0
0.002    0
0.003    5.9278E-256
0.004    2.5915E-135
0.005    1.38338E-80
0.006    3.94036E-52
0.007    7.84145E-36
0.008    1.29616E-25
0.009    4.5817E-19
0.01     1.77258E-30
0.011    3.45746E-24
0.012    2.09305E-29
0.013    2.59634E-24
0.014    2.39061E-20
0.015    3.45618E-17
```

0.016	1.2358E−14
0.017	1.35538E−12
0.018	6.22218E−11
0.019	1.44399E−09
0.02	1.99505E−08
0.021	1.81924E−07
0.022	1.16961E−06
0.023	5.66381E−06
0.024	2.18341E−05
0.025	0.000069468
0.026	0.000188501
0.027	0.000450927
0.028	0.000961239
0.029	0.001864125
0.03	0.003354478
0.031	0.00565105
0.032	0.00894764
0.033	0.013470278
0.034	0.019397811
0.035	0.026764605
0.036	0.035626446
0.037	0.046149759
0.038	0.058383899
0.039	0.071799416
0.04	0.086377925

0.041	0.102248319
0.042	0.119098733
0.043	0.136750501
0.044	0.154604272
0.045	0.173231638
0.046	0.190799671
0.047	0.208800496
0.048	0.227937709
0.049	0.244981076
0.05	0.260938526
0.051	0.278099534
0.052	0.294851071
0.053	0.308155872
0.054	0.321291609
0.055	0.334562634
0.056	0.347088528
0.057	0.359713468
0.058	0.578149456
0.059	1
0.06	0.806141813
0.061	0.411486427
0.062	0.419043821
0.063	0.400806762
0.064	0.406557205
0.065	0.410565589

0.066	0.411450944
0.067	0.608131224
0.068	0.613934226
0.069	0.458457862
0.07	0.041912579
0.071	0.035800841
0.072	0.038958556
0.073	0.041859564
0.074	0.04472359
0.075	0.047961056
0.076	0.051171122
0.077	0.054025585
0.078	0.057218707
0.079	0.060189503
0.08	0.063258474
0.081	0.06658476
0.082	0.069299247
0.083	0.071485823
0.084	0.073624811
0.085	0.076023922
0.086	0.078306547
0.087	0.080904739
0.088	0.083293699
0.089	0.084679603
0.09	0.085977959

0.091	0.087516819
0.092	0.088196014
0.093	0.088909403
0.094	0.090230984
0.095	0.090830201
0.096	0.091667361
0.097	0.092622011
0.098	0.092570685
0.099	0.092349555
0.1	0.092901848
0.101	0.092989928
0.102	0.09244198
0.103	0.092294377
0.104	0.092337259
0.105	0.091037442
0.106	0.089105012
0.107	0.087902648
0.108	0.086128523
0.109	0.085160648
0.11	0.084756659
0.111	0.083338289
0.112	0.081550806
0.113	0.078405614
0.114	0.07514073
0.115	0.073304842

0.116	0.071489751
0.117	0.068382337
0.118	0.066327009
0.119	0.063471445
0.12	0.060366916
0.121	0.058395701
0.122	0.055817489
0.123	0.053229885
0.124	0.050380735
0.125	0.046467356
0.126	0.042339071
0.127	0.039127032
0.128	0.034788964
0.129	0.031094742
0.13	0.027282649
0.131	0.022784397
0.132	0.020094482
0.133	0.016952626
0.134	0.012878785
0.135	0.009443342
0.136	0.006616777
0.137	0.004256079
0.138	0.002124588
0.139	0.000236323
0.14	0

0.141 0

0.142 0

0.143 0

0.144 0

0.145 0

0.146 0

0.147 0

0.148 0

0.149 0

0.15 0

6.3 MATLAB Scripts

Listing 6.31: MATLAB script to process digitised RCF images

```
% Input and output directories. Change for 100, 125, and 140 kV accordingly
input_folder = 'C:\Users\neiso\YandexDisk\MSc\Results\GafChromic\Halcyon kV\100 kV\Exposed\Original';
output_folder = 'C:\Users\neiso\YandexDisk\MSc\Results\GafChromic\Halcyon kV\100 kV\Exposed\Edited';
result_file = 'C:\Users\neiso\YandexDisk\MSc\Results\GafChromic\Halcyon kV\100 kV\Exposed\Edited\results.txt';

% Ensure the output folder exists. If not, create it.
if ~exist(output_folder, 'dir')
    mkdir(output_folder);
end

% Threshold for white detection in 16-bit images
white_threshold = 56000; % Adjust if necessary

% List all TIFF files in the input folder
tifFiles = dir(fullfile(input_folder, '*.tif*'));
```

```
% Open the results file for writing
fid = fopen(result_file, 'w');
fprintf(fid, 'Image Name\tChannel\tMean\tStandard Deviation\n');

% Loop through each TIFF file
for i = 1:length(tifFiles)
    % Read the image
    img = imread(fullfile(input_folder, tifFiles(i).name));

    % Convert to binary mask where true indicates non-white regions
    mask = ~(img(:,:,1) > white_threshold & img(:,:,2) > white_threshold & img(:,:,3) > white_threshold);

    % Find the bounding boxes of the non-white regions
    stats = regionprops(mask, 'BoundingBox');

    if isempty(stats)
        warning(['No object found in image: ', tifFiles(i).name]);
```

```
    continue;
end

% Find the largest object
bbs = cat(1, stats.BoundingBox);
areas = bbs(:,3) .* bbs(:,4);
[~, idx] = max(areas);
bb = stats(idx).BoundingBox;

% Crop the image based on bounding box
cropped_img = imcrop(img, bb);

% Save the cropped image to the output folder
imwrite(cropped_img, fullfile(output_folder, tifFiles(i).name), 'tif');

% Split into RGB channels
R = cropped_img(:,:,1);
```

```
G = cropped_img(:,:,2);

B = cropped_img(:,:,3);


% Get the center coordinates

[height, width, ~] = size(cropped_img);

center_x = floor(width/2);

center_y = floor(height/2);


% Define the ROI around the center

half_len = floor(5/2);

roi = [center_x - half_len, center_y - half_len, 4, 4];


% Extract the 5x5 region from each channel

roi_R = imcrop(R, roi);

roi_G = imcrop(G, roi);

roi_B = imcrop(B, roi);
```

```
    % Calculate the mean and standard deviation for each ROI
    fprintf(fid, '%s\tRed\t%f\t%f\n', tifFiles(i).name, mean(roi_R(:)), std(double(roi_R(:))));
    fprintf(fid, '%s\tGreen\t%f\t%f\n', tifFiles(i).name, mean(roi_G(:)), std(double(roi_G(:))));
    fprintf(fid, '%s\tBlue\t%f\t%f\n', tifFiles(i).name, mean(roi_B(:)), std(double(roi_B(:))));
end

% Close the results file
fclose(fid);

disp('Processing completed.');
```

Listing 6.32: MATLAB script to plot GATE PDDs

```
% Define the folder containing the .txt files
folder_path = 'C:\Users\neiso\YandexDisk\MSc\Results\Halcyon kV\montecarlo\mcpdds';

% Get a list of all .txt files in the folder
file_list = dir(fullfile(folder_path, '*.txt'));
```

```
% Loop through each file in the folder
for i = 1:numel(file_list)
    file_name = file_list(i).name;

    % Open the file for reading
    fileID = fopen(fullfile(folder_path, file_name), 'r');

    % Skip the first 6 lines (header lines)
    % for j = 1:6
    %     fgetl(fileID);
    % end

    % Read the numeric data
    data = textscan(fileID, '%f');

    % Close the file
    fclose(fileID);
```

```
% Extract the data from the cell array
data = data{1};

% Reverse the order of appearance of the data
reversed_data = flipud(data);

% Create x-axis values (indices)
x = 1:length(reversed_data);

% Create a plot
plot(x/10, reversed_data*100);

% Set plot labels and title (customize as needed)
xlabel('Depth (cm)');
ylabel('PDD (%)');
title([file_name(1:5),' Percent Depth Dose']);
```

```
    % Save the plot as a PNG file using the first five characters of the file name
    plot_file_name = fullfile(folder_path, [file_name(1:5), '.fig']);
    saveas(gcf, plot_file_name);

    % Close the current figure to prepare for the next plot
    close(gcf);
end
```

Listing 6.33: MATLAB script to plot GATE Profiles

```
% Define the folder containing the .txt files
folder_path = 'C:\Users\neiso\YandexDisk\MSc\Results\Halcyon kV\montecarlo\mcpdds';

% Get a list of all .txt files in the folder
file_list = dir(fullfile(folder_path, '*.txt'));

% Loop through each file in the folder
for i = 1:numel(file_list)
```

```
file_name = file_list(i).name;


% Open the file for reading
fileID = fopen(fullfile(folder_path, file_name), 'r');


% Skip the first 6 lines (header lines)
% for j = 1:6
%     fgetl(fileID);
% end


% Read the numeric data
data = textscan(fileID, '%f');


% Close the file
fclose(fileID);


% Extract the data from the cell array
```

```
data = data{1};

% Reverse the order of appearance of the data
reversed_data = flipud(data);

% Create x-axis values (indices)
x = 1:length(reversed_data);

% Create a plot
plot(x/10, reversed_data*100);

% Set plot labels and title (customize as needed)
xlabel('Depth (cm)');
ylabel('PDD (%)');
title([file_name(1:5),' Percent Depth Dose']);

% Save the plot as a PNG file using the first five characters of the file name
```

```
    plot_file_name = fullfile(folder_path, [file_name(1:5), '.fig']);
    saveas(gcf, plot_file_name);

    % Close the current figure to prepare for the next plot
    close(gcf);
end
```

Listing 6.34: MATLAB script to compare Measured and GATE PDDs

```
% Define the folders
folder1_path = 'C:\\Users\\neiso\\YandexDisk\\MSc\\Results\\Halcyon kV\\scans\\pdd';
folder2_path = 'C:\\Users\\neiso\\YandexDisk\\MSc\\Results\\Halcyon kV\\montecarlo\\mcpdds\\modified';
folder3_path = 'C:\\Users\\neiso\\YandexDisk\\MSc\\Results\\Halcyon kV\\comparisons';

% Get file lists
file_list1 = dir(fullfile(folder1_path, '*.txt'));
file_list2 = dir(fullfile(folder2_path, '*.txt'));

% Loop through files in the first folder
```

```
for i = 1:numel(file_list1)
    file1_name = file_list1(i).name;

    % Loop through files in the second folder
    for j = 1:numel(file_list2)
        file2_name = file_list2(j).name;

        % Check if the first 5 characters of the file names match
        if strcmp(file1_name(1:5), file2_name(1:5))

            % Read data from both files
            data1 = dlmread(fullfile(folder1_path, file1_name));
            data2 = dlmread(fullfile(folder2_path, file2_name));

            % Add data from the second file as a new column to the first data
            combined_data = [data1, data2];
```

```
% Calculate the percentage difference and add as a new column
percentage_diff = (combined_data(:,3) - combined_data(:,2));
combined_data = [combined_data, percentage_diff]; %#ok<AGROW>

% Save the combined data to a new .txt file
save_file_name = fullfile(folder1_path, [file1_name(1:5), '.txt']);
dlmwrite(save_file_name, combined_data, 'precision', 10);

% Create a plot
figure;
plot(combined_data(:,1), combined_data(:,2),'ok', 'DisplayName', 'Measured');
hold on;
plot(combined_data(:,1), combined_data(:,3), 'DisplayName', 'GATE');
plot(combined_data(:,1), combined_data(:,4),'xb', 'DisplayName', 'Difference (%)');
yline(5,'--g','DisplayName','+/-5%');
yline(-5,'--g','HandleVisibility', 'off');
xlabel('Depth (mm)');
```

```
            ylabel('PDD (%)');
            legend;
            hold off;

            % Save the plot
            saveas(gcf, fullfile(folder3_path, [file1_name(1:5), '.fig']));
            close(gcf);

            break; % Break out of the second loop since a match was found
        end
    end
end
```

Listing 6.35: MATLAB script to compare Measured and GATE Profiles

```
% Define the folders
folder1_path = 'C:\\Users\\neiso\\YandexDisk\\MSc\\Results\\Halcyon kV\\scans\\profs';
folder2_path = 'C:\\Users\\neiso\\YandexDisk\\MSc\\Results\\Halcyon kV\\montecarlo\\mcprofs\\modified';
folder3_path = 'C:\\Users\\neiso\\YandexDisk\\MSc\\Results\\Halcyon kV\\comparisons\\profs';
```

```
% Get file lists
file_list1 = dir(fullfile(folder1_path, '*.txt'));
file_list2 = dir(fullfile(folder2_path, '*.txt'));

% Loop through files in the first folder
for i = 1:numel(file_list1)
    file1_name = file_list1(i).name;

    % Loop through files in the second folder
    for j = 1:numel(file_list2)
        file2_name = file_list2(j).name;

        % Check if the first 5 characters of the file names match
        if strcmp(file1_name(1:5), file2_name(1:5))

            % Read data from both files
```

```
data1 = dlmread(fullfile(folder1_path, file1_name));
data2 = dlmread(fullfile(folder2_path, file2_name));

% Add data from the second file as a new column to the first data
combined_data = [data1, data2];

% Calculate the percentage difference and add as a new column
percentage_diff = (combined_data(:,3) - combined_data(:,2));
combined_data = [combined_data, percentage_diff]; %#ok<AGROW>

% Save the combined data to a new .txt file
save_file_name = fullfile(folder3_path, [file1_name(1:5), '.txt']);
dlmwrite(save_file_name, combined_data, 'precision', 10);

% Create a plot
figure;
plot(combined_data(:,1), combined_data(:,2),'ok', 'DisplayName', 'Measured');
```

```
            hold on;
            plot(combined_data(:,1), combined_data(:,3), 'DisplayName', 'GATE');
            plot(combined_data(:,1), combined_data(:,4),'xb', 'DisplayName', 'Difference (%)');
            yline(5,'--g','DisplayName','+/-5%');
            yline(-5,'--g','HandleVisibility', 'off');
            xlabel('Depth (mm)');
            ylabel('PDD (%)');
            legend;
            hold off;

            % Save the plot
            saveas(gcf, fullfile(folder3_path, [file1_name(1:5), '.fig']));
            close(gcf);

            break; % Break out of the second loop since a match was found
        end
    end
```

```
end
```